U. S. DEPARTMENT OF THE INTERIOR

U. S. GEOLOGICAL SURVEY

Geophysical Tracking of the Injection of Trench Stabilization Material at U. S. DOE Hanford Site, Richland, Washington

by

G. R. Olhoeft[1], J. E. Lucius[1] and S. J. Phillips[2]

Open File Report 94-146

[1]U. S. Geological Survey, Box 25046 DFC MS964, Denver, CO 80225-0046

[2]Westinghouse Hanford, P.O.Box 1970 MS L7-10, Richland, WA 99352

1994

Introduction

The U. S. Department of Energy's Hanford Site near Richland, Washington, has many environmental challenges. This report outlines an experiment performed to address isolation and stabilization of burial grounds, trenches and landfills containing leachable materials and void space (Ames and Phillips, 1979; Banno and Yoshida, 1992; Cline and others, 1980; Francis, 1991; Fruland and others, 1989; Harris and others, 1992; Henckel and Johnson, 1991; Khaleel and LeGore, 1990; Loomis and Low, 1988; McLaughlin and others, 1992; Morgan and Bostick, 1990; Phillips and Raymond, 1975; Phillips and others, 1977, 1980, 1993; Phillips and Stewart, 1993; Phillips, 1978; Swanson and others, 1988; Voogd, 1992; Wakeley and Ernzen, 1992).

In October, 1988, an experiment was performed to test the ability of geophysical methods to track where stabilization material actually invades when injected into the void space within the gravel layer of the trench fill material. Injected stabilization material is intended to reduce or eliminate ground water contact with wastes to minimize leaching (Jones and Skaggs, 1989; Khaleel and LeGore, 1990; Francis and Spalding, 1991; Wakeley and others, 1992), and to minimize corrosion of waste containers (James, 1987, 1988; Merz and others, 1987). Results were initially presented in Olhoeft and others (1989). Under the highly resistive soil conditions at the Hanford Site, ground penetrating radar proved to be the most effective surface geophysical technique to track the stabilization material.

Site Description

Geology (condensed from Newcomb and others, 1972, and Myers and Price, 1979)

The Hanford Site is located on the broad sandy terraces along the Columbia River in the semiarid Pasco Basin of south-central Washington (Figure 1). Elevations range from 100 m to about 240 m on the terraces, reach 1074 m in the mountains adjacent on the west, and extend above 300 m on a few bedrock knobs which rise prominently above the surrounding terraces.

The bedrock of the region is the basalt of the Columbia River Group which is about 1460 m thick below the site. The basalt is warped and locally is severely deformed. The Ringold Formation, of middle or late Pleistocene age, overlies the basalt; it consists of up to 365 m of bedded silts and fine sands containing some gravel, clay and volcanic ash, and one prominent conglomerate train (Figure 2). The eroded surface of the Ringold Formation has been covered by various thicknesses, up to about 60 m, of glaciofluviatile and fluvial deposits (from the ancestral Columbia River) which underlie the land surface in most of the site. These deposits consist of granule gravel, sand and pebble gravel with some intermixed and interlayered silt as well as interbedded and included cobbles and boulders. Most of the site is terrace land underlain by 15 to 30 m glaciofluviatile and fluvial deposits. The differences between these deposits and the underlying Ringold Formation are summarized in Table 1.

See also: Bjornstad (1990), Carson and others (1987), Delaney (1991), Gaylord and Poeter (1991), Heller and others (1985), Hunter and Busacca (1990), LaSala and Doty (1975), Lasmanis (1989), Last and others (1989), Lindsey and others (1989), Newcomb and others (1972), Swanson (1982), and Weskes and others (1987).

Hydrology (condensed from Newcomb and others, 1972, and Myers and Price, 1979)

The climate of the Pasco Basin is semiarid indicating 25 to 50 cm of annual precipitation. Within the site, the regional water table lies mostly in the Ringold Formation, specifically, within the conglomerate zone (figure 2). The Columbia and Yakima Rivers are the base level drainage. The water table remains relatively flat for about 3 km from the Columbia River then slopes up at about 0. 6 to 2. 8 m/km toward the higher elevations. Few bodies of perched ground water occur naturally. The glaciofluviatile and fluviatile deposits, much of the alluvium, and the colluvium are sufficiently permeable to permit water to infiltrate readily to transfer downward to the water table. Regional flow direction is toward the rivers. Surface runoff is minimal and there is no annual recharge through the soil. The zone of aeration effectively separates the precipitation from the water table. Recharge is mainly from Cold Creek to the west of the site. The effective porosity of the Ringold conglomerate is approximately 11%, and that of the overlying deposits is about twice as much.

See also: Bjornstad (1990), Delaney (1991), Drost and others (1989), Gaylord and Poeter (1991), Gee and Heller (1985), Heller and others (1985), LaSala and Doty (1975), Last and others (1989), Mitchell and Freshley (1987), Naugle (1989), Newcomb and others (1972), Newcomer and McDonald (1990), Poeter and Gaylord (1990), Rouston and Johnson (1990), Schalla and others (1988), and Weskes and others (1987).

Environmental Challenges

Environmental problems at Hanford include contaminated surface and near-surface soil, sediment, and water and contaminated ground water. Some man-made basins and ponds are contaminated with low-level radioactive waste (LLRW) mixed with organic and inorganic hazardous materials and heavy metals. Soil beneath the units may also be contaminated. These areas are unlined and pose a current and potential source of vadose zone and ground water contamination. There are areas where surface soils that have been contaminated with LLRW mixed with hazardous constituents that are associated with above or underground storage tanks, piping, or sewer lines. Some soils are contaminated with some combination of petroleum, polychlorinated biphenyls (PCBs), volatile organic compounds (VOCs), and heavy metals. Other soils are contaminated only by LLRW. Vegetation and animals on the site have bioaccumulated LLRW. There are landfills, trenches, or other burial grounds containing LLRW mixed with hazardous materials such as organic and inorganic materials and metals. Other burial grounds contain only non-radioactive hazardous materials. Burial trenches are major sources of vadose zone and ground water contamination. There is LLRW mixed with hazardous materials contained in above ground storage tanks and associated piping. There are also facilities and equipment on site that require decontamination and decommissioning (D&D). A potential exists for generating mixed waste through the D&D procedure. Ground water beneath the site has been contaminated with tritium and other radiologic and hazardous constituents.

See also: Battelle (1991), Bryce and Gorst (1990), Elder and others (1989), Evans and Murphy (1988), Gerber (1991, 1992), Gray (1988, 1989, 1990), Jacquish and Bryce (1989), Jacquish and Mitchell (1988), Marshall (1987), Price and others (1987), Schmidt and others (1990, 1991, 1992), Shulman (1989), U.S. DOE (1987, 1989, 1990, 1991, 1992), USGS (1987), Westinghouse Hanford (1989, 1992).

Geophysics

Phillips and others (1977) demonstrated the utility of metal detector, magnetometer, acoustics, and ground penetrating radar to map buried waste materials, waste containers and trench boundaries. Piciulo and others (1985) measured in situ and laboratory soil resistivity from the Hanford site in the range of 100 to 1,000 ohm-m. Sandness (1991) used electromagnetic induction and ground penetrating radar to locate abandoned sewers, burial trenches and pits, determine depth of fill, and locate waste, including any outside perimeter fences. Bergstrom and others (1993) used ground penetrating radar and electromagnetic induction to investigate several landfill, trench and mound sites. The lack of clay minerals and high resistivity of the site makes ground penetrating radar the most useful high resolution tool.

Preparation

Laboratory investigations demonstrated an electrical properties contrast between the stabilization material to be injected and the Hanford soil. The electrical properties that control electromagnetic propagation through a material are the complex dielectric permittivity and the DC (direct current) electrical conductivity (or its reciprocal: electrical resistivity). The electrical conductivity describes the ability of electric charge to be transported through the material. The dielectric permittivity describes the ability of opposite electric charges within the material to be separated by a distance (polarized). At frequencies above 10^6 Hz, the electrical conductivity is a fixed, frequency-independent, real number. The dielectric permittivity is a frequency dependent complex quantity. The dielectric permittivity is presented here as the relative permittivity (dielectric permittivity of the material divided by the permittivity of vacuum or free space, ϵ_o = 8.854x10^{-12} Farad/meter).

To parameterize the data, the electrical properties are described by the Cole-Cole model (Cole and Cole, 1941), all relative to the free space permittivity:

$$\epsilon_r' - i\,\epsilon_r'' = \epsilon_\infty + (\epsilon_\iota - \epsilon_\infty) / (1 + (i\,\omega\,\tau_\epsilon)^{\alpha_\epsilon})$$

with the electric loss tangent given as:

$$\tan\delta_\epsilon = \epsilon_r''/\epsilon_r' + \sigma/(\omega\epsilon_r'\epsilon_o)$$

where ϵ_r' = real part of the relative complex dielectric permittivity
ϵ_r'' = imaginary part of the relative complex dielectric permittivity
ϵ_ι = low frequency limit of permittivity
ϵ_∞ = high frequency limit of permittivity
$\omega = 2\,\pi f$ = radian frequency [f is frequency in 10^6 Hz]
$i = \sqrt{(-1)}$
τ_ϵ = time constant of relaxation [10^{-6} seconds]
α_ϵ = Cole-Cole relaxation breadth distribution parameter
(= 0 for infinitely broad, = 1 for single relaxation)
σ = DC conductivity [Siemens/m].

The magnetic property that controls electromagnetic propagation through a material is the complex magnetic permeability. The magnetic permeability is commonly assumed to be that of free space, $\mu_o = 4\,\pi$x10^{-7} Henry/meter, and a real,

fixed parameter, independent of frequency. This was confirmed by these laboratory measurements.

To parameterize the data, the magnetic properties are also described by the Cole-Cole model (Olhoeft, 1972), all relative to the free space permeability:

$$\mu_r' - i\,\mu_r'' = \mu_\infty + (\mu_\iota - \mu_\infty) / (1 + (i\,\omega\tau_\mu)^{\alpha_\mu})$$

with the magnetic loss tangent given as:

$$\tan\delta_\mu = \mu_r''/\mu_r'$$

where μ_r' = real part of the relative complex magnetic permeability
μ_r'' = imaginary part of the relative complex magnetic permeability
μ_ι = low frequency limit of permeability
μ_∞ = high frequency limit of permeability
$\omega = 2\,\pi f$ = radian frequency [f is frequency in 10^6 Hz]
$i = \sqrt{(-1)}$
τ_μ = time constant of relaxation [10^{-6} seconds]
α_μ = Cole-Cole relaxation breadth distribution parameter
(= 0 for infinitely broad, = 1 for single relaxation)

Figures 3 through 14 show the electrical properties of the stabilization material and the Hanford soil from 10^{-3} to 10^{+9} Hz. Figure 3 shows the time dependence of the electrical resistivity at 1 Hz for a stabilization material mixed with 28 percent distilled water. The resistivity is about 1 ohm-m for nearly 1,000 seconds after mixing, rapidly increasing thereafter. The low-frequency complex resistivity spectra of the stabilization material are shown in Figures 4 through 6. These measurements may be simply described by only the DC conductivity parameter. Figures 7 through 10 show the low-frequency complex resistivity spectra of Hanford soil. Note that even water saturated (12 weight percent water), there is a 100 to 1 contrast between the soil and the fresh, uncured stabilization material. Note in the wet soils of Figures 8 through 10, there is a slight induced polarization response near a few Hertz (evidenced as the peak in the phase versus frequency) and there is no induced polarization response at all in the stabilization materials. This difference in induced polarization response might be sufficient to distinguish the stabilization material from the soil if both were water saturated, but is insufficient for the dry soil (which has no induced polarization response and a resistivity of thousands of ohm-m). See Olhoeft (1985) for further information about measuring and interpreting low frequency electrical properties.

Figures 11 through 14 show the high frequency electrical and magnetic properties of the Hanford soil. In each figure, the upper left plot is the relative dielectric permittivity, the lower left plot is the electric loss tangent, the upper right plot is the relative magnetic permeability, and the lower right plot is the magnetic loss tangent, each versus log frequency. Each plot shows the forward and reverse measurements (the jagged lines) and a smooth curve showing the fit of the model parameters. The unchanging line with a minimum near 100 MHz in both loss tangent plots represents the minimum resolvable losses for the sample holder and measurement system. Also labelled on the plots are the dry bulk density (upper left), water content (lower right), and dielectric and magnetic Cole-Cole model parameters (lower plots). See Olhoeft (1987) and Olhoeft and Capron (1993) for further information about measuring and interpreting high frequency electrical properties. Note again, that even water saturated (Figure 14), the soil is resistive enough for good radar penetration. The magnetic properties are essentially those of free space and may be neglected.

At the isolation and stabilization site, Geonics EM-31 and EM-34 electromagnetic induction conductivity meters were used to measure the in situ electrical properties. The EM-31 measured 7 mS/m (139 ohm-m) in both coil orientations (vertical and horizontal) and both azimuths (line between the coils parallel and perpendicular to the trench). The EM-34 measured:

line between coils parallel to trench
- 10 m vertical coil 2.1 mS/m (476 ohm-m)
- 10 m horizontal coil 2.7 mS/m (370 ohm-m)
- 20 m vertical coil 3.5 mS/m (285 ohm-m)
- 20 m horizontal coil 5.1 mS/m (196 ohm-m)

line between coils perpendicular to trench
- 10 m vertical coil 2.2 mS/m (454 ohm-m)
- 10 m horizontal coil 2.7 mS/m (370 ohm-m)
- 20 m vertical coil 3.6 mS/m (277 ohm-m)
- 20 m horizontal coil 5.0 mS/m (200 ohm-m).

The trench was 3.6 to 4.3 m deep. The in situ measurements of high resistivity suggest less than one percent moisture content in the soil.

A Geophysical Survey Systems Inc. SIR-7 ground penetrating radar system was used with a pair of antennas having a center frequency in air of 300 MHz. Figures 15 and 16 show ground penetrating radar measurements of relative dielectric permittivity determined in situ from a large volume average. These are performed by walking one antenna away from a second fixed antenna. The first arrival is the electromagnetic wave through the air between the two antennas. The second arrival is the wave travelling just beneath the surface of the earth. The relative dielectric permittivity is the square of the ratio of the slopes of the two wave arrival times versus distance. From these large volume average in situ measurements, a relative dielectric permittivity value of 5 was used to convert two-way travel time into depth for the ground penetrating radar cross-sections. This is consistent with the laboratory measurements in Figures 12 and 13, again suggesting less than 1 percent moisture content in the soil.

Stabilization Material Injection

A particulate slurry of stabilization material (cement, grout, fly ash and water) was injected into a simulated low-level radioactive waste disposal crib of known morphology and dimensions. The trench was nominally 4.4 m deep and filled with 0.7 m thickness of gravel with a porosity of 46 percent. The gravel was covered by a plastic sheet, and the hole backfilled to a level surface. 13.7 m^3 of slurry was injected (1.4 m^3 more than the volume of the gravel void). Figures 17 through 19 show the topography of the surface before and after the injection. The mounding evident in the difference plot (Figure 19) is the result of the excess injection beyond the gravel void volume. Electromagnetic induction conductivity meter and ground penetrating radar measurements were performed before, during and after the injection.

Results

On exhumation of the crib, the stabilization material was found to fully penetrate the gravel aggregate layer located at the base of the trench. In addition, a layer of clean stabilization material was found directly above the gravel approximately

0.4 m thick at the injection riser and decreasing to less than 0.05 m at the longitudinal terminus of the crib.

The electromagnetic induction conductivity meter EM-34 measured no difference between the before and after injection measurements. The EM-34 volume of investigation includes too large a volume of dry soil compared to the volume of injected stabilization material to be measurable. The EM-31 placed on the ground surface in the middle of the trench measured an 8 percent increase in conductivity as the injection occurred, but no measurable difference when measured at 1 m height traversing across the trench.

The 300 MHz center-frequency ground penetrating radar directly observed the change from air filled gravel to stabilization material slurry filled gravel trench. The ground penetrating radar data, in Figures 20 through 55, was processed through the following steps:

1) a 60 MHz high pass filter was applied (to remove long period undulations in each scan),
2) each scan's mean was adjusted to a value of 127 (the middle of the 8-bit grayscale plotting palette),
3) a global average background scan was then subtracted (to reduce the effects of antenna ringing),
4) a contrast stretch was applied (to compensate for contrast loss in printing), and
5) the vertical and horizontal scales were applied and rubbersheeted by a cubic spline to topographic locations surveyed by an Sokhisha total station SET-2 electronic distance measuring device (to compensate for variations in antenna movement and position during the data acquisition process).

A relative dielectric permittivity of 5 was used to convert two-way travel time into depth. The horizontal scale was determined by marks recorded on the radar data that correlated with the surveying information. Note that slight variations in the range gain settings of different data acquisition runs produce amplitude variations between radar cross sections that have not been compensated.

Figures 20 through 31 show a time sequence (Table 2) of measurements before, during and after the stabilization material is injected along a line (5/6, between lines 5 and 6 in Figure 19) over the top of and down the middle of the gravel filled trench. In Figures 21 through 28, data are missing from 0 to 10 m horizontal distance as injection hoses were occupying that space. In Figure 20, the air filled gravel is visible at about 4 m depth between 7 and 17 m horizontal distance. The trench construction disturbance is visible as a reflector coming down from the surface at each end (first visible going down to the left at 2 m depth near 3 m horizontal distance and coming back up to the surface near 22 m horizontal distance). In Figure 21, 12 minutes after injecting water and 9 minutes after stabilization material injection started, the stabilization material begins to appear as a bright reflector at 10 m horizontal distance. In Figure 22, the stabilization material reflector appears between 10 and 11 m, with a break, and then between 14 and 16 m horizontal distance, suggesting the stabilization material filled in the gravel by a sinuous path in and out of the plane of the radar data. In Figure 23, the stabilization material has filled in the break, showing a continuous reflector from 10 to 16 m horizontal distance. In Figure 24, reflector brightness variations along the length of the stabilization material suggest higher stabilization material invasion near line C than line D. These apparent invasion variations continue in Figures 25 through 31, only stabilizing after injection stops. Note also the successive lightening of the reflector

contrast in Figures 29 through 31 as the stabilization material cures and dries. Also note the slight dip to the trench going down from C towards E.

Figures 32 through 34 show the results from line B, perpendicular to and beyond the end of the gravel trench. There is no evidence of the stabilization material penetrating beyond the end of the gravel.

Figures 35 through 38 show the results from line C, perpendicular to and just over the end of the gravel filled trench near the injection riser. Note the bright reflector that appears between 21 to 25 m horizontal distance as the stabilization material is injected. Note also that there are diffractions (tailing from 21 towards 19 m and from 25 towards 28 m horizontal distance) appearing at the edges of the trench reflection in Figures 36 through 38 that are not present in Figure 35. These diffractions indicate a sharp transition on the scale of about a third of a wavelength from stabilization material filled gravel to no stabilization material filling at the edge of the trench. The other radar sections lack these features, suggesting a more gradual transition. The 300 MHz antenna center frequency in air is pulled down to an effective center frequency in the ground of 100 MHz by ground loading and dispersion. A 100 MHz wavelength in relative dielectric permittivity 5 material is about 1.3 m.

Figures 39 through 42 show the results from line D, perpendicular to and across the middle of the gravel filled trench. Note the bright reflector that appears between 21 to 24 m horizontal distance as the stabilization material is injected. Note the flatter and slightly tilted shape of the reflector here compared to line C in Figures 36 through 38, where the surface of the stabilization material appears more rounded. Note also (more clearly here than for line C) that the brightest reflector in Figure 39 is slightly lower than in Figures 40 through 42. In Figure 39, there are reflections from both the top and bottom of the gravel filled trench, with the bottom reflection being slightly brighter caused by the instrument range gain setting (a variable gain with reception time to partially compensate for geometric spreading and material attenuation losses) and a slight curvature to the bottom of the trench which produces a focussing effect from 22 to 23.5 m horizontal distance. The reflection from the top of the gravel filled trench is just above the bright reflection between 21 and 24 m horizontal distance and much lower contrast (harder to see). In Figures 40 through 42, only the top of the gravel filled trench produces a reflection as the stabilization material is too attenuating to also allow measurement of a reflection from the bottom of the gravel filled trench. These data are full waveform modeled below.

Figures 43 through 46 show the results from line E, perpendicular to and just beyond the end of the gravel filled trench at the opposite end from the injection riser. There is no evidence of the stabilization material penetrating beyond the end of the gravel.

Figures 47 through 49 show the results from line 5, parallel to and outside the edge of the gravel filled trench. There is no evidence of the stabilization material penetrating beyond the edge of the gravel.

Figures 50 through 52 show the results from line 6, parallel to and down the middle of the gravel filled trench. The gravel filled trench and injected stabilization material appear between 7 and 17 m horizontal distance.

Figures 53 through 55 show the results from line 7, parallel to and outside the edge of the gravel filled trench. There is no evidence of the stabilization material penetrating beyond the edge of the gravel.

Full waveform forward modeling of the ground penetrating radar data was performed using the model of Powers and others (1992). Figures 56 through 59 show the model results for the middle of the trench from cross section line D (Figures 39 through 42). The direct arrivals and stratigraphic radar reflectors above the gravel level in the trench were removed to scale just the reflection from the gravel layer. In each figure, the left half shows the radar data (dashed line) with range gain removed and the model result (solid line) versus two-way travel time. The right half of the figure shows the model. The rightmost number is depth in meters. Remaining numbers in each layer are the real (K') and imaginary (K") relative dielectric permittivities and the DC electrical conductivity (con) in mS/m. The bottom two numbers are the zero offset (Offs) for the dataset (an arbitrary number for a GSSI SIR-7) and the coupling ratio, Cr. The coupling ratio compensates for the pull-down of the center frequency of the antenna (nominally measured in air and 300 MHz in this data set) when the antenna is placed on the surface of a dielectric material (a ground loaded antenna). In these examples, it is also used to compensate for the frequency dependent electrical properties of the soil which cause pulse broadening or dispersion (requiring an apparent center frequency of 100 MHz for this data). The high frequency ripple seen in the model (most pronounced in Figure 59) is the result of truncation and rounding errors in the double precision calculations.

Figure 56 shows the results before injection when the gravel voids are air filled. Figures 57, 58, and 59 show the results at 0.25, 16.5 and 62 hours after the injection ended. In each of these figures, the 3.4 m depth reflector overlain by relative permittivity 5.0 material should produce a reflection at 50.7 ns two-way travel time. However, dispersion in the soil (the freqency dependent properties seen in Figures 11-14) causes the transmitted pulse to be low pass filtered as it passes through the soil and to see an apparently increasing permittivity with depth as the center frequency of the pulse decreases. This causes a later arrival time. As this model is non-dispersive, a compensating factor was added to the offset parameter, Offs, to align the model and field pulse arrivals. Note the reversal in the sign of the pulse as the air filled voids become wet stabilization material slurry filled voids (compare Figures 56 and 57). The air filled voids also allow a reflection from the bottom of the gravel as well as the top (Figure 56) but the slurry filled voids are too attenuating (from high electrical conductivity) to see the bottom reflection. Note also that the electrical properties in the lowest layer decrease with time as the stabilization material cures. The coupling ratio for the transmitted pulse was adjusted to fit the pulse width in Figure 56 (the ground loading of the surface relative permittivity of 5 plus the dispersive scattering of the dry gravel layer). Note how the field data pulse from the wet gravel reflector is even more dispersive in Figure 57 (broader compared to the model with the same coupling ratio as Figure 56), and then declines slightly in Figures 58 and 59 as the stabilization material begins to cure.

Conclusions

Complex resistivity (also known as induced polarization) has no contrast and poor resolution, insufficient to locate the stabilization material. Electromagnetic induction conductivity mapping also has little contrast and poor resolution, insufficient to locate the stabilization material. Ground penetrating radar demonstrated high contrast and resolution sufficient to locate and track the stabilization material. As the stabilization material cures over more than a few tens of hours, the contrast reduces, making location with any electrical method (including ground penetrating radar) difficult.

Acknowledgements

This project was funded under Interagency Agreement No. DE-A107-85ID12609 between the U. S. Geological Survey and the U. S. Department of Energy. Edgar Ethington made the laboratory measurements in Figures 3-10. Dennis Capron made the laboratory measurements in Figures 11-14.

References

Ames, L. L. and Phillips, S. J., 1979, Characterization of the Hanford 300 area burial grounds. Task II. Geochemical analysis: Battelle-Pacific Northwest Lab., Richland, Wash., PNL-2658, 68p.

Banno, K. and Yoshida, H., 1992, Immobilization of contaminated soil using jet grouting method: in Waste Management '92: working towards a cleaner environment, Proc. of a Symp., R. G. Post, ed., 1-5 March 1992, Tucson, AZ, CONF-920307, p. 575-578.

Battelle Pacific Northwest Labs., 1991, Resource book; Decommissioning of contaminated facilities at Hanford; Volume 1: Battelle Pacific Northwest Labs., Richland, WA, Report No. PNL-7008-VOL. 1, PNL-MA-588-VOL. 1, NTIS DE92001760/XAB, 349p.

Battelle Pacific Northwest Labs., 1991, Resource book; Decommissioning of contaminated facilities at Hanford; Volume 2: Battelle Pacific Northwest Labs., Richland, WA, Report No. PNL-7008-VOL. 2, BNWL-MA-88-APP. 1, PNL-MA-588-Vol. 2, NTIS DE92001759/XAB, 158p.

Battelle Pacific Northwest Labs., 1991, Resource book; Decommissioning of contaminated facilities at Hanford; Volume 3: Battelle Pacific Northwest Labs., Richland, WA, Report No. PNL-7008-VOL. 3, PNL-MA-588-VOL. 3, NTIS DE92001761/XAB, 280p.

Bergstrom, K. A., Mitchell, T. H. and Kunk, J. R., 1993, Interpretation of radar data at the Hanford Site, Richland, Washington: in Proc. 2nd Government Workshop on GPR, Advanced Ground Penetrating Radar: Technologies and Applications, 26-28 October 1993, Ohio State Univ., Columbus, Ohio, p. 157-174.

Bjornstad, B. N., 1990, Geohydrology of the 218-W-5 Burial Ground, 200-West Area, Hanford Site: Battelle Pacific Northwest Labs., Richland, WA, Report No. PNL-7336, NTIS DE90010853/XAB, 198p.

Bryce, R. W., and Gorst, W. R., 1990, Hanford Site environmental data for calendar year 1989-Ground Water: Battelle Pacific Northwest Labs., Richland, WA, Report No. PNL-7390, NTIS DE91007874/XAB, 573p.

Carson, R. J., Tolan, T. L., and Reidel, S. P., 1987, Geology of the Vantage area, south-central Washington; an introduction to the Miocene flood basalts, Yakima fold belt, and the Channeled Scabland: in Hill, M. L., Cordilleran section of the Geological Society of America, Whittier, CA, Geol. Soc. Am., Boulder, CO, p. 357-362.

Cline, J. F., Gano, K. A., and Rogers, L. E., 1980, Loose rock as biobarriers in shallow land burial: Health Physics, v. 39, p. 497-504.

Cole, K. S. and Cole, R. S., 1941, Dispersion and adsorption in dielectrics, I, alternating current characteristics: J. Chem. Phys., v. 9, p. 341-351.

Delaney, C. D., 1991, Hydrogeology of the Hanford Site in South-Central Washington State: Westinghouse Hanford Co., Richland, WA, Report No. WHC-SA-1155, CONF-9110190-1, NTIS DE91016629/XAB, 22p.

Drost, B. W., Schurr, K. M., and Lum, W. E., 1989, Selected ground-water information for the Pasco Basin and adjacent areas, Washington, 1986-89: Open File Report OF 89-0228, U. S. Geol. Surv., Tacoma, WA, 91 p.

Elder, R. E., McKinney, S. M., and Osborne, W. L., 1989, Westinghouse Hanford Company environmental surveillance annual report-200/600 Areas, calendar year 1988: Westinghouse Hanford Co., Richland, WA, Report No. WHC-EP-0145-1, NTIS DE90008201/XAB, 127p.

Evans, J. C., and Murphy, E., 1988, Characterization of Contaminants in the Subsurface of the Hanford Site: Battelle Pacific Northwest Labs., Richland, WA, Report No. PNL-SA-15958, CONF-8806159-3, NTIS DE89008126/XAB, 34p.

Francis, C. W. and Spalding, B. P., 1991, In situ grouting of low-level burial trenches with a cement-based grout: Environment remediation '91: cleaning up the environment for the 21st century, D. E. Wood, ed., Proc. of a conf., Pasco, WA, 8-11 September 1991, NTIS CONF-910981, p. 107-113.

Francis, C. W., 1991, Task plan to evaluate the effectiveness of in situ grouting of an ORNL waste burial trench with a cement-based grout: Oak Ridge, TN, Oak Ridge National Laboratory report ORNL/ER-24, 15p.

Fruland, R. M., Hagan, R. A., Cline, C. S., Bates, D. J., and Evans, J. C., 1989, Interim Site Characterization Report and Ground-Water Monitoring Program for the Hanford Site Solid Waste Landfill: Battelle Pacific Northwest Labs., Richland, WA., Report No. PNL-6823, NTIS No. DE89014963/HDM, 263p.

Gaylord, D. R., and Poeter, E. P., 1991, Geology and hydrology of the 300 Area and vicinity, Hanford Site, south-central Washington: Westinghouse Hanford Co., Richland, WA, Report No. WHC-EP-0500, NTIS DE92006495/XAB, 97p.

Gee, G. W., and Heller, P. R., 1985, Unsaturated Water Flow at the Hanford Site; A Review of Literature and Annotated Bibliography: Battelle Pacific Northwest Labs., Richland, WA, Report No. PNL-5428, NTIS DE85013172/XAB, 82p.

Gerber, M. S., 1991, Historical genesis of the Hanford Site wastes: in Proc. Environmental Remediation '91: cleaning up the environment for the 21st century, D. E. Wood, ed., Pasco, WA, Sept. 8-11, 1991, NTIS CONF-910981, p. 649-654.

Gerber, M. S., 1992, Legend and legacy: fifty years of defense production at the Hanford site: Westinghouse Hanford Co., Richland, WA, WHC-MR-0293 (rev. 1), 64p.

Gray, R. H., 1988, Environmental Monitoring at the US Department of Energy's Hanford Site, Washington: Battelle Pacific Northwest Labs., Richland, WA, Report No. PNL-SA-16150, CONF-881054-29, NTIS DE89001994/XAB, 12p.

Gray, R. H., 1989, Monitoring for Potential Environmental Problems at a Nuclear Research Facility at Hanford, Washington, USA: Battelle Pacific Northwest Labs., Richland, WA, Report No. PNL-SA-16538, CONF-890223-1, NTIS DE89008246/XAB, 15p.

Gray, R. H., 1990, Environmental monitoring and surveillance on the Hanford Site, Washington: Battelle Pacific Northwest Labs., Richland, WA, Report No. PNL-SA-17769, CONF-9005159-2, NTIS DE91011241/XAB, 34p.

Gray, R. H., 1990, Long-term environmental monitoring at Hanford, Washington: Battelle Pacific Northwest Labs., Richland, WA, Report No. PNL-SA-18459, CONF-901191-4, NTIS DE91005707/XAB, 30p.

Gray, R. H., 1990, Twenty-eighth Hanford symposium on Health and the environment; Environmental monitoring, restoration and assessment; what have we learned?: in Twenty-eighth Hanford Symposium on Health and the Environment, v. 28, unknown p.

Harris, D., Wooden, C. E. and Motl, G. P., 1992, Application of jet grouting as an in-situ technology for the White Oak Creek Embayment time critical removal

action: in Waste management and environmental restoration, Proc. of the 8th Ann. DOE Model Conf., 18-22 Oct 1992, Oak Ridge, TN, CONF-921029, 7p.

Heller, P. R., Gee, G. W., and Myers, D. A., 1985, Moisture and Textural Variations in Unsaturated Soils/Sediments Near the Hanford Wye Barricade: Battelle Pacific Northwest Labs., Richland, WA, Report No. PNL-5377, NTIS DE85009499/XAB, 84p.

Henckel, G. C., and Johnson, W. L., 1991, Accelerated cleanup of the 316-5 Process Trenches at the Hanford Site: Westinghouse Hanford Co., Richland, WA, Report No. WHC-SA-1202, CONF-910981-56, NTIS DE92008380/XAB, 11p.

Hunter, C. R., and Busacca, A. J., 1990, Feasibility study of modeling pedogenic carbonates in soils and sediments at the US Department of Energy's Hanford Site: Battelle Pacific Northwest Labs., Richland, WA, Report No. PNL-7413, NTIS DE91000063/XAB, 55p.

Jacquish, R. E., and Bryce, R. W., 1989, Hanford Site environmental report for calendar year 1988: Battelle Pacific Northwest Labs., Richland, WA, Report No. PNL-6825, NTIS DE90005687/XAB, 293p.

Jacquish, R. E., and Mitchell, P. J., 1988, Environmental Monitoring at Hanford for 1987: Battelle Pacific Northwest Labs., Richland, WA, Report No. PNL-6464, NTIS DE88011766/XAB, 272p.

James, L. A., 1987, Environmentally assisted cracking behavior of a candidate nuclear waste repository container material in simulated Hanford groundwater: Nuclear and Chemical Waste Management, v. 7, p. 227-237.

James, L. A., 1988, Cracking of a nuclear waste container material by irradiation in a simulated groundwater: Nuclear and Chemical Waste Management, v. 8, p. 75-82.

Jones, T. L., and Skaggs, R. L., 1989, Influence of hydrologic factors on leaching of solidified low-level waste forms at an arid-site filed-scale lysimeter facility: in Cote, P., Gilliam, M., Environmental aspects of stabilization and solidification of hazardous and radioactive wastes, ASTM Special Technical Publication STP 1033, Environ. Can., Burlington, ON, Canada, p. 358-380.

Khaleel, R., and LeGore, T., 1990, Effects of varying recharge of radionuclide flux rates to the water table at a low-level solid waste burial site: Westinghouse Hanford Co., Richland, WA, Report No. WHC-SA-0699, CONF-900210-14, NTIS DE90007211/XAB, 16p.

Kutrubes, D. L., 1986, Dielectric permittivity measurements of soils saturated with hazardous fluids: MSc Thesis, Dept. of Geophysics, Colo. School of Mines, Golden, CO, 300p.

LaSala, A. M., Jr., and Doty, G. C., 1975, Geology and hydrology of radioactive solid waste burial grounds at the Hanford Reservation, Wash: Open File Report OF 75-0625, U. S. Geological Survey, Reston, VA, 70 p.

Lasmanis, R., 1989, Hanford defense waste program and its geologic setting: Washington Geologic Newsletter, v. 17, p. 3-8.

Last, G. V., Bjornstad, B. N., Bergeron, M. P., Wallace, D. W., and Newcomer, D. R., 1989, Hydrogeology of the 200 Areas Low-Level Burial Grounds; An Interim Report; Volume 1; Text: Battelle Pacific Northwest Labs., Richland, WA, Report No. PNL-6820-VOL. 1, NTIS DE89014008/XAB, 261p.

Last, G. V., Bjornstad, B. N., Bergeron, M. P., Wallace, D. W., and Newcomer, D. R., 1989, Hydrogeology of the 200 Areas Low-Level Burial Grounds; An Interim Report; Volume 2; Appendixes: Battelle Pacific Northwest Labs., Richland, WA, Report No. PNL-6820-VOL. 2, NTIS DE89014005/XAB, 770p.

Lindsey, K. A., Gaylord, D. R., and Poeter, E. P., 1989, Sedimentary and stratigraphic examination of the Ringold Formation, Hanford Nuclear Reservation, Washington; applied lithofacies analysis: in The Geological Society of America, Cordilleran Section, 85th annual meeting and Rocky Mountain Section, 42nd

annual meeting. Abstracts with Programs Geological Society of America, v. 21, p. 107.

Loomis, G. G. and Low, J. O., 1988, In situ grouting for improved confinment of buried TRU waste at the Idaho National Engineering Laboratory: in Nuclear and hazardous waste management, Proc. of an Int'l. Topical Meeting, 11-15 Sept 1988, Pasco, WA, American Nuclear Society, La Grange Park, IL, CONF-880903, p. 496-498.

Marshall, E., 1987, Hanford's radioactive tumbleweed: Science, v. 236, p. 1616-1620.

McLaughlin, T. J., Airhart, S. P., Beattie, K. L., Rouse, J. K. and Phillips, S. J., 1992, Subsurface barrier technologies as potential interim actions for Department of Energy underground storage tanks: in Spectrum '92: Nuclear and hazardous waste management, Proc. of an Int'l. Topical Meeting, 23-27 April 1992, Boise, ID, American Nuclear Society, La Grange Park, IL, p. 1200-1205.

Merz, M. D., Gerber, F., and Wang, R., 1987, MCC corrosion tests at reference testing conditions for A27 cast steel in Hanford ground water: in Bates, J. K., Seefeldt, W. B., Scientific basis for nuclear waste management X, Argonne Natl. Lab., Argonne, IL, Materials Research Society Symposia Proceedings, v. 84, p. 215-226.

Mitchell, P. J., and Freshley, M. D., 1987, Ground-Water Monitoring and Modeling at the Hanford Site: Battelle Pacific Northwest Labs., Richland, WA, Report No. PNL-SA-14263, CONF-870306-34, NTIS DE87006434/XAB, 6p.

Morgan, I. L. and Bostick, W. D., 1990, Performance testing of grout-based wasteforms for anion exchange resins: in Spectrum '90: Nuclear and hazardous waste management, Proc. of an Int'l. Topical Meeting, 30 Sept - 4 Oct 1990, Knoxville, TN, American Nuclear Society, La Grange Park, IL, p. 288-290.

Myers, C. W. and Price, S. M., 1979, Geologic Studies of the Columbia Plateau -- A Status Report, October 1979: Basalt waste Isolation Project/Geosciences Group, Rockwell Hanford Operations, RHO-BWI-ST-4, various pagination.

Naugle, G. D., 1989, Characterization of hydrofacies in the 300 area, Hanford Nuclear Reservation, Washington: Master's Thesis, Colorado School of Mines, 152 p.

Newcomb, R. C., Strand, J. R. and Frank, F. J., 1972, Geology and Ground-Water Characteristics of the Hanford Reservation of the U. S. Atomic Energy Commission, Washington: U. S. Geological Survey Professional Paper 717, 78 p.

Newcomer, D. R., and McDonald, J. P., 1990, Water-table elevations on the Hanford Site, December 1989: Battelle Pacific Northwest Labs., Richland, WA, Report No. PNL-7374, NTIS DE90013374/XAB, 37p.

Olhoeft, G. R. and Capron, D. E., 1993, Laboratory Measurements of the Radiofrequency Electrical and Magnetic Properties of Soils from near Yuma, Arizona: U. S. Geological Survey Open File Report 93-701, 214p.

Olhoeft, G. R., 1972, Time dependent magnetization and magnetic loss tangents: MSc Thesis, Dept. of Electrical Engineering, Massachusetts Institute of Technology, Cambridge, MA, 94p.

Olhoeft, G. R., 1985, Low-frequency electrical properties: Geophysics, v. 50, p. 2492-2503.

Olhoeft, G. R., 1987, Electrical properties from 10^{-3} to 10^{+9} Hz -- physics and chemistry: in Proc. of the 2nd Int'l. Symp. on the Physics and Chemistry of Porous Media, Schlumberger-Doll, Ridgefield, CT, October, 1986, Am. Inst. Phys., Conf. Proc. 154, J. R. Banavar, J. Koplik and K. W. Winkler, eds., NY, AIP, p. 281-298.

Olhoeft, G. R., Lucius, J. E., and Phillips, S. J., 1989, Ground penetrating radar monitoring of grout injection for trench stabilization: in Eleventh Annual Dept. of Energy Low-level Waste Management Conf., 22-24 August 1989, Pittsburgh, CONF-890854-Absts, p. RA-8.

Phillips, S. J. and Raymond, J. R., 1975, Monitoring and characterization of radionuclide transport in the hydrologic system: Battelle-Pacific Northwest Lab., Richland, Wash., BNWL-SA-5494(Pt. 1), 23p.

Phillips, S. J. and Stewart, W. E., 1993, Interim subsurface barriers for U. S. Department of Energy underground storage tanks: in Waste treatment, retrieval and processing, Proc. of the U. S. Department of Energy Information Exchange Meeting, 15-17 March 1993, Houston, TX, p. 494-500.

Phillips, S. J., 1978, Characterization of 300 area burial ground, PNL-2500 Part 5, Pacific Northwest Lab. Ann. report for 1977 to the DOE Assistant Secretary for Environment, Part 5--Control, Technology, Overview, Health, Safety and Policy Analysis: p. 1. 23-1. 26.

Phillips, S. J., Alexander, R. G., England, J. L., Stewart, W. E., and Kemp, C. J., 1993, Monolithic confinement of RWMC contaminated geologic media: in Waste treatment, retrieval and processing, Proc. of the U. S. Department of Energy Information Exchange Meeting, 15-17 March 1993, Houston, TX, p. 501-505.

Phillips, S. J., Ames, L. L. and Fitsner, R. E., 1980, Characterization of the Hanford 300 area burial grounds. Final report--Decontamination and decommissioning: Battelle-Pacific Northwest Lab., Richland, Wash., PNL-2557, 255p.

Phillips, S. J., Reisenauer, A. E., Rickard, W. H. and Sandness, G. A., 1977, Initial site characterization and evaluation of radionuclide contaminated solid waste burial grounds: Battelle-Pacific Northwest Lab., BNWL-2184, UC-70, 59p.

Piciulo, P. L., Shea, C. E. and Barletta, R. E., 1985, Analyses of soils from the low-level radioactive waste disposal sites at Barnwell, SC, and Richland, WA: U. S. Nuclear Regulatory Comm., NUREG/CR-4083, 54p.

Poeter, E. P., and Gaylord, D. R., 1990, Influence of aquifer heterogeneity on contaminant transport at the Hanford site: Ground Water, v. 28, p. 900-909.

Powers, M. H., Duke, S. K., Huffman III, A. C., and Olhoeft, G. R., 1992, GPRMODEL: one-dimensional full waveform forward modelling of ground penetrating radar data: U. S. Geological Survey Open File Report 92-532, 22p.

Price, K. R., Mitchell, P. J., and Freshley, M. D., 1987, Environmental monitoring at Hanford for 1986: , Report PNL-06120, Battelle Mem. Inst., Richland, VA, variously paginated p.

Rouston, R. C., and Johnson, V. G., 1990, Recharge estimates for the Hanford Site 200 Acres Plateau: Northwest Science, v. 64, p. 150-158.

Sandness, G. A., 1991, Report on geological surveys in the 300-FF-1 operable unit: Battelle Pacific Northwest Labs., Richland, WA. Environmental Management Operations., Report No. EMO-1032, NTIS No. DE91011327/HDM, 126p.

Schalla, R., Aaberg, R. L., Bates, D. J., Carlile, J. V. M., and Freshley, M. D., 1988, Revised Ground-Water Monitoring Compliance Plan for the 300 Area Process Trenches: Battelle Pacific Northwest Labs., Richland, WA, Report No. PNL-6671, NTIS DE89001462/XAB, 431p.

Schmidt, J. W., Huckfeldt, C. R., Johnson, A. R., and McKinney, S. M., 1990, Westinghouse Hanford Company environmental surveillance annual report-200/600 Areas; Calendar year 1989: Westinghouse Hanford Co., Richland, WA, Report No. WHC-EP-0145-2, NTIS DE90012640/XAB, 153p.

Schmidt, J. W., Huckfeldt, C. R., Johnson, A. R., and McKinney, S. M., 1991, Westinghouse Hanford Company Environmental surveillance annual report-200/600 Areas; Calendar year 1990: Westinghouse Hanford Co., Richland, WA, Report No. WHC-EP-0145-3, NTIS DE91018137/XAB, 126p.

Schmidt, J. W., Webb, C. R., Johnson, A. R., and McKinney, S. M., 1992, Westinghouse Hanford Company Environmental Surveillance annual report; 200/600 Areas; Calendar year 1990; Revision 4: Westinghouse Hanford Co., Richland, WA, Report No. WHC-EP-0145-4-REV. 4, NTIS DE92014220/XAB, 197p.

Shulman, S., 1989, Nuclear waste disposal; daunting costs for clean-up at Hanford: Nature (London), v. 339, p. 241.

Spalding, B. P., 1991, Task plan for TARA-II compaction and grouting demonstration - environmental restoration program: Oak Ridge National Laboratory, Oak Ridge, TN, report ORNL/ER-25, 17p.

Swanson, D. A., 1982, Geologic mapping of the Columbia Plateau: Schneider, R., Roseboom, E. H., JR., Robertson, J. B., Stevens, P. R., U. S. Geological Survey research in radioactive waste disposal; fiscal year 1979. Circular. p. 19 20, Report C 0847, U. S. Geological Survey, Reston, VA, p. 19-20.

Swanson, D. A., 1982, Geologic mapping of the Columbia Plateau: Schneider, R., Trask, N. J., U. S. Geological Survey research in radioactive waste disposal; fiscal year 1980. Open File Report OF 82-0509, U. S. Geological Survey, Reston, VA, p. 28-31.

Swanson, L. C., Weekes, D. C., Luttrell, S. P., Mitchell, R. M., and Landeen, D. S., 1988, Grout Treatment Facility Environmental Baseline and Site Characterization Report: Westinghouse Hanford Co., Richland, WA, Report No. WHC-EP-0150, NTIS DE89002503/XAB, 249p.

U. S. DOE, 1987, Environmental Survey preliminary report, Hanford Site, Richland, Washington: Department of Energy, Washington, DC, Office of Environmental Audit, Report No. DOE/EH/OEV-05P, NTIS DE91001067/XAB, 490p.

U. S. DOE, 1989, Draft Remedial Investigation/Feasibility Study Work Plan for the 300-FF-5 Operable Unit, Hanford Site, Richland, Washington: Department of Energy, Richland, WA, Richland Operations Office, Report No. DOE/RL-89-14-DR-A, NTIS DE90001139/XAB, 366p.

U. S. DOE, 1990, Remedial investigation/feasibility study work plan for the 200-BP-1 operable unit, Hanford Site, Richland, Washington; Revision 1: Department of Energy, Richland, WA, Richland Operations Office, Report No. DOE/RL-88-32-REV. 1, NTIS DE90009857/XAB, 666p.

U. S. DOE, 1990, Tiger Team Assessment of the Hanford Site; Volume 1: Department of Energy, Washington, DC. Assistant Secretary for Environment, Safety and Health., Report No. DOE/EH-0139-VOL. 1, NTIS No. DE91004627/HDM, 633p.

U. S. DOE, 1990, Tiger Team Assessment of the Hanford Site; Volume 2, Appendices: Department of Energy, Washington, DC. Assistant Secretary for Environment, Safety and Health., Report No. DOE/EH-0139-VOL. 2, NTIS No. DE91004626/HDM, 480p.

U. S. DOE, 1991, Annual report for RCRA groundwater monitoring projects at Hanford Site facilities for 1990: Department of Energy, Richland, WA, Richland Operations Office, Report No. DOE/RL-91-03, NTIS DE91010033/XAB, 402p.

U. S. DOE, 1991, Engineering evaluation of the 618-9 Burial Ground expedited response action; Draft A: Department of Energy, Richland, WA, Richland Operations Office, Report No. DOE/RL-91-38-DRAFTA, NTIS DE92000232/XAB, 132p.

U. S. DOE, 1991, Environmental restoration and waste management site-specific plan for Richland Operations Office: DOE/RL-91-25, 380p.

U. S. DOE, 1991, Hanford Central Waste Complex; Radioactive mixed waste storage facility dangerous waste permit application; Volume 1: Department of Energy, Richland, WA, Richland Operations Office, Report No. DOE/RL-91-17-VOL. 1, NTIS DE92003982/XAB, 619p.

U. S. DOE, 1991, Hanford Federal Facility Agreement and Consent Order quarterly progress report for the period ending September 30, 1991: Department of Energy, Richland, WA, Richland Operations Office, Report No. DOE/RL-91-41, NTIS DE92004568/XAB, 97p.

U. S. DOE, 1991, Remedial investigation phase 2 supplemmental work plan for the Hanford site 1100-EM-1 operable unit: DOE/RL-90-37 (rev. 1), 127p.

U. S. DOE, 1992, RCRA groundwater monitoring data; Quarterly report, January 1, 1992--March 31, 1992: Department of Energy, Richland, WA, Richland Operations Office, Report No. DOE/RL-92-26-1, NTIS DE92018209/XAB, 672p.

U. S. DOE, 1992, Remedial investigation/feasibility study work plan for the 100-BC-5 operable unit, Hanford Site, Richland, Washington: Department of Energy, Richland, WA, Richland Operations Office, Report No. DOE/RL-90-08, NTIS DE92018160/XAB, 368p.

U. S. G. S., 1987, Subsurface transport of radionuclides in shallow deposits of the Hanford Nuclear Reservation, Washington; review of selected previous work and suggestions for further study: U. S. Geological Survey, Open File Report OF-87-0222, 61p.

Voogd, J. A., 1992, The Hanford grout treatment facility: in Radioactive, hazardous, and/or mixed waste sludge management, Proc. of a Workshop, T. F. Lomenick, ed., 4-5 Dec 1990, Knoxville, TN, CONF-901264, p. 19-34.

Wakeley, L. D. and Ernzen, J. J., 1992, Grout for closure of the demonstration vault at the U. S. DOE Hanford facility: U. S. Army Waterways Experiment Station, Vicksburg, MS, report WES/TR/SL-92-21, 164p.

Wakeley, L. D., Ernzen, J. J., McDaniel, E. W. and Voogd, J., 1992, Grout for closure of waste-disposal vaults at the US DOE Hanford Site: The use of fly ash, silica fume, slag and natural pozzolans in concrete, Proc. of the 4th Int'l. Conf., Istanbul, Turkey, 3-8 May 1992, NTIS CONF-920559, 21p.

Weskes, D. C., Luttrell, S. P., and Fuchs, M. R., 1987, Interim hydrogeologic characterization report and groundwater monitoring system for the nonradioactive dangerous waste landfill, Hanford Site, Washington: Report WHC-EP-0021, Westinghouse Hanford Co., Richland, WA, 170 p.

Westinghouse Hanford Co., 1989, Hanford Site Groundwater Protection Management Program: Westinghouse Hanford Co., Richland, WA, Report No. DOE/RL-89-12, NTIS DE90003494/XAB, 102p.

Westinghouse Hanford Co., 1989, Preliminary Operable Units Designation Project: Westinghouse Hanford Co., Richland, WA, Report No. WHC-EP-0216, NTIS DE89013925/XAB, 229p.

Westinghouse Hanford Co., 1992, Remedial investigation/feasibility study work plan for the 100-BC-5 Operable Unit, Hanford Site, Richland, Washington: Westinghouse Hanford Co., Richland, WA, Report No. DOE/RL-90-08-DRAFTC, NTIS DE92012251/XAB, 397p.

Table 1. Lithologies and alterations of the Ringold Formation and glaciofluvatile and fluvatile deposits near Hanford Site (from Myers, and Price 1979).

Characteristic	Ringold Formation	Glaciofluviatile and fluviatile deposits
Lithology:		
Rock types	Upper Columbia River materials predominate, almost exclusively below medium-sand sizes.	Nearby basaltic materials predominate in gravel sizes and are relatively high in sand sizes.
Grain sizes	Silt and fine sand predominate; many thick and continuous silt and clay strata present.	Except for Touchet Beds, gravel and coarse to medium sand predominate; little clay present - only discontinuous silt beds and lenses.
Induration	Silt and clay compact; gravel and sand compact and contain strongly cemented beds; only newly exposed silt and sand vulnerable to wind erosion.	Material mostly loose; finer-grained material blows badly in desert situations.
Sorting	Well sorted but uniform sand fills interstices of gravel; gravel and sand are clean washed.	Mostly poorly sorted except in parts of the Touchet Beds. Gravel particles mostly silt dusted.
Grain shapes	Gravel well rounded; silt and finer sand is angular.	Gravel well rounded; boulder blocks, silt, and sand are angular.
Alterations:		
Rinds	Alteration of rinds 1/32 to 1/8 in. thick on basalt pebbles.	No appreciable alterations.
Cementation	Caliche impregnations; concretions in some clays; some sand beds contain well cemented layers.	No known concretions; no appreciable cementation; only slight caliche accumulations.
Secondary	Secondary gypsum; fossil bone is petrified.	No known secondary gypsum; no known petrified bone.

Table 2 - Time sequence of events.

Time	Event	Figure
16:04	Begin injecting Water	
16:07	Begin injecting stabilization material slurry	
16:16	Ground penetrating radar line 5/6	21
16:30	Ground penetrating radar line 5/6	22
16:45	Ground penetrating radar line 5/6	23
17:00	First truck empty Ground penetrating radar line 5/6	24
17:38	Begin injecting second truck load	
17:45	Ground penetrating radar line 5/6	25
18:00	Ground penetrating radar line 5/6	26
18:15	Ground penetrating radar line 5/6	27
18:30	End injection Ground penetrating radar line 5/6	28
18:45	Ground penetrating radar line 5/6 (0.25 hour after injection ends)	29
	Ground penetrating radar line 5/6 (16.5 hours after injection ends)	30
	Ground penetrating radar line 5/6 (62 hours after injection ends)	31

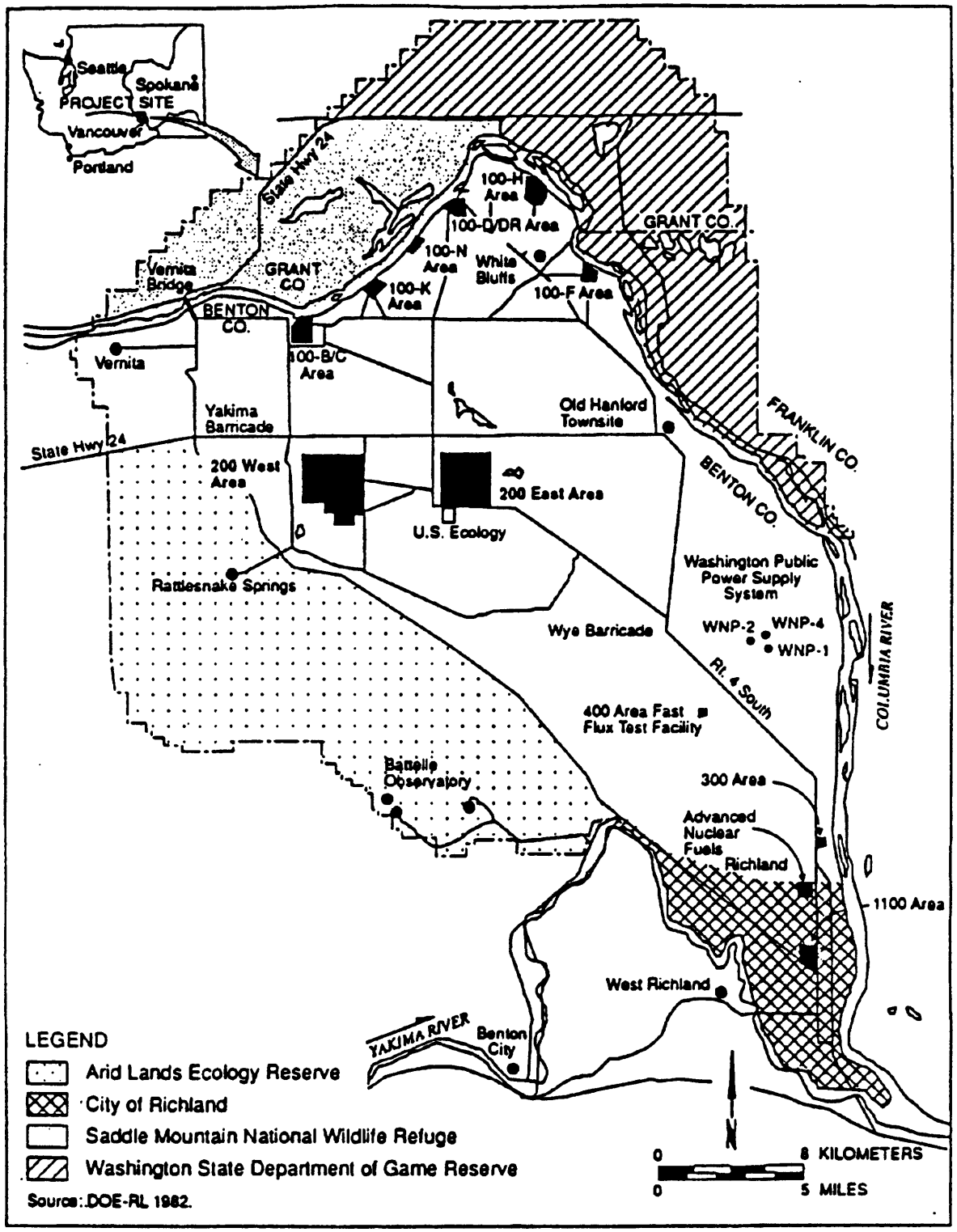

Figure 1. Location of the Hanford Site (from Bergstrom and others, 1993).

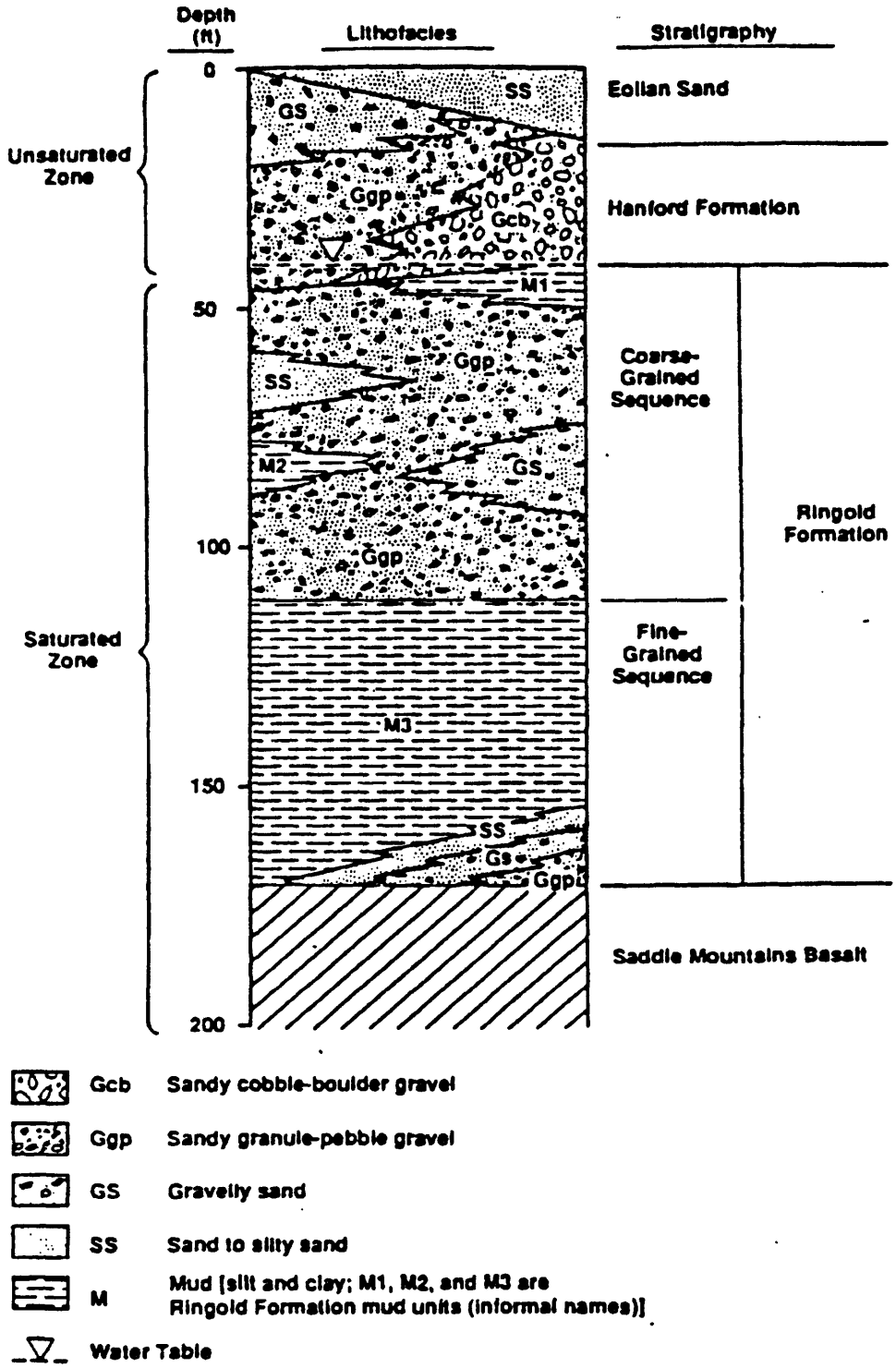

Figure 2. Stratigraphic section of the Hanford Site (from Bergstrom and others, 1993).

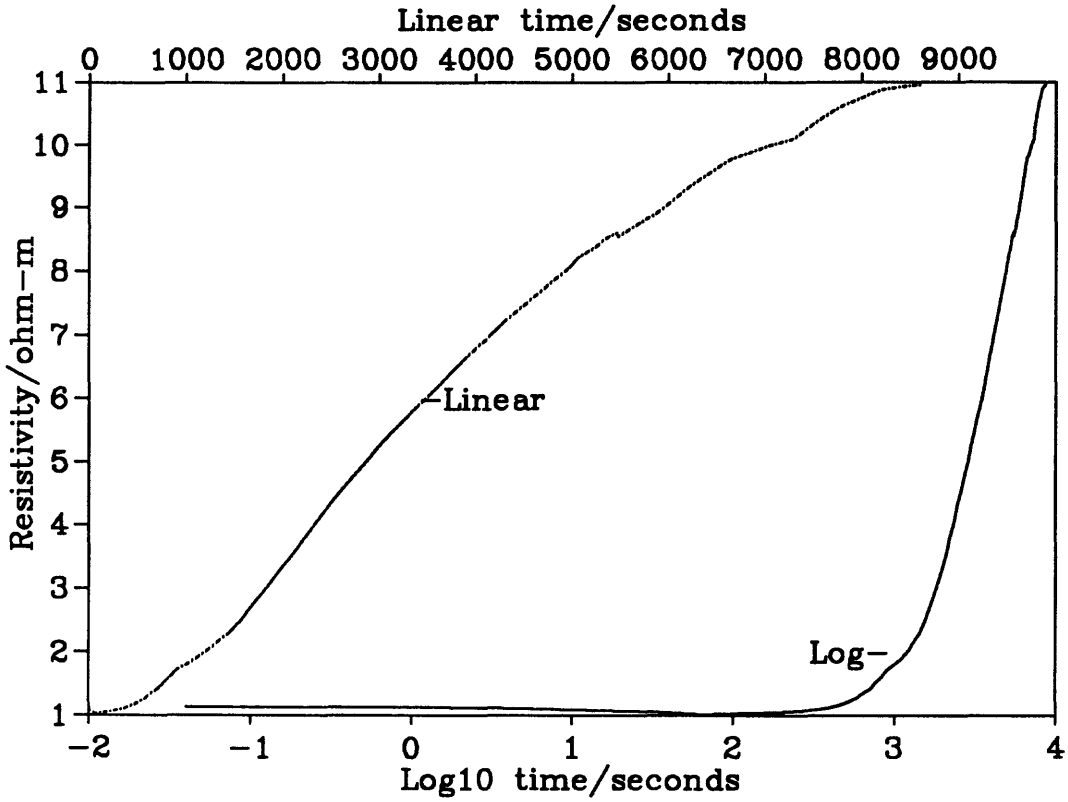

Figure 3 -

Variation in 1 Hz electrical resistivity of a mixture of 28 weight percent water in stabilization material as it cures. Solid line is versus log time; dashed line is versus linear time.

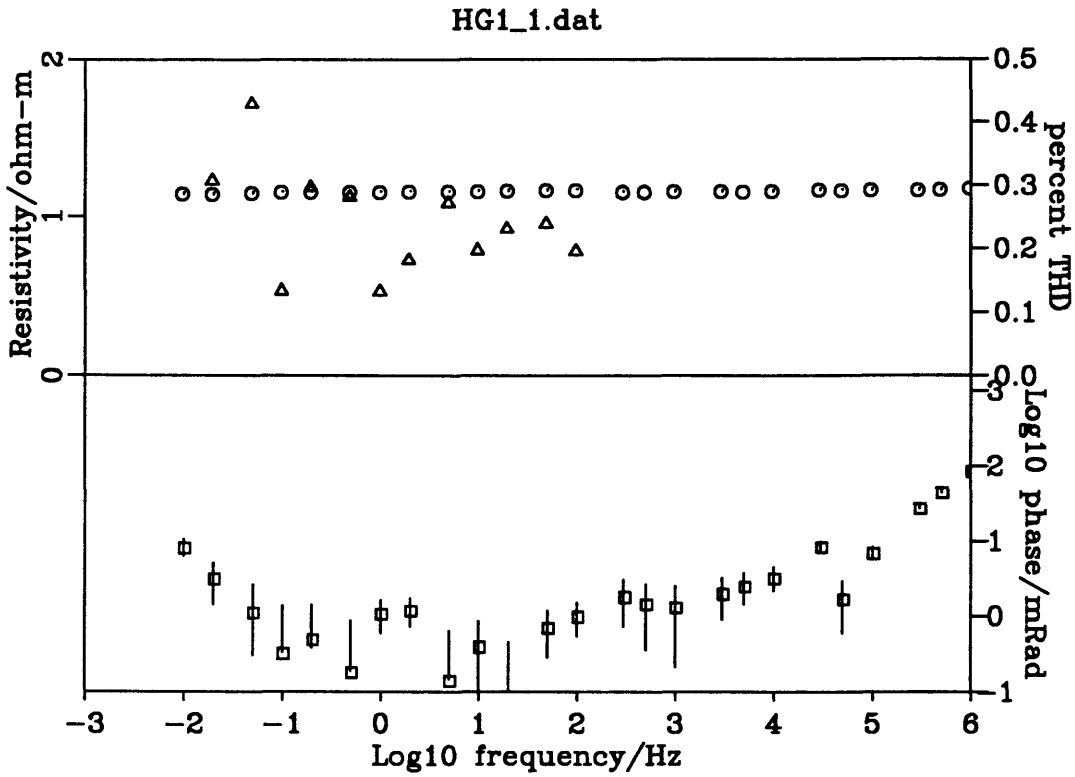

Figure 4 -

Complex resistivity versus frequency of stabilization material mixed with 28 weight percent water just after mixing. Circles are the resistivity. Triangles are the total harmonic distortion (one measure of nonlinearity, see Olhoeft, 1985). Squares are the phase between the applied current and resultant voltage response (a measure of polarization and usually indicative of chemical reactivity below 10^3 Hz). Error bars are shown where larger than the plotting symbol.

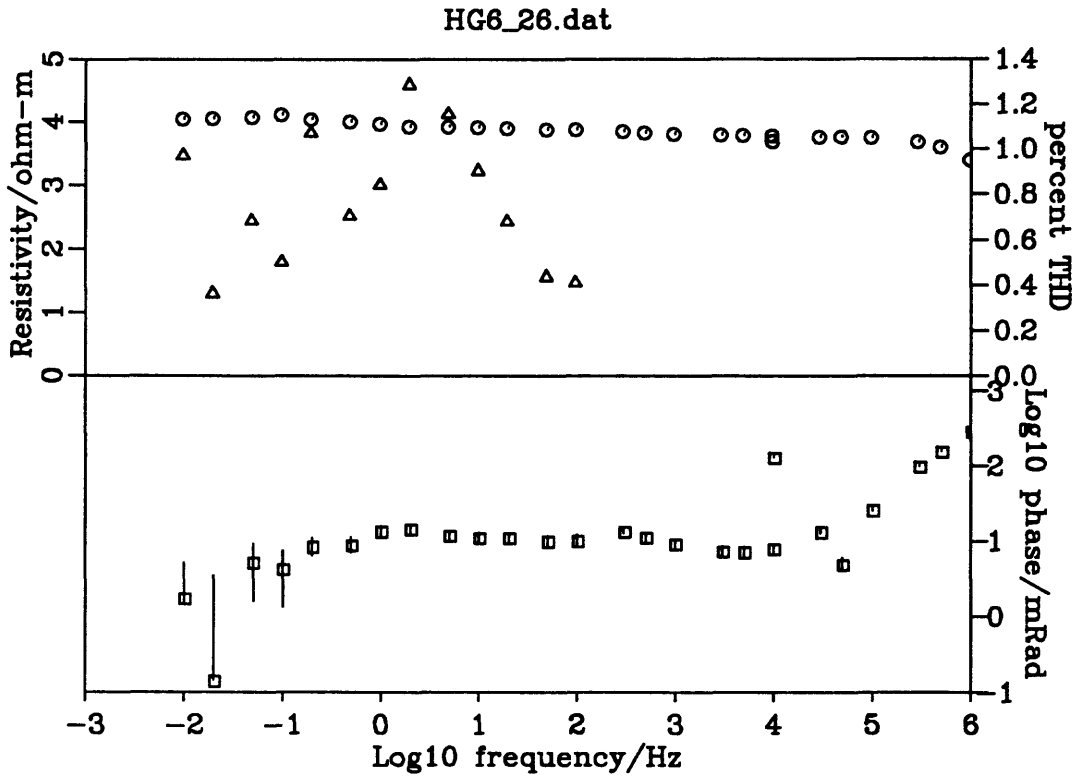

Figure 5 -

Complex resistivity versus frequency of stabilization material mixed with 22 weight percent water 3 days after mixing. Circles are the resistivity. Triangles are the total harmonic distortion (one measure of nonlinearity, see Olhoeft, 1985). Squares are the phase between the applied current and resultant voltage response (a measure of polarization and usually indicative of chemical reactivity below 10^3 Hz). Error bars are shown where larger than the plotting symbol.

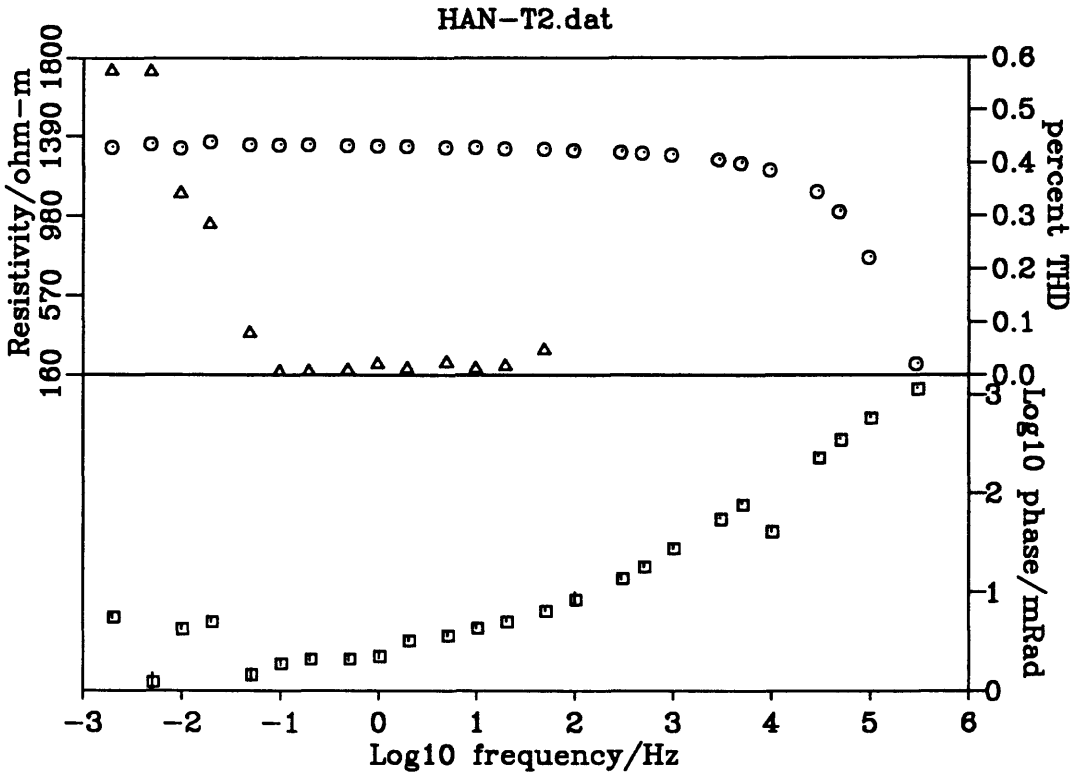

Figure 6 -

Complex resistivity versus frequency of cured stabilization material saturated with tap water. The sample had 36.5 volume percent water accessible porosity and 39.3 percent helium accessible porosity. Dry bulk density was 1.426 g/cm^3 and grain specific gravity from helium pycnometry was 2.352 g/cm^3. Circles are the resistivity. Triangles are the total harmonic distortion (one measure of nonlinearity, see Olhoeft, 1985). Squares are the phase between the applied current and resultant voltage response (a measure of polarization and usually indicative of chemical reactivity below 10^3 Hz). Error bars are shown where larger than the plotting symbol.

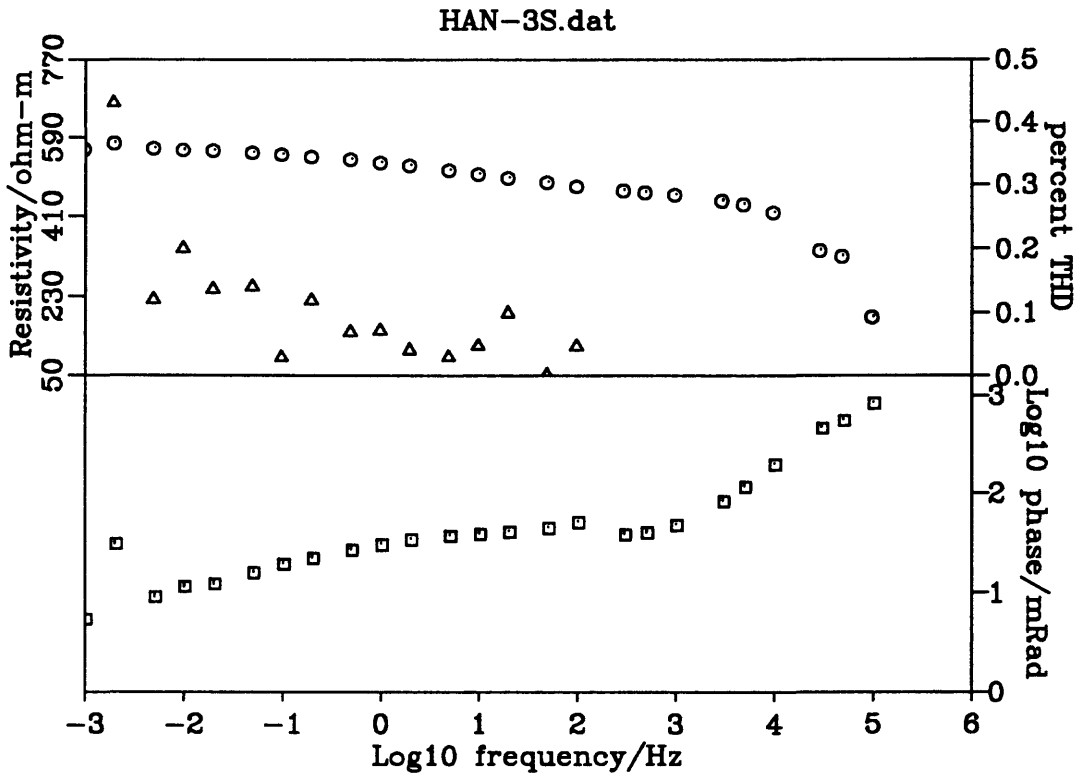

Figure 7 -

Complex resistivity versus frequency of Hanford soil with 3 weight percent distilled water. The soil had a grain specific gravity by helium pycnometry of 2.890 g/cm^3 and a specific surface area by Brunauer-Emmet-Teller nitrogren adsorption isotherm of 6.12 m^2/g. Circles are the resistivity. Triangles are the total harmonic distortion (one measure of nonlinearity, see Olhoeft, 1985). Squares are the phase between the applied current and resultant voltage response (a measure of polarization and usually indicative of chemical reactivity below 10^3 Hz). Error bars are shown where larger than the plotting symbol.

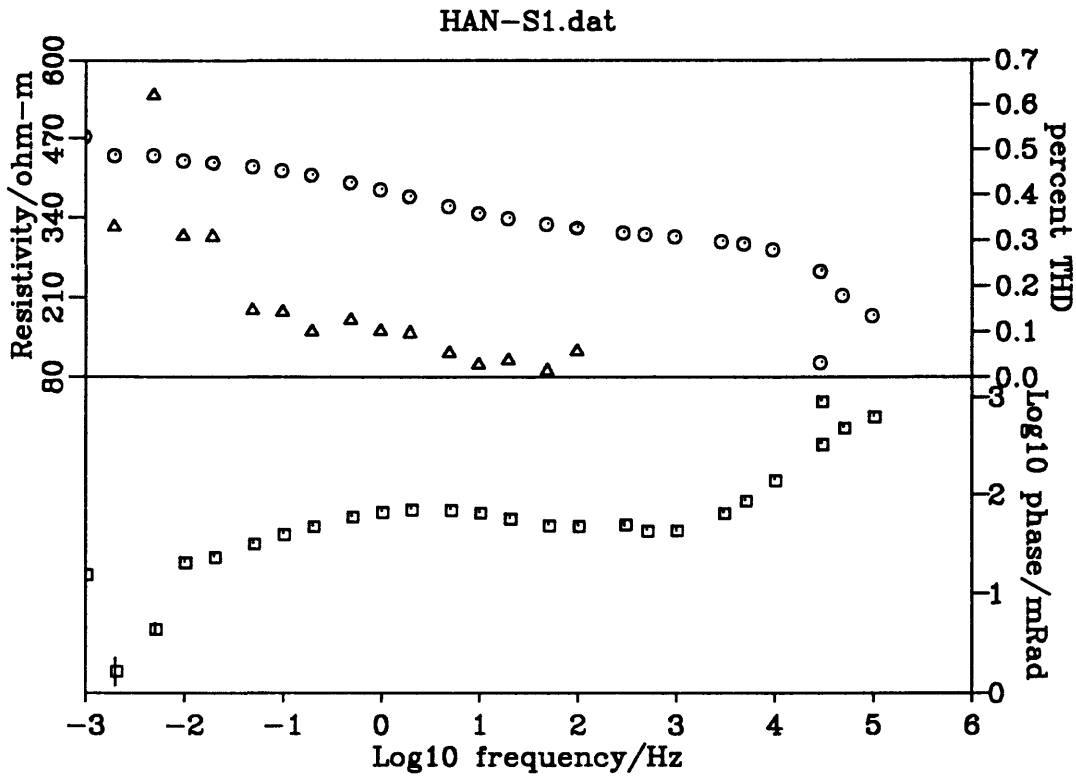

Figure 8 -

Complex resistivity versus frequency of Hanford soil with 5 weight percent distilled water as in Figure 7. Circles are the resistivity. Triangles are the total harmonic distortion (one measure of nonlinearity, see Olhoeft, 1985). Squares are the phase between the applied current and resultant voltage response (a measure of polarization and usually indicative of chemical reactivity below 10^3 Hz). Error bars are shown where larger than the plotting symbol.

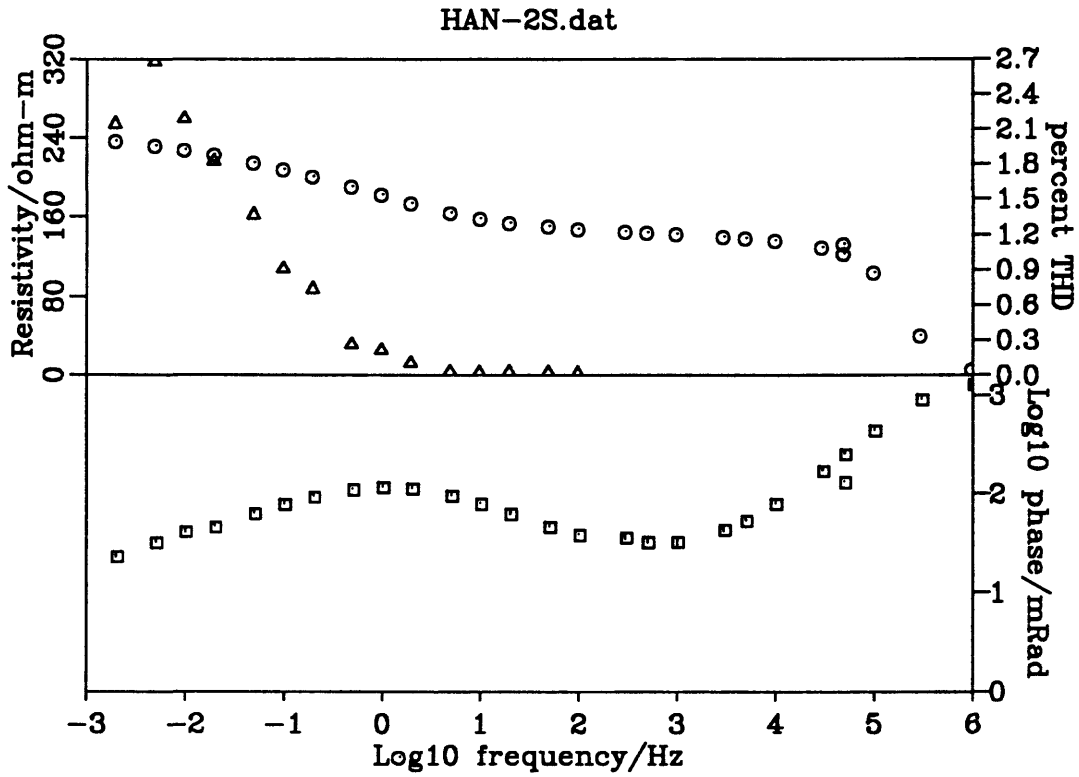

Figure 9 -

Complex resistivity versus frequency of Hanford soil with 10 weight percent distilled water as in Figure 7. Circles are the resistivity. Triangles are the total harmonic distortion (one measure of nonlinearity, see Olhoeft, 1985). Squares are the phase between the applied current and resultant voltage response (a measure of polarization and usually indicative of chemical reactivity below 10^3 Hz). Error bars are shown where larger than the plotting symbol.

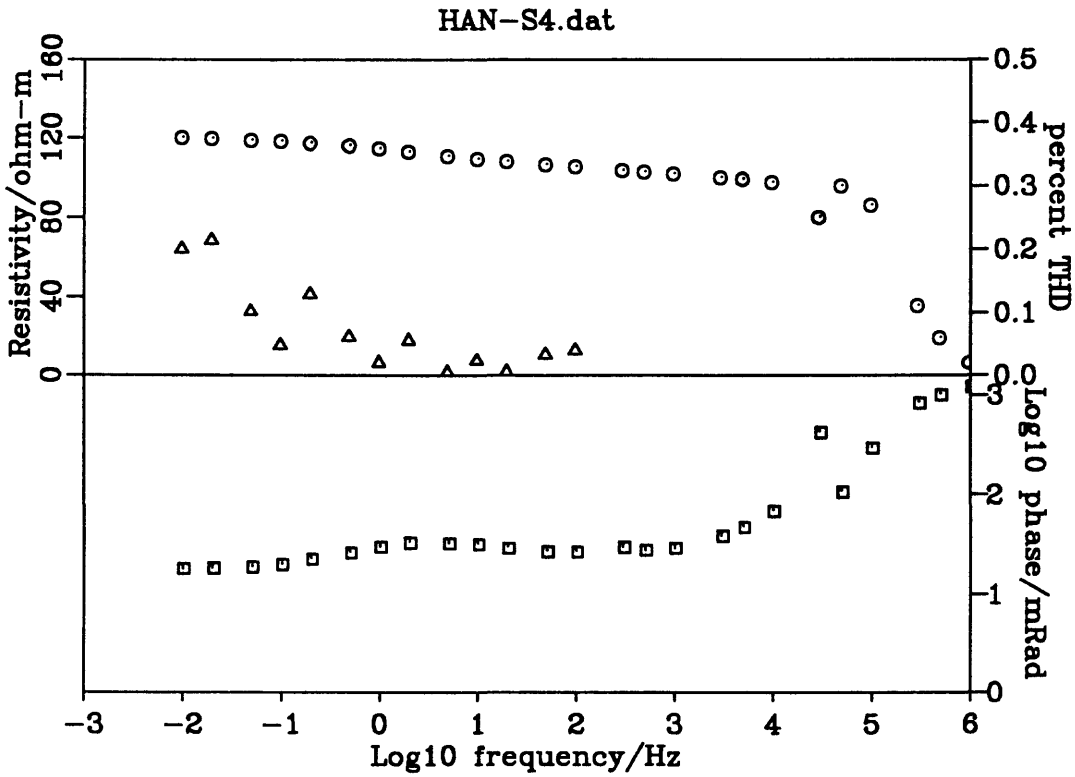

Figure 10 -

Complex resistivity versus frequency of Hanford soil with 12 weight percent distilled water as in Figure 7. Circles are the resistivity. Triangles are the total harmonic distortion (one measure of nonlinearity, see Olhoeft, 1985). Squares are the phase between the applied current and resultant voltage response (a measure of polarization and usually indicative of chemical reactivity below 10^3 Hz). Error bars are shown where larger than the plotting symbol.

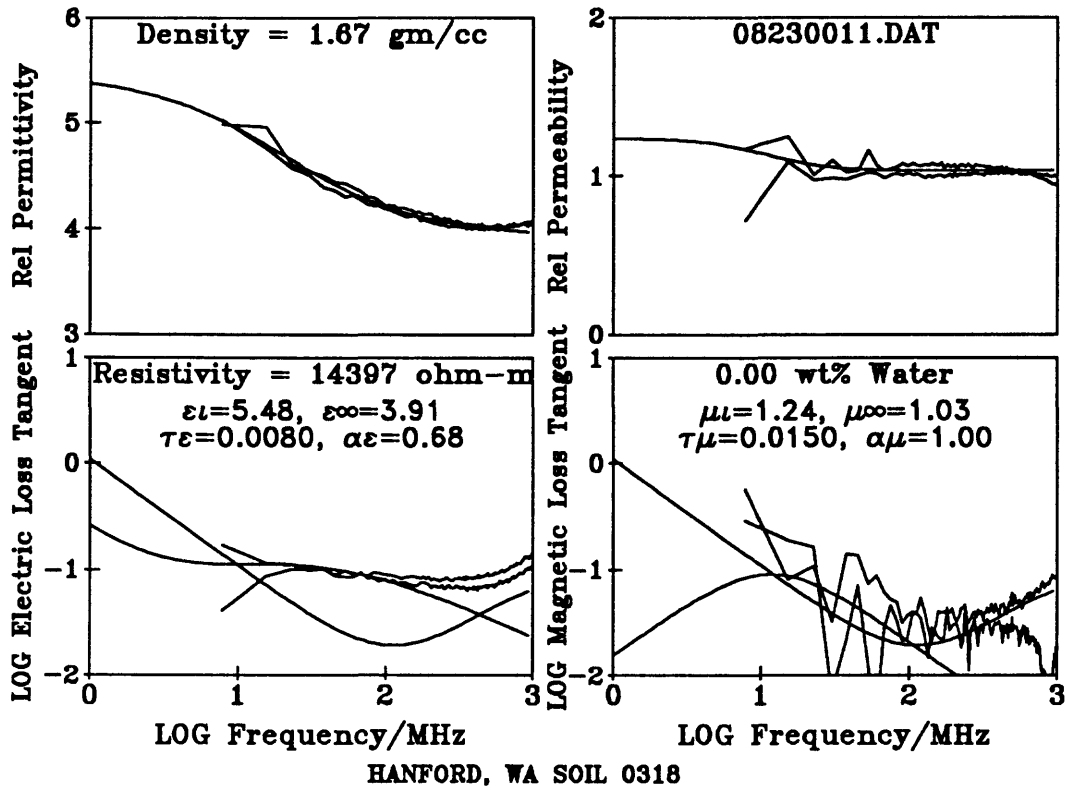

Figure 11 -

Complex relative permittivity and permeability versus frequency of dry Hanford soil as in Figure 7. The jagged lines are the forward and reverse measurements (measuring a coaxial sample holder independently from each end). The smooth solid lines are the model fits with the parameters shown (see text). The solid line in the loss tangent plots with a minimum near 10^2 MHz is the residual loss of the measurement system.

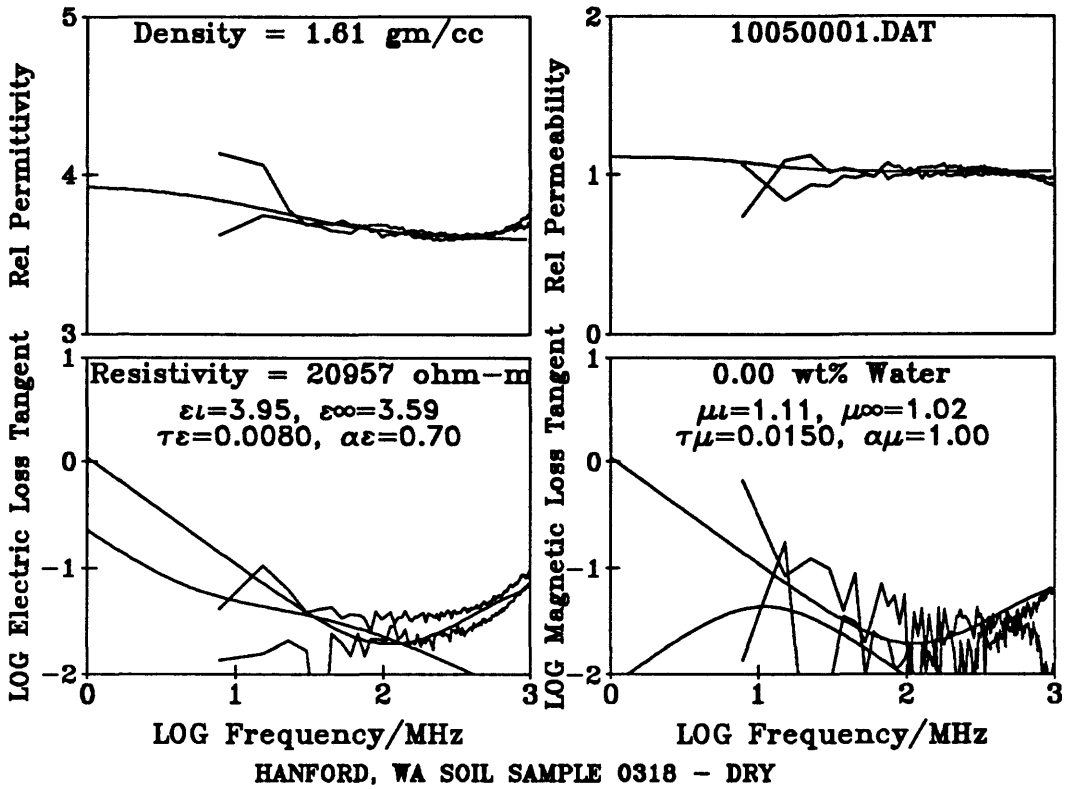

Figure 12 -

Complex relative permittivity and permeability versus frequency of vacuum dry Hanford soil as in Figure 7. The jagged lines are the forward and reverse measurements (measuring a coaxial sample holder independently from each end). The smooth solid lines are the model fits with the parameters shown (see text). The solid line in the loss tangent plots with a minimum near 10^2 MHz is the residual loss of the measurement system.

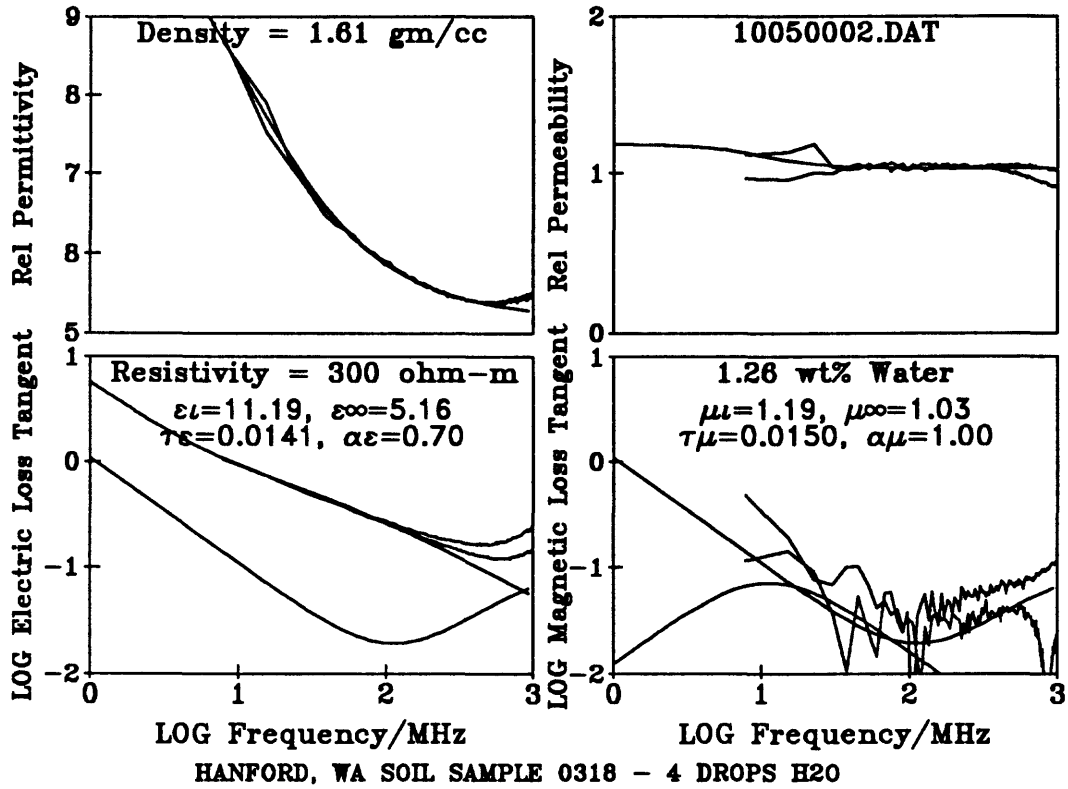

Figure 13 -

Complex relative permittivity and permeability versus frequency of Hanford soil with 1.26 weight percent water as in Figure 7. The jagged lines are the forward and reverse measurements (measuring a coaxial sample holder independently from each end). The smooth solid lines are the model fits with the parameters shown (see text). The solid line in the loss tangent plots with a minimum near 10^2 MHz is the residual loss of the measurement system.

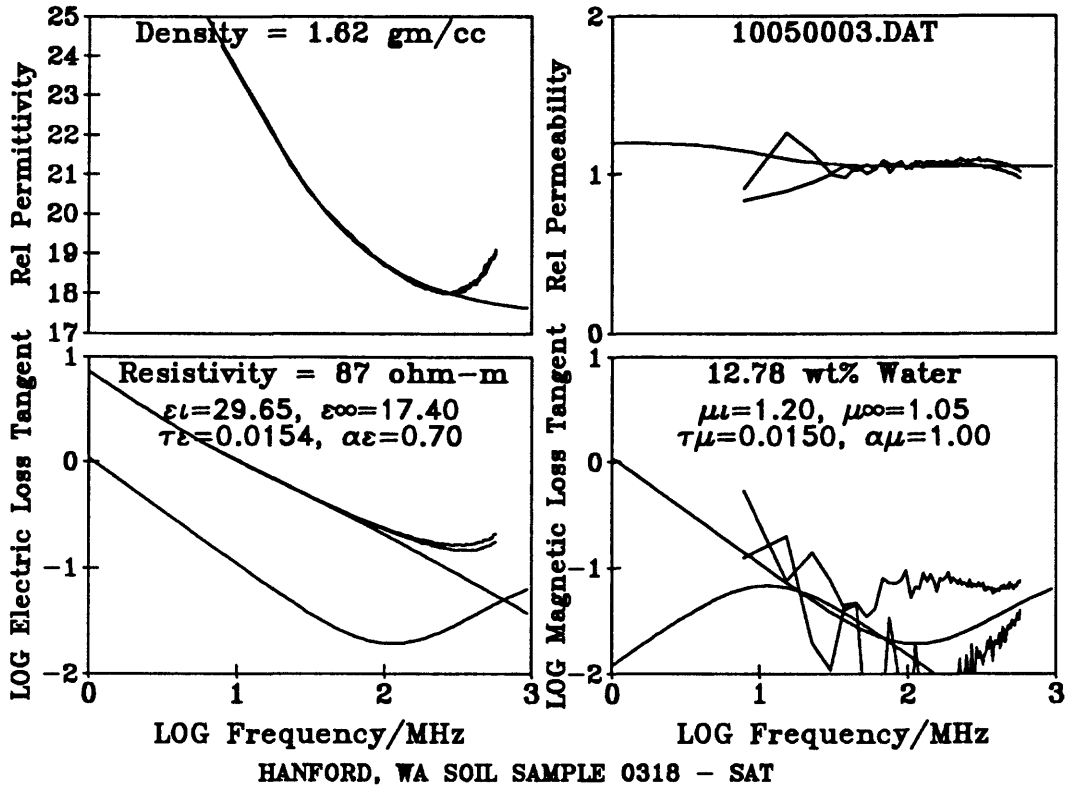

Figure 14 -

Complex relative permittivity and permeability versus frequency of Hanford soil with 12.78 weight percent water as in Figure 7. The jagged lines are the forward and reverse measurements (measuring a coaxial sample holder independently from each end). The smooth solid lines are the model fits with the parameters shown (see text). The solid line in the loss tangent plots with a minimum near 10^2 MHz is the residual loss of the measurement system.

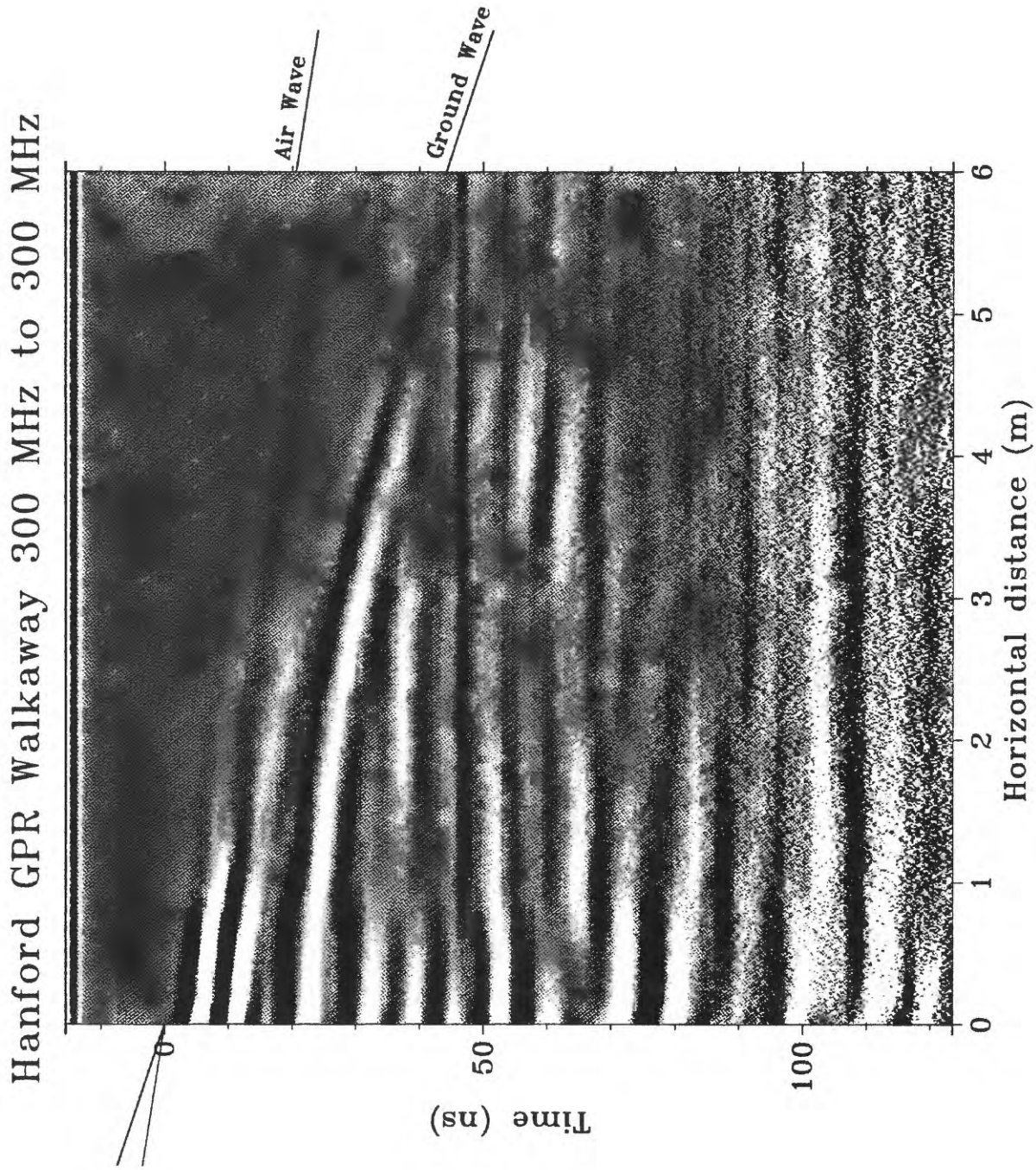

Figure 15 -

Paired antenna walkaway using two 300 MHz ground penetrating radar antennas to determine in situ relative dielectric permittivity = 4.6.

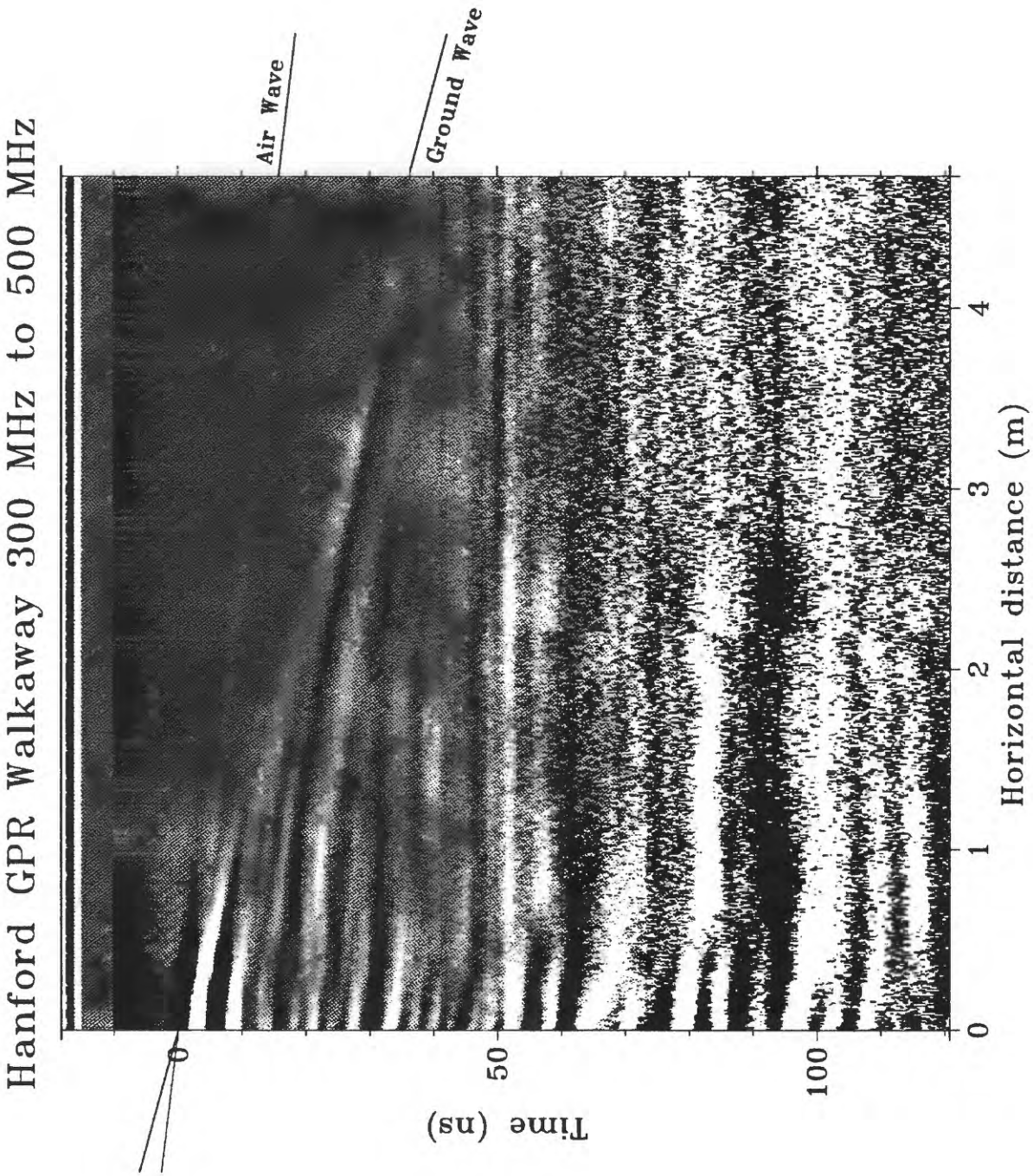

Figure 16 -

Paired antenna walkaway using 300 MHz ground penetrating radar transmit and 500 MHz receive antennas to determine in situ relative dielectric permittivity = 5.3.

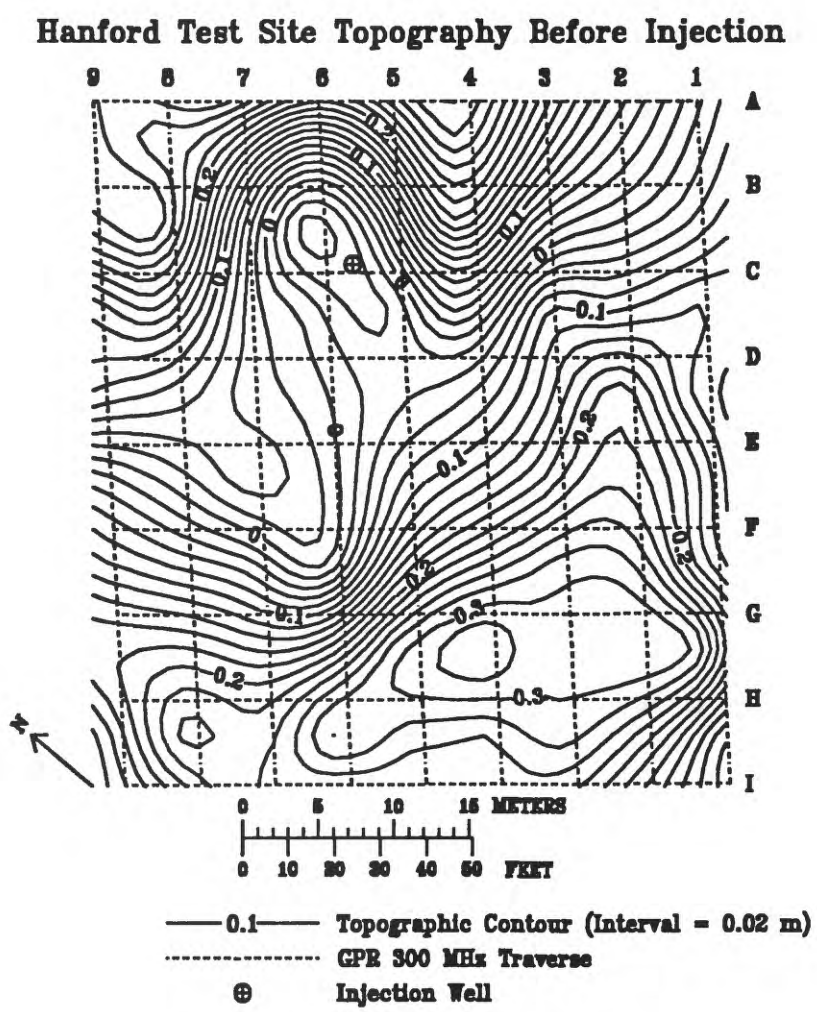

Figure 17 -

Topography before stabilization material injection. Letters and numbers around the top and right edges of the plot are the designations of the surface ground penetrating radar lines across the site.

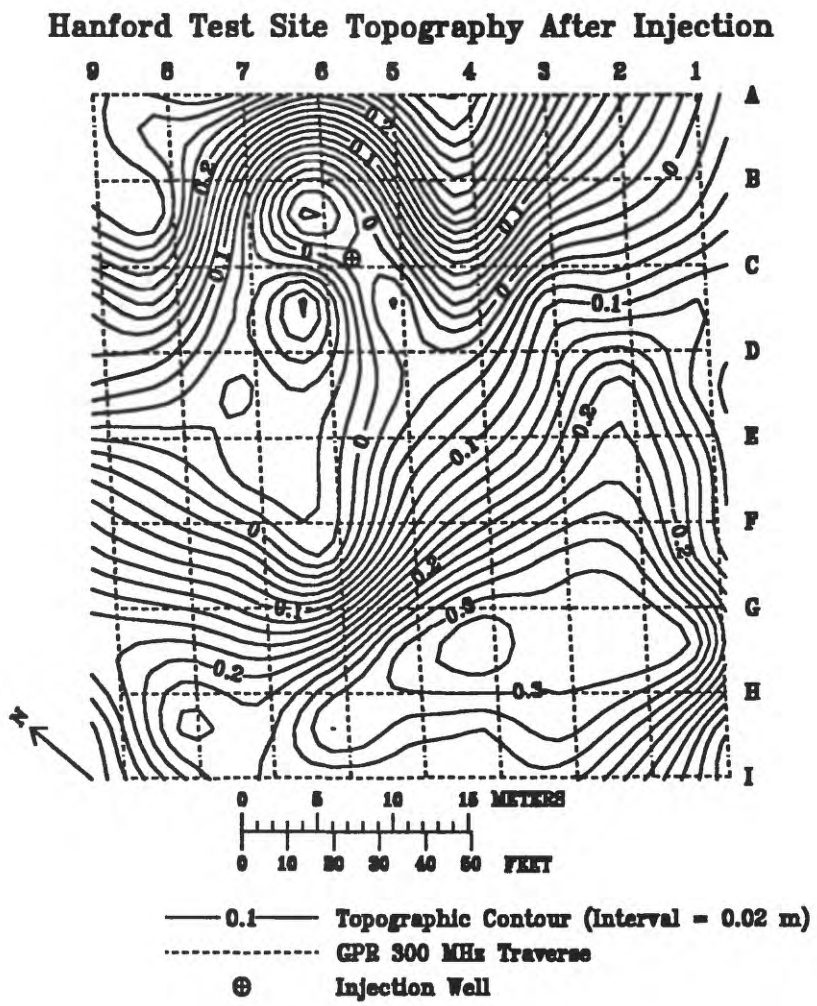

Figure 18 -

Topography after stabilization material injection.

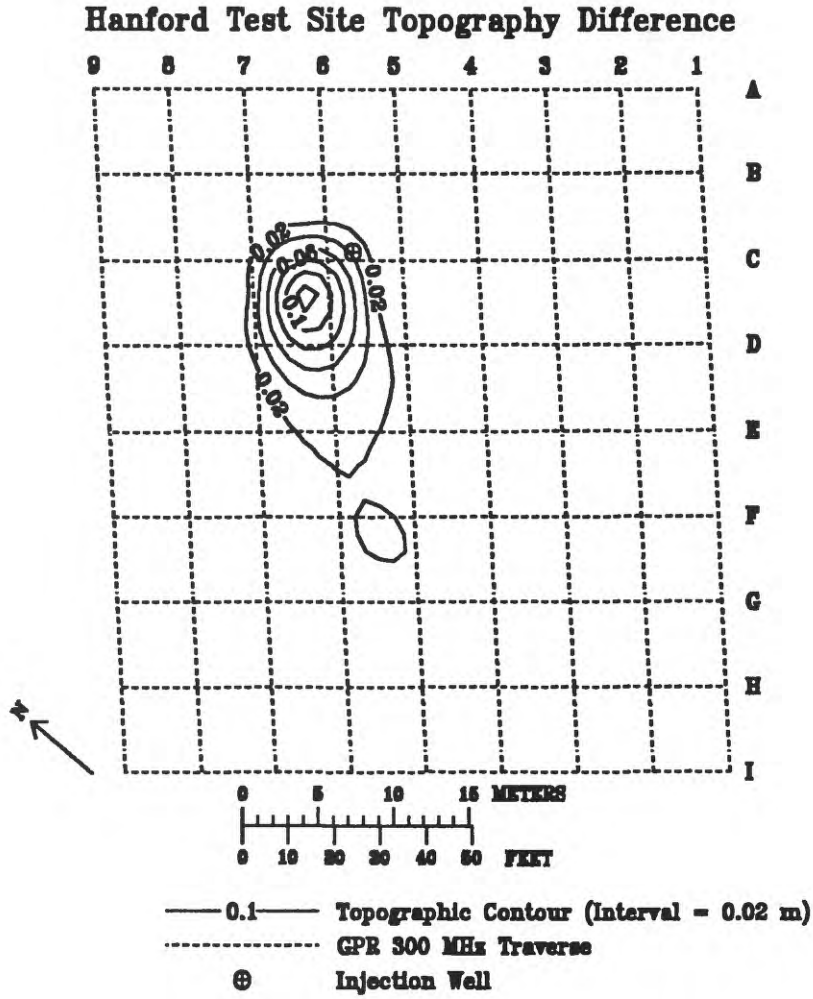

Figure 19 -

Difference in topography between before and after injection. Note mounding near injection point indicative of excess injected slurry volume over available gravel void volume.

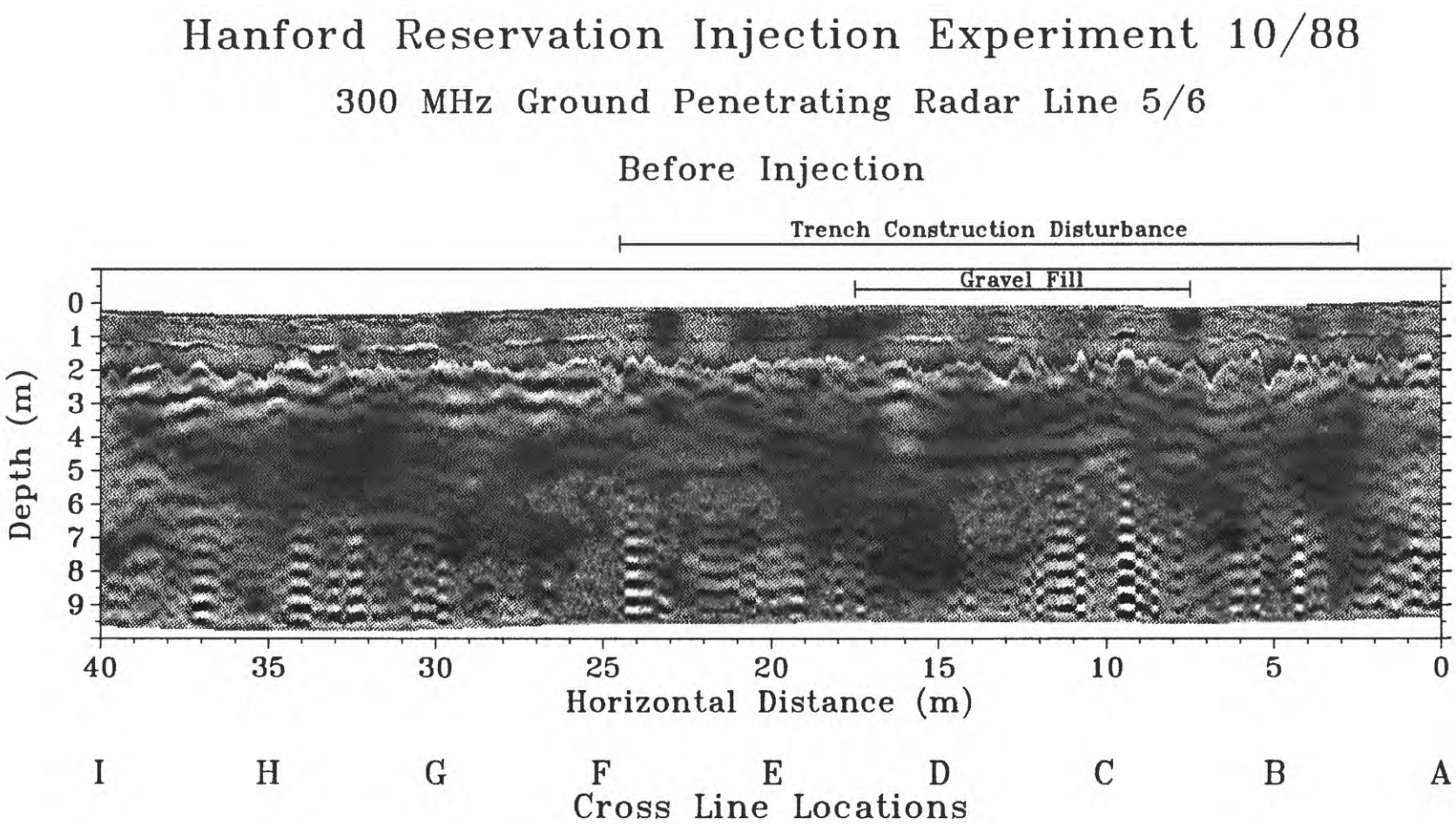

Figure 20 -

300 MHz ground penetrating radar section along line 5/6 (midway between lines 5 and 6, see location key in Figure 19) along the length of the gravel trench, before injection.

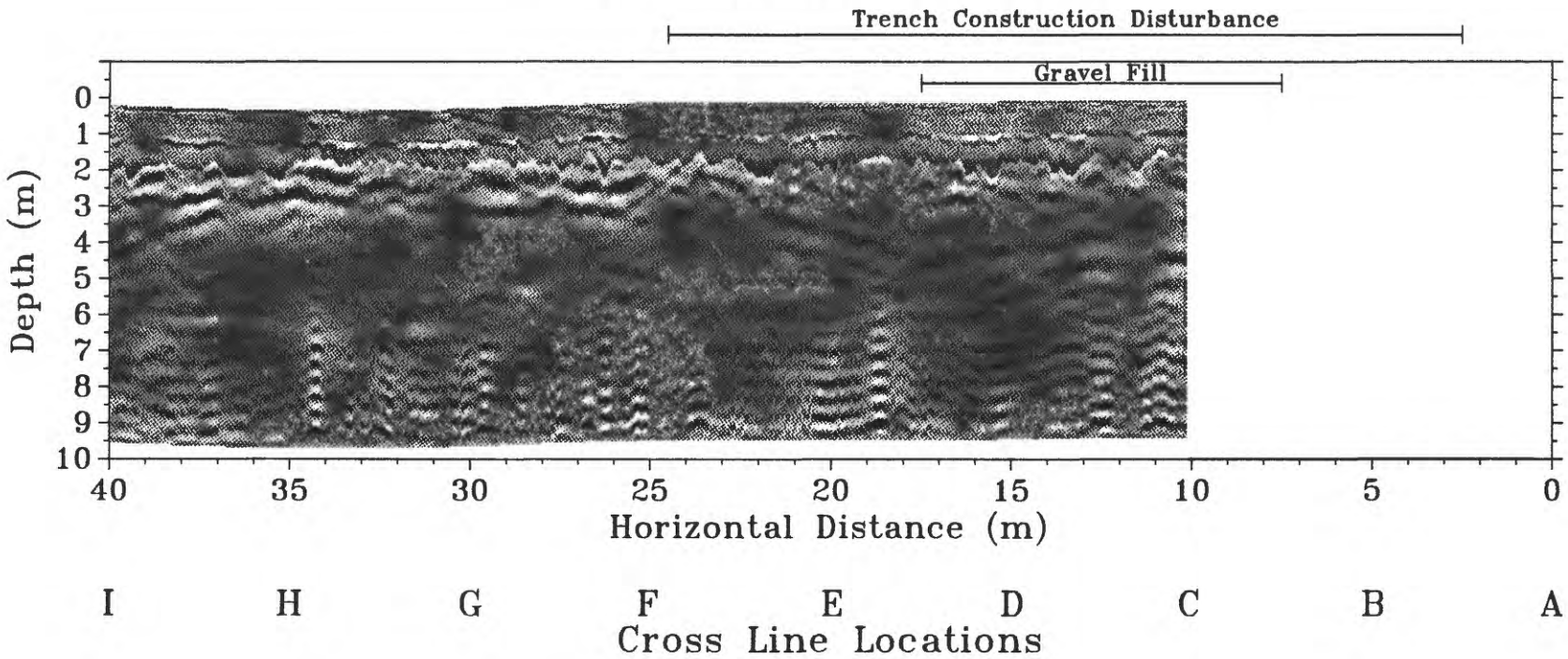

Figure 21 -

300 MHz ground penetrating radar section along line 5/6 (midway between lines 5 and 6, see location key in Figure 19) along the length of the gravel trench at time 16:16 during injection (see Table 2).

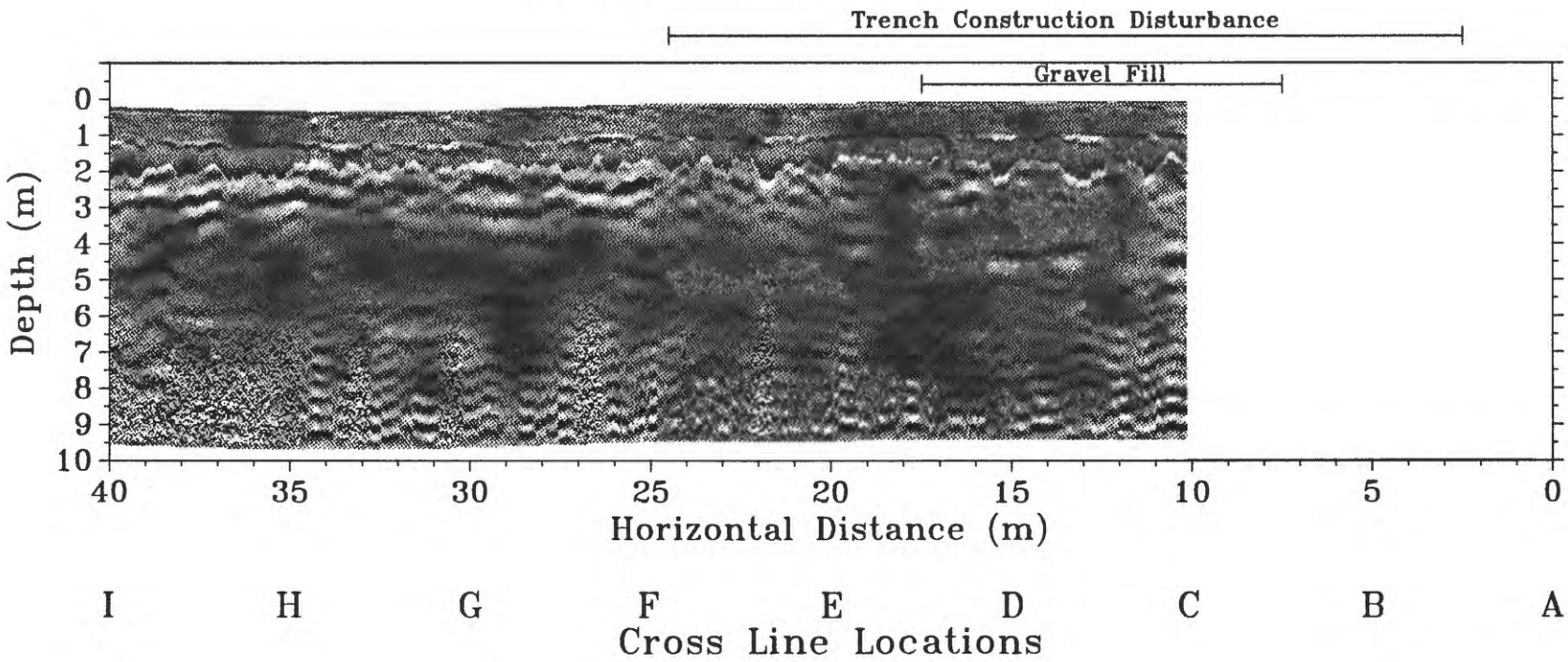

Figure 22 -

300 MHz ground penetrating radar section along line 5/6 (midway between lines 5 and 6, see location key in Figure 19) along the length of the gravel trench at time 16:30 during injection (see Table 2).

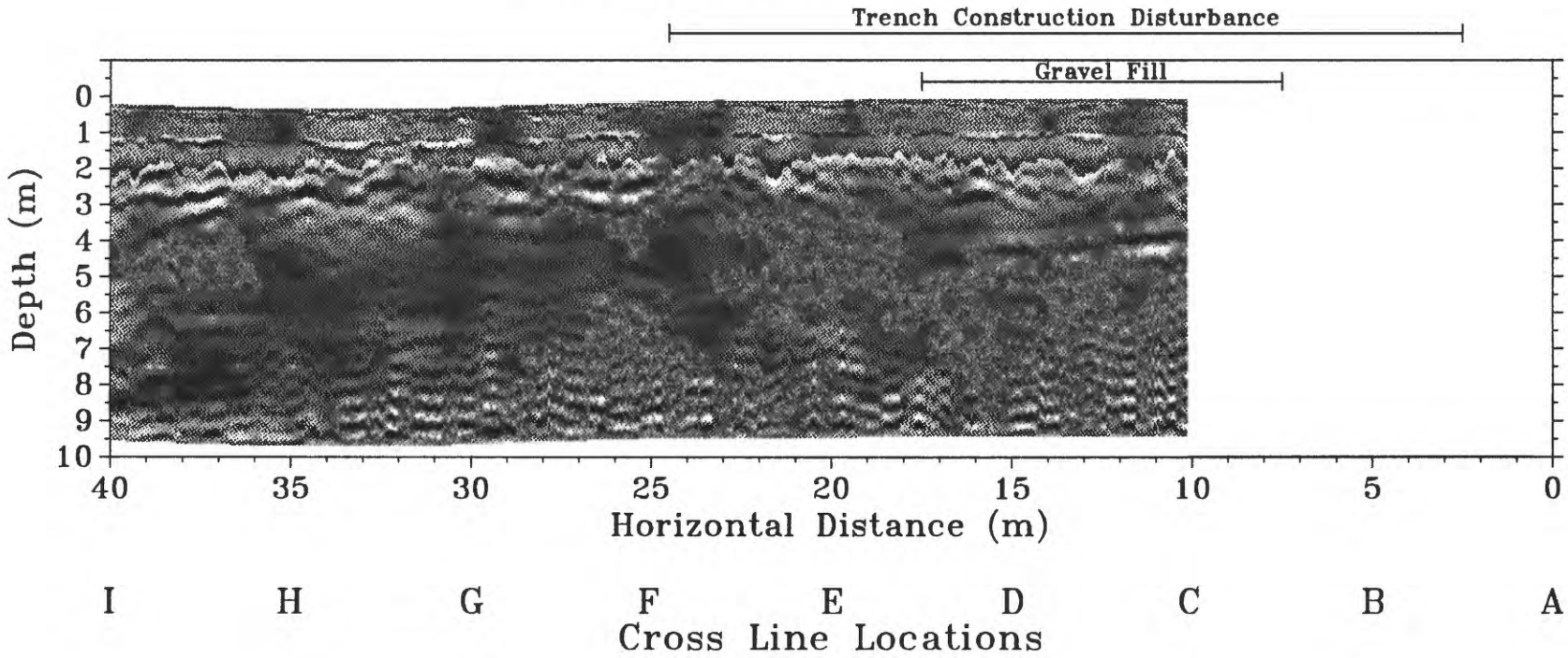

Figure 23 -

300 MHz ground penetrating radar section along line 5/6 (midway between lines 5 and 6, see location key in Figure 19) along the length of the gravel trench at time 16:45 during injection (see Table 2).

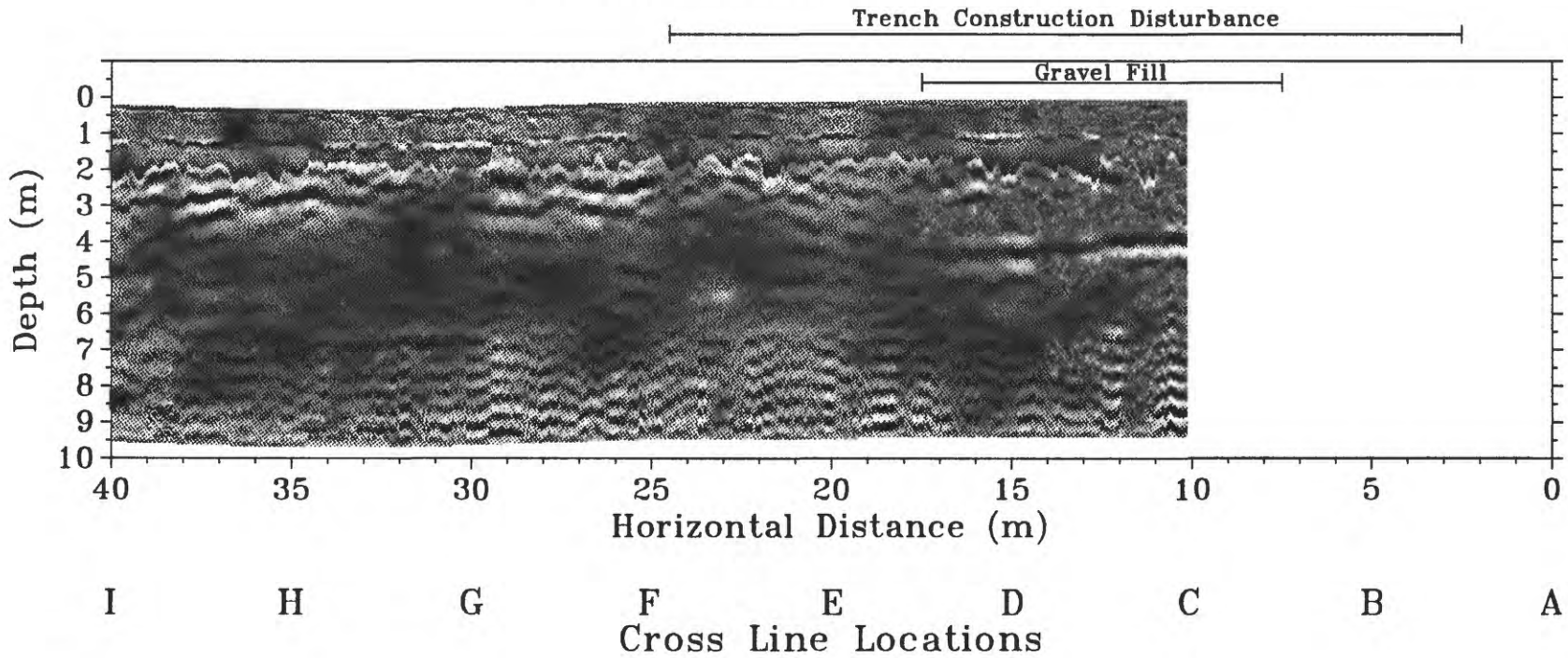

Figure 24 -

300 MHz ground penetrating radar section along line 5/6 (midway between lines 5 and 6, see location key in Figure 19) along the length of the gravel trench at time 17:00 during injection (see Table 2).

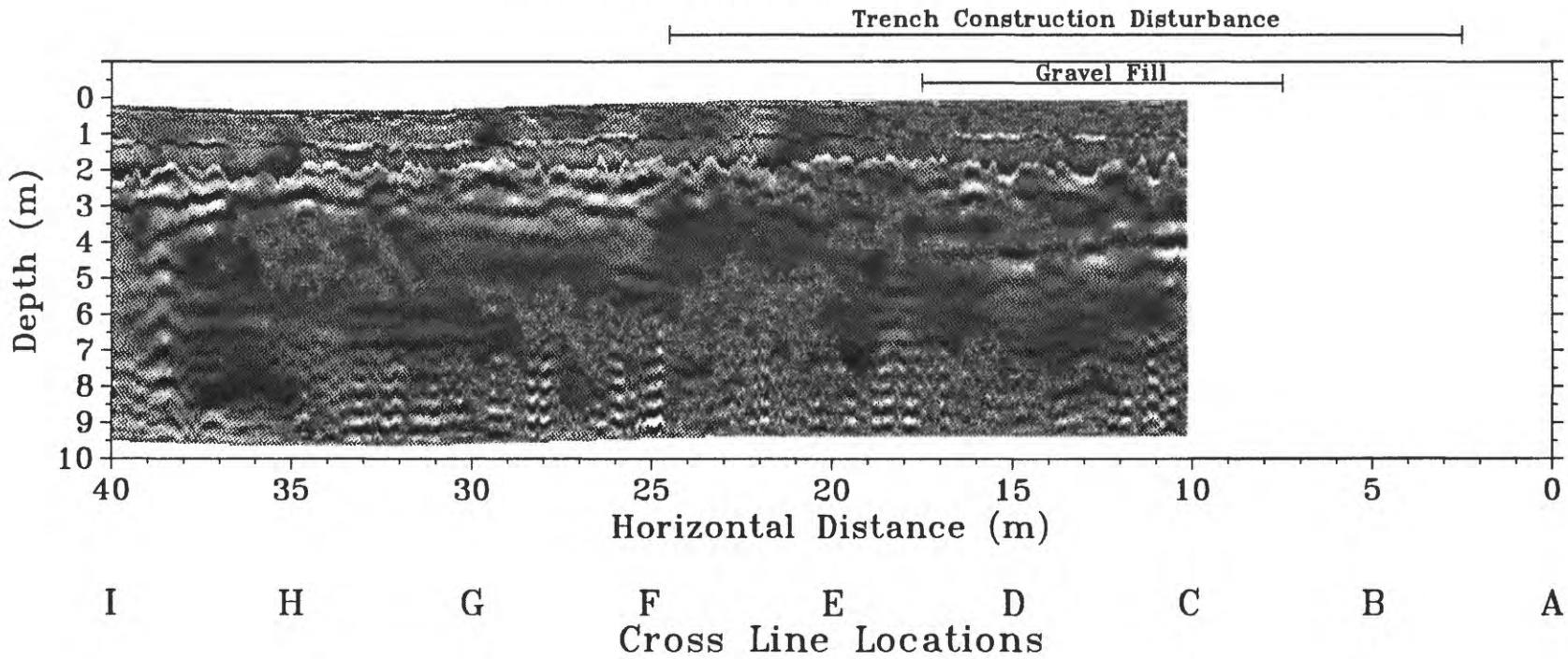

Figure 25 -

300 MHz ground penetrating radar section along line 5/6 (midway between lines 5 and 6, see location key in Figure 19) along the length of the gravel trench at time 17:45 during injection (see Table 2).

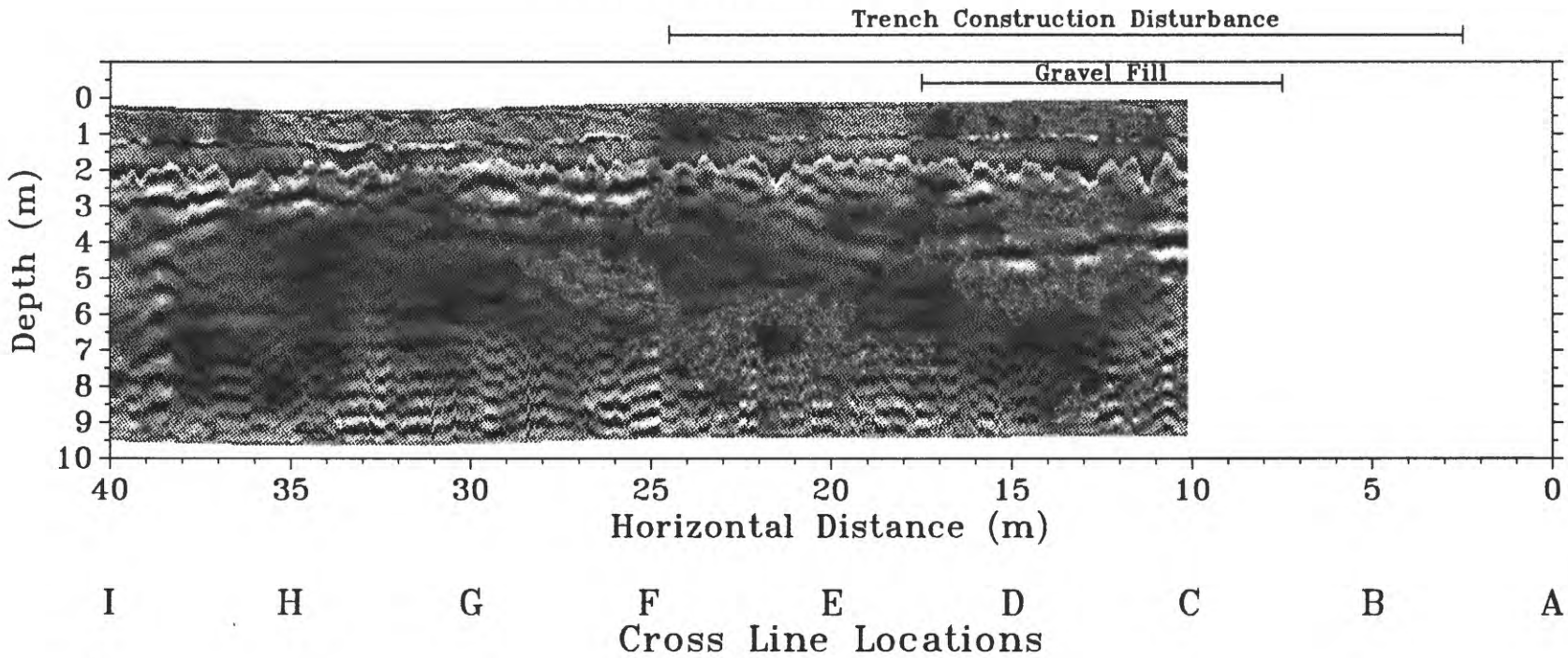

Figure 26 -

300 MHz ground penetrating radar section along line 5/6 (midway between lines 5 and 6, see location key in Figure 19) along the length of the gravel trench at time 18:00 during injection (see Table 2).

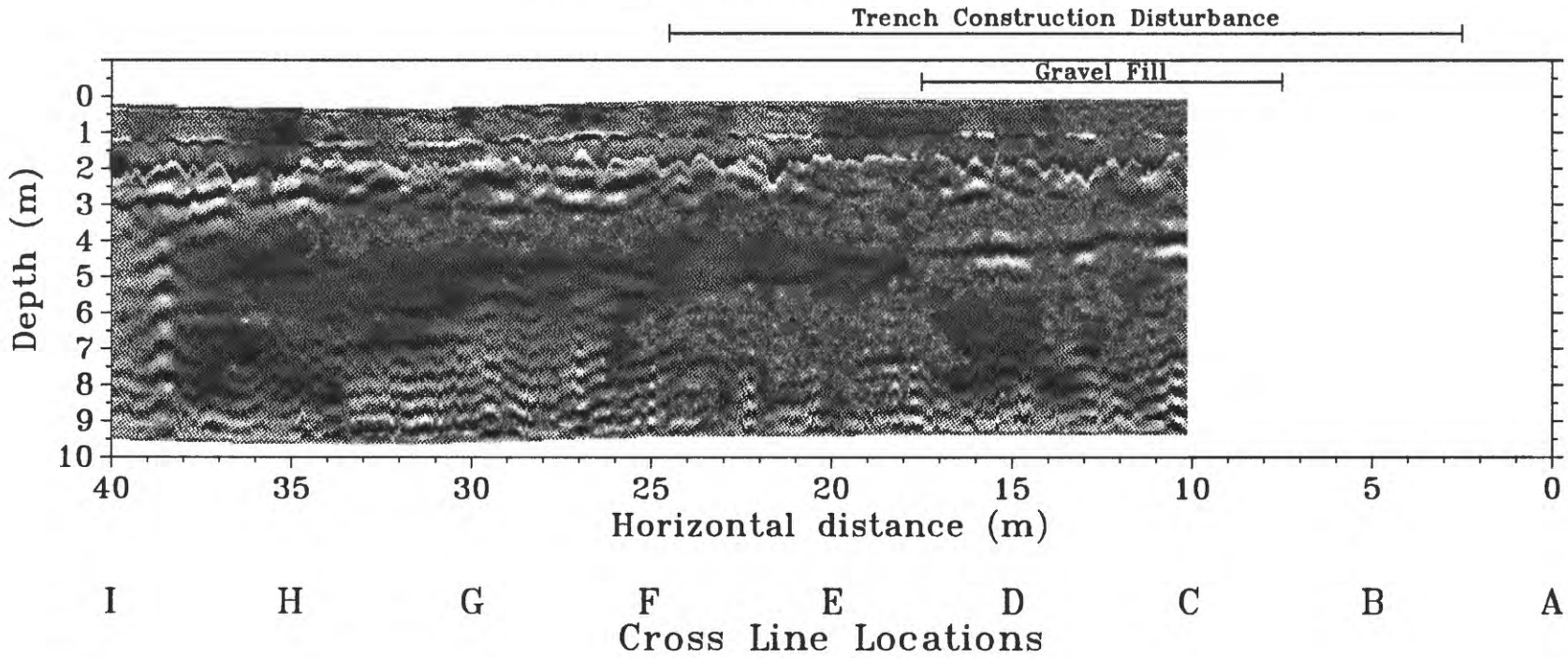

Figure 27 -

300 MHz ground penetrating radar section along line 5/6 (midway between lines 5 and 6, see location key in Figure 19) along the length of the gravel trench at time 18:15 during injection (see Table 2).

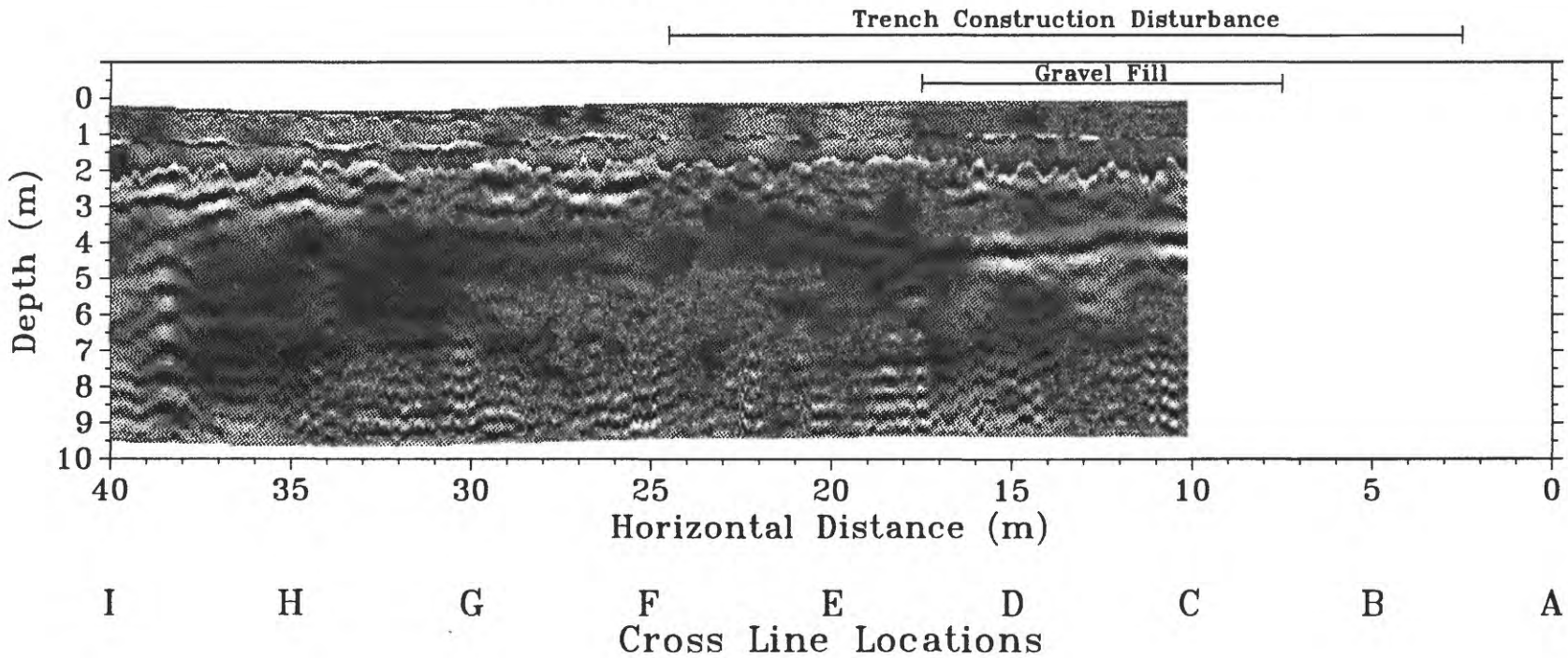

Figure 28 -

300 MHz ground penetrating radar section along line 5/6 (midway between lines 5 and 6, see location key in Figure 19) along the length of the gravel trench at time 18:30 during injection (see Table 2).

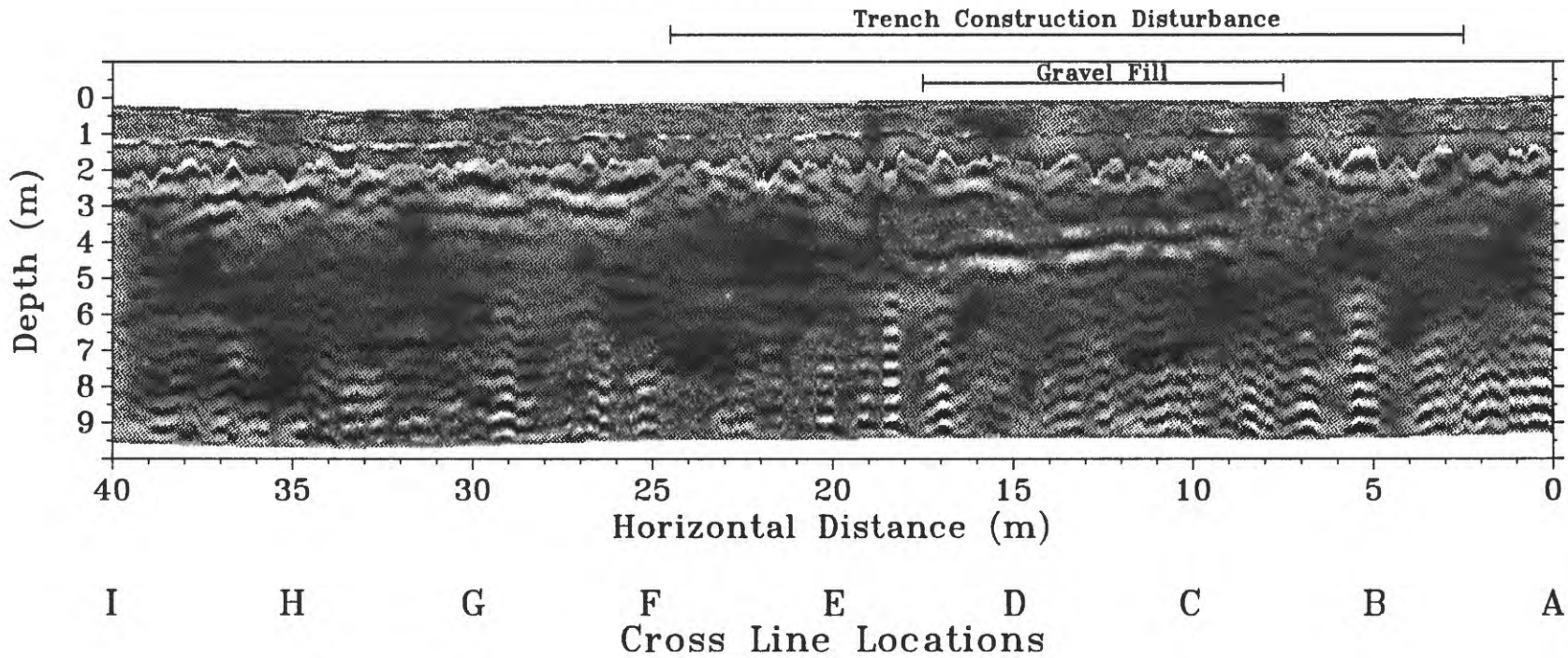

Figure 29 -

300 MHz ground penetrating radar section along line 5/6 (midway between lines 5 and 6, see location key in Figure 19) along the length of the gravel trench at time 18:45, 0.25 hour after injection ended (see Table 2).

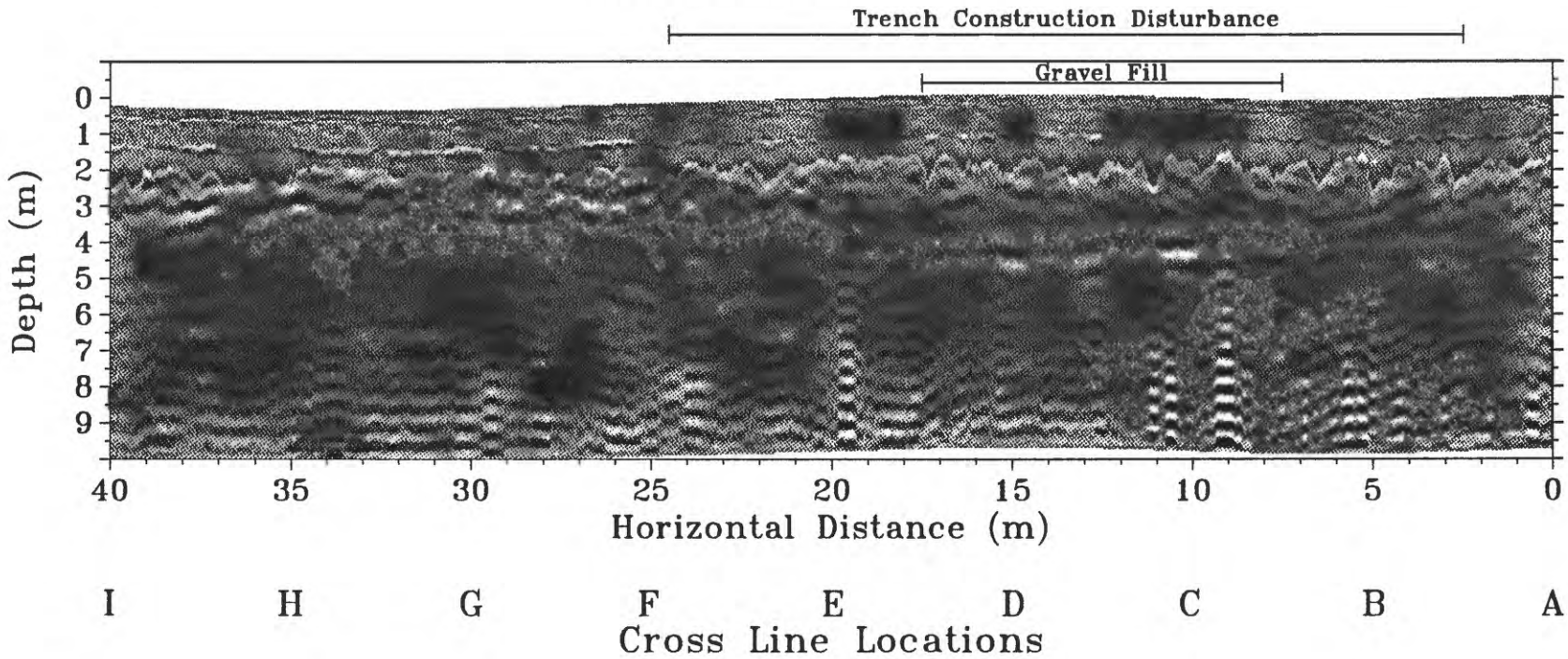

Figure 30 -

300 MHz ground penetrating radar section along line 5/6 (midway between lines 5 and 6, see location key in Figure 19) along the length of the gravel trench, 16.5 hours after injected ended.

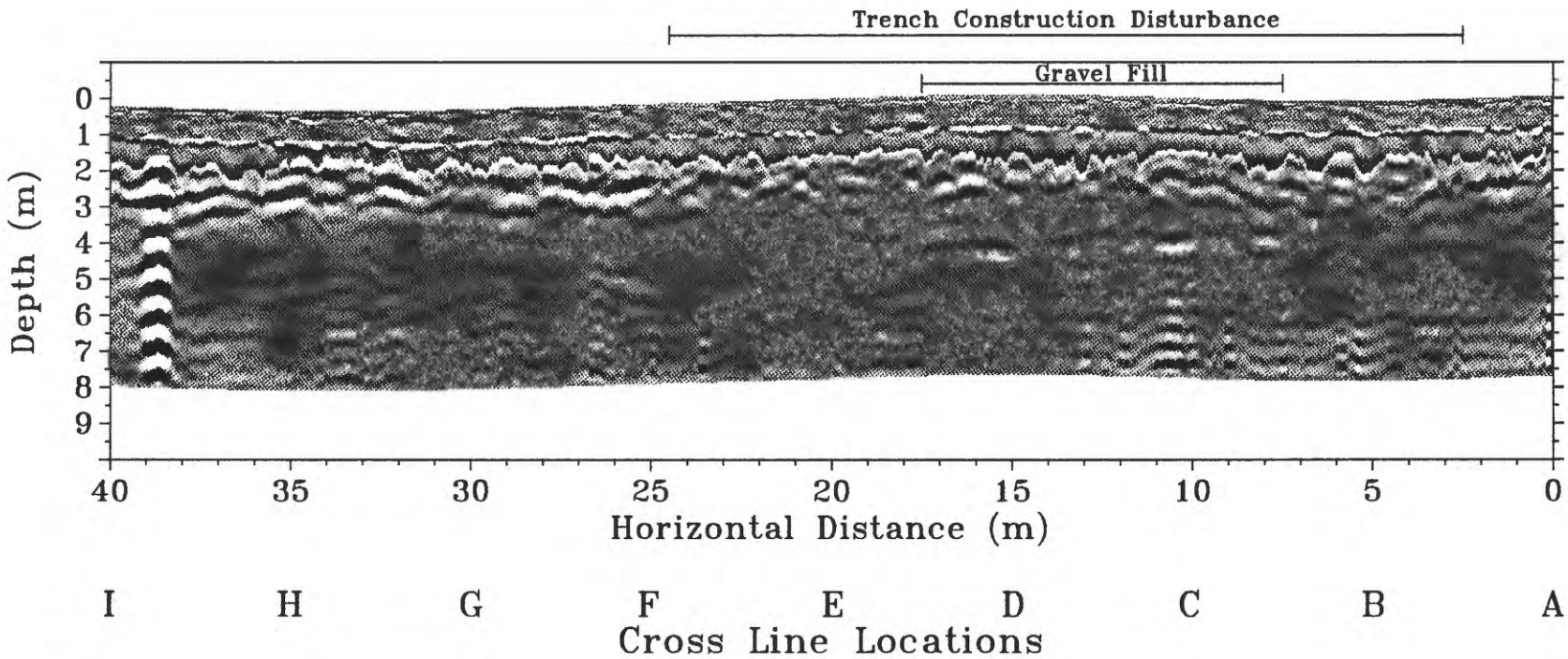

Figure 31 -

300 MHz ground penetrating radar section along line 5/6 (midway between lines 5 and 6, see location key in Figure 19) along the length of the gravel trench, 62 hours after injected ended.

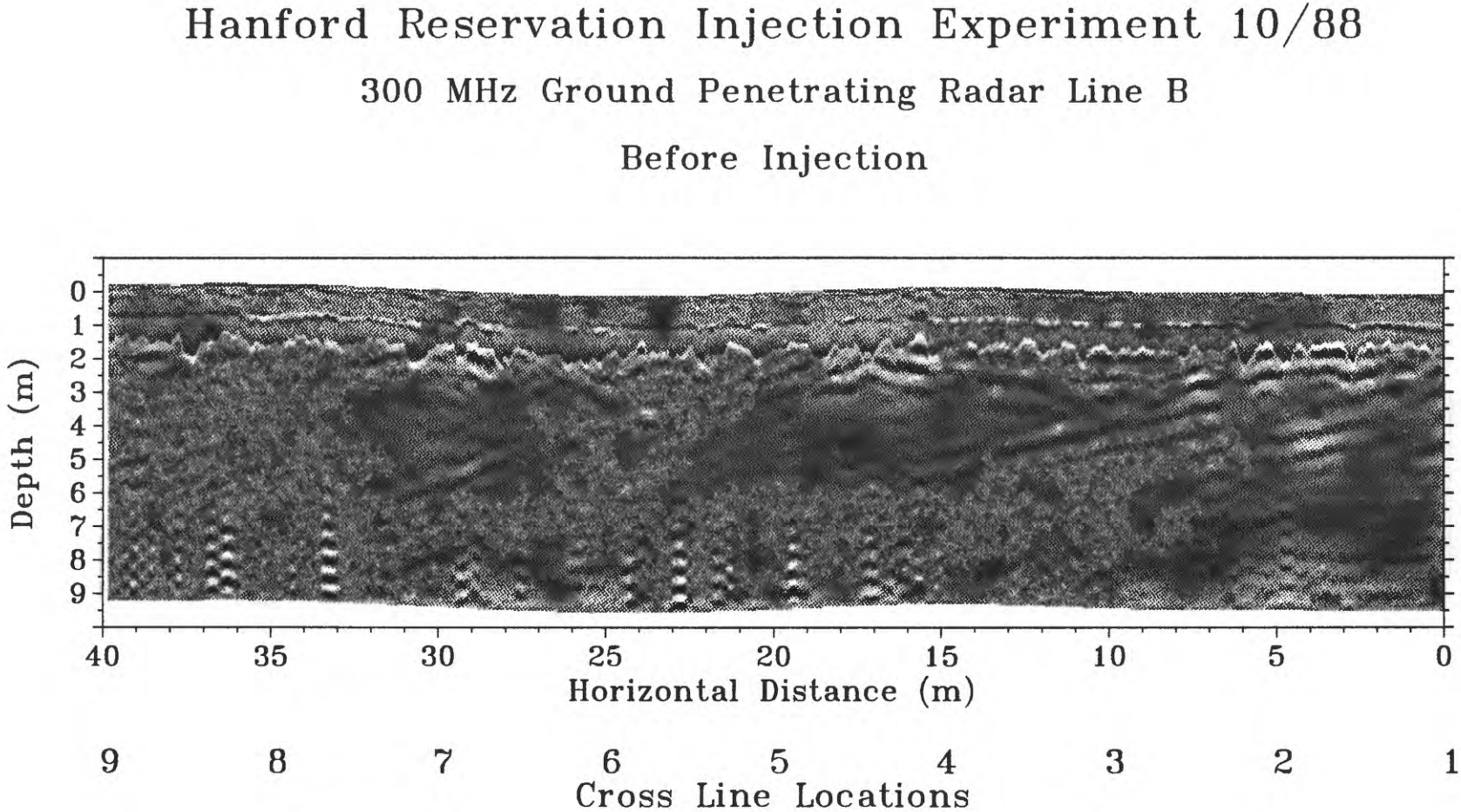

Figure 32 -

300 MHz ground penetrating radar section along line B (see location key in Figure 19) beyond the end of the trench before injection.

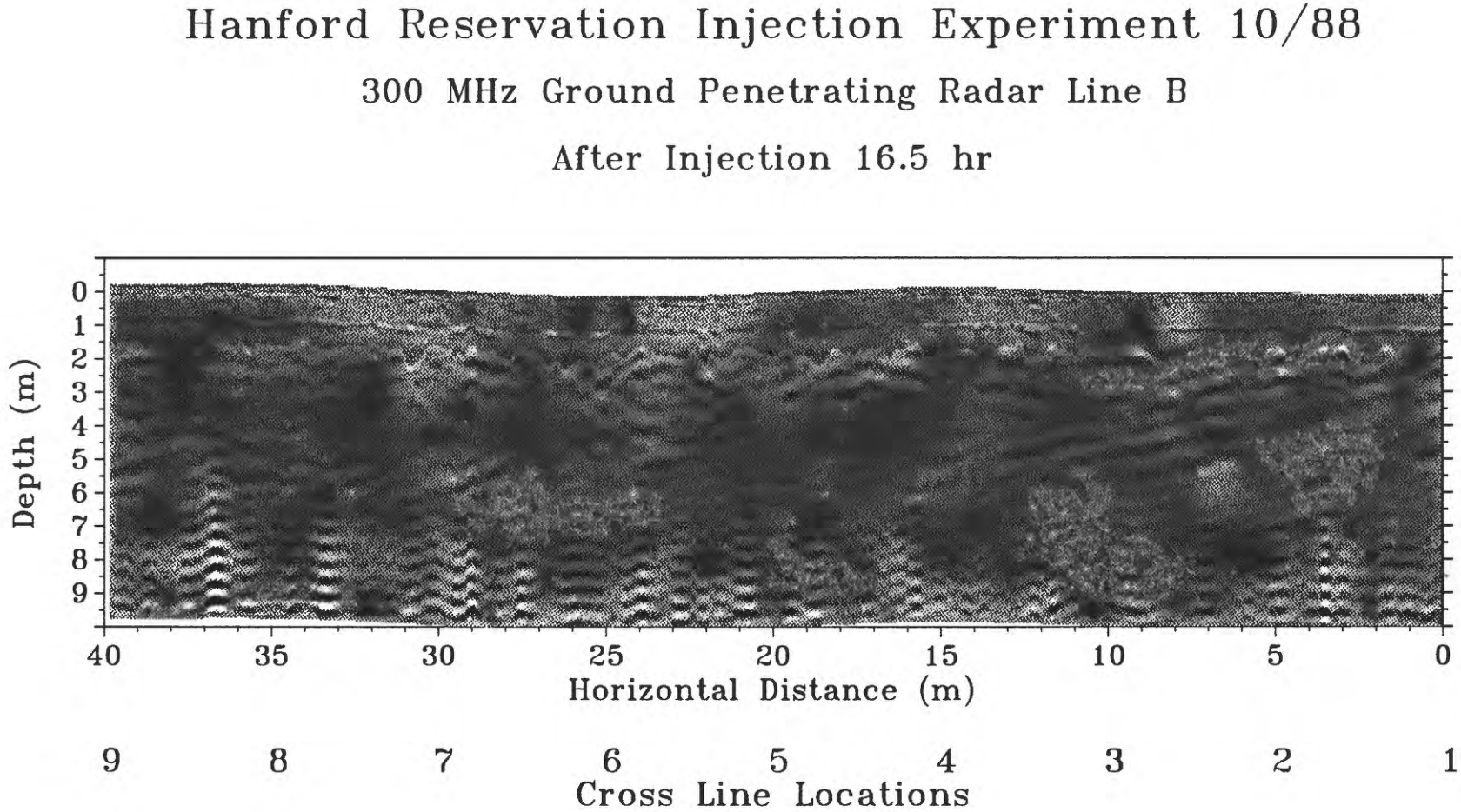

Figure 33 -

300 MHz ground penetrating radar section along line B (see location key in Figure 19) beyond the end of the trench 16.5 hours after injected ended.

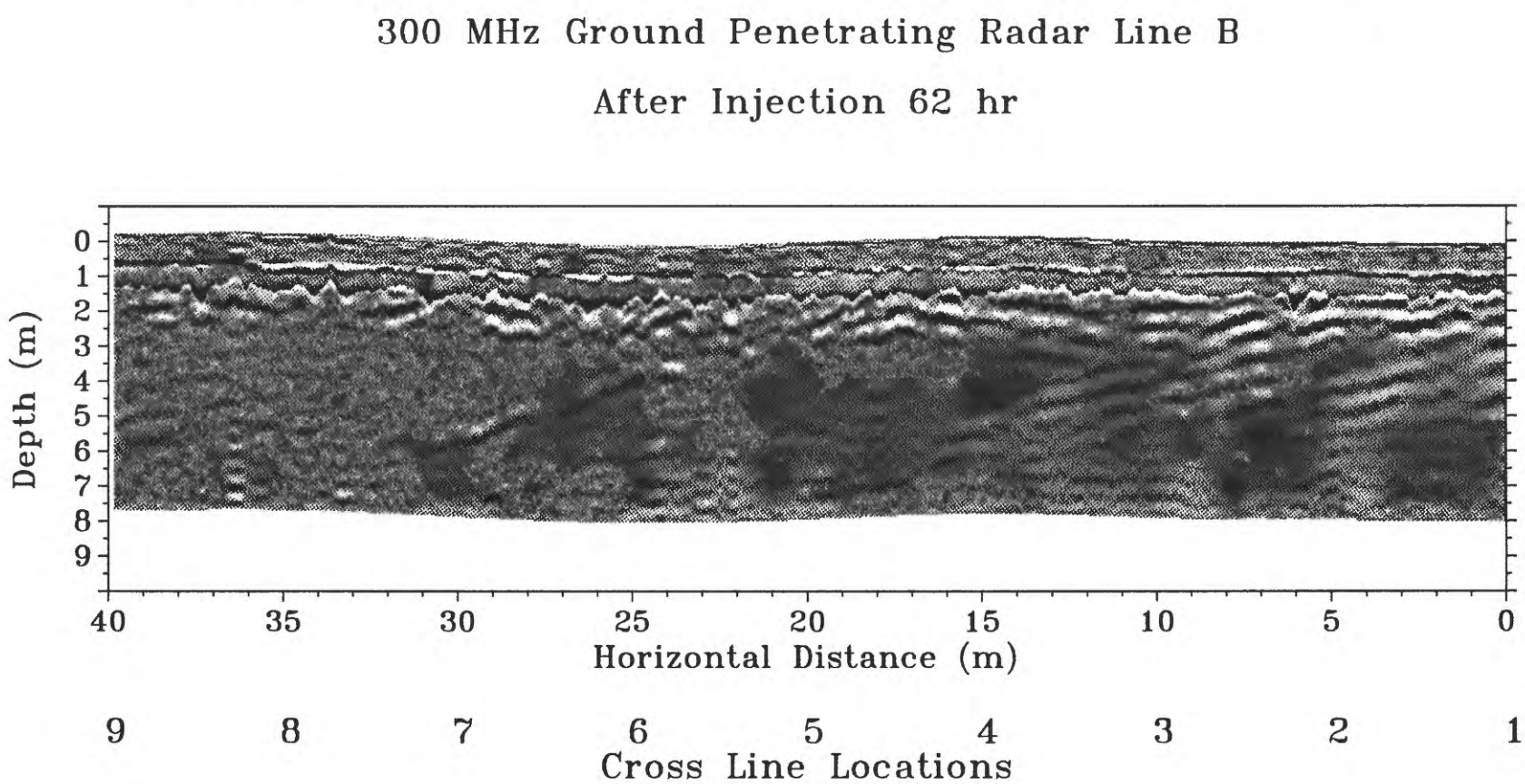

Figure 34 -

300 MHz ground penetrating radar section along line B (see location key in Figure 19) beyond the end of the trench 62 hours after injected ended.

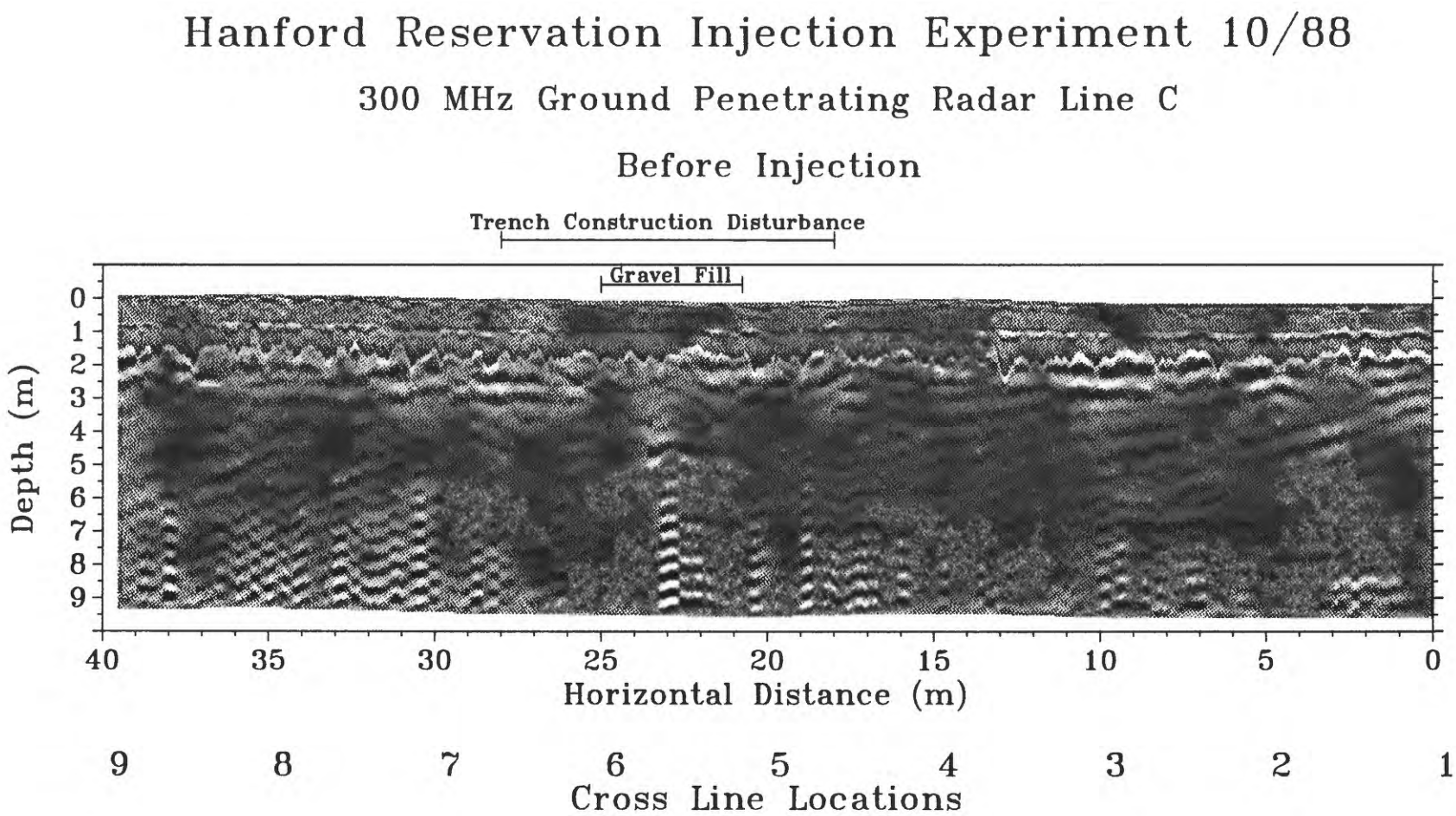

Figure 35 -

300 MHz ground penetrating radar section along line C (see location key in Figure 19) across the end of the trench near the injection riser before injection.

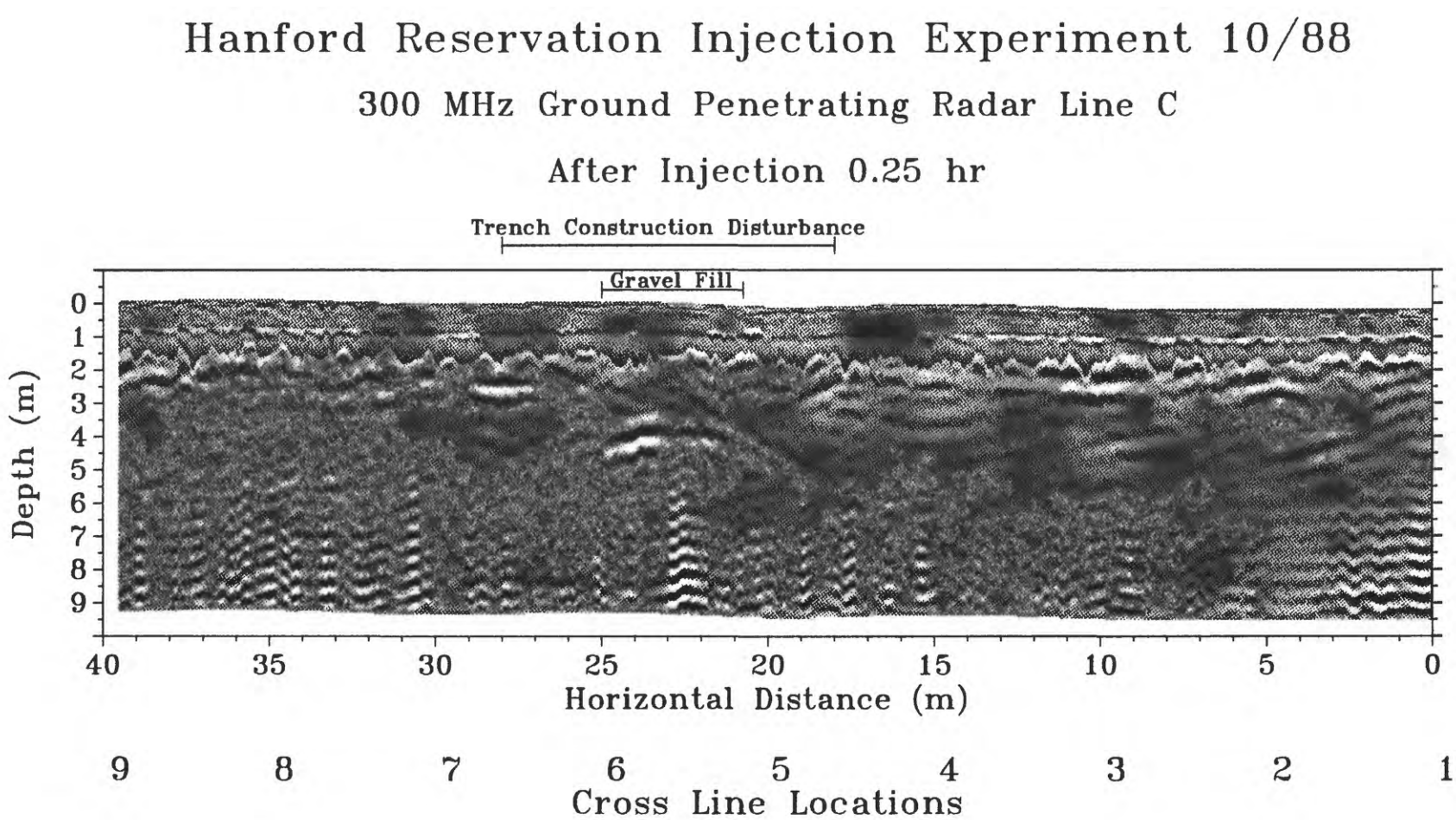

Figure 36 -

300 MHz ground penetrating radar section along line C (see location key in Figure 19) across the end of the trench near the injection riser, 0.25 hour after injected ended.

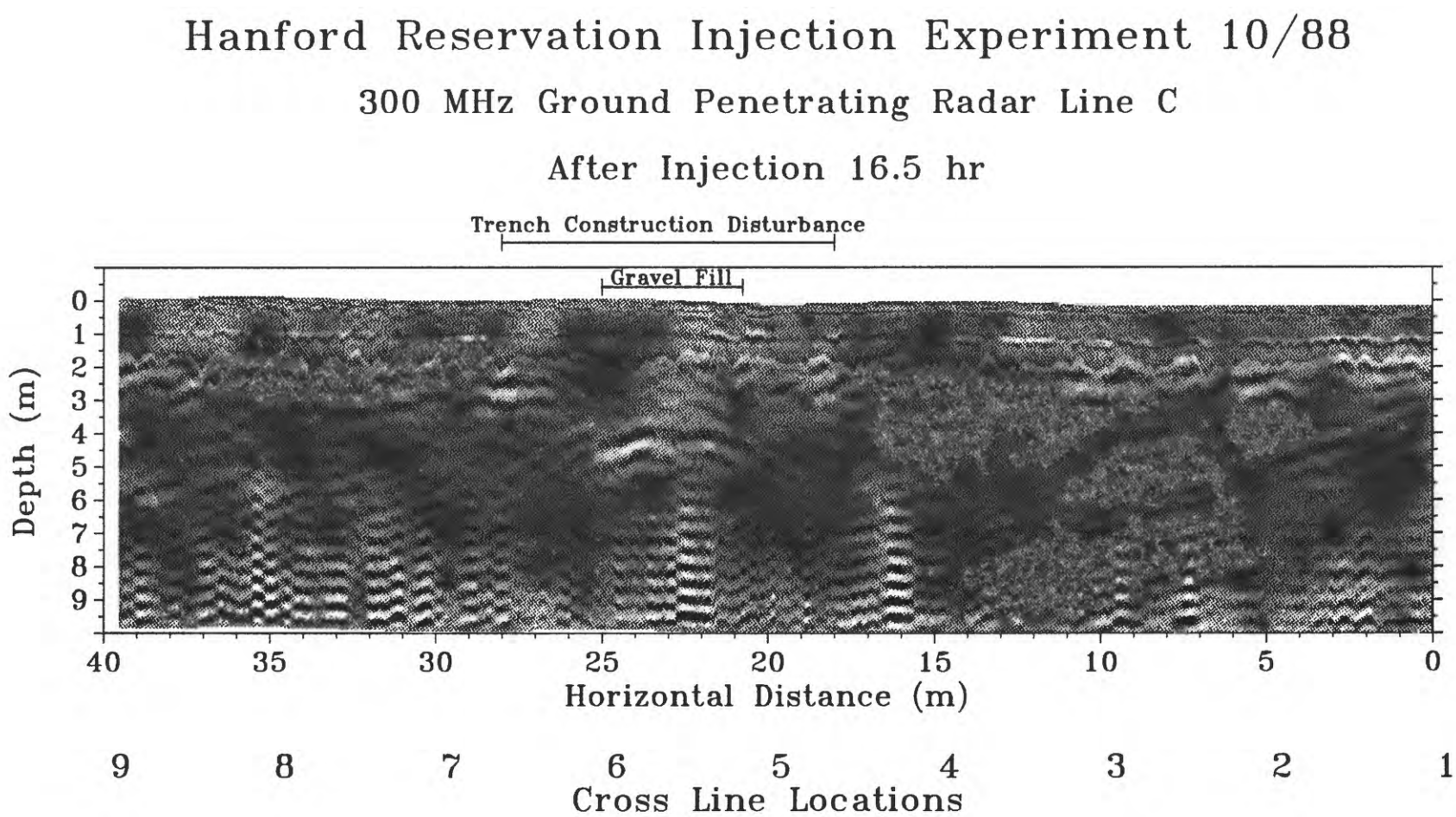

Figure 37 -

300 MHz ground penetrating radar section along line C (see location key in Figure 19) across the end of the trench near the injection riser 16.5 hours after injected ended.

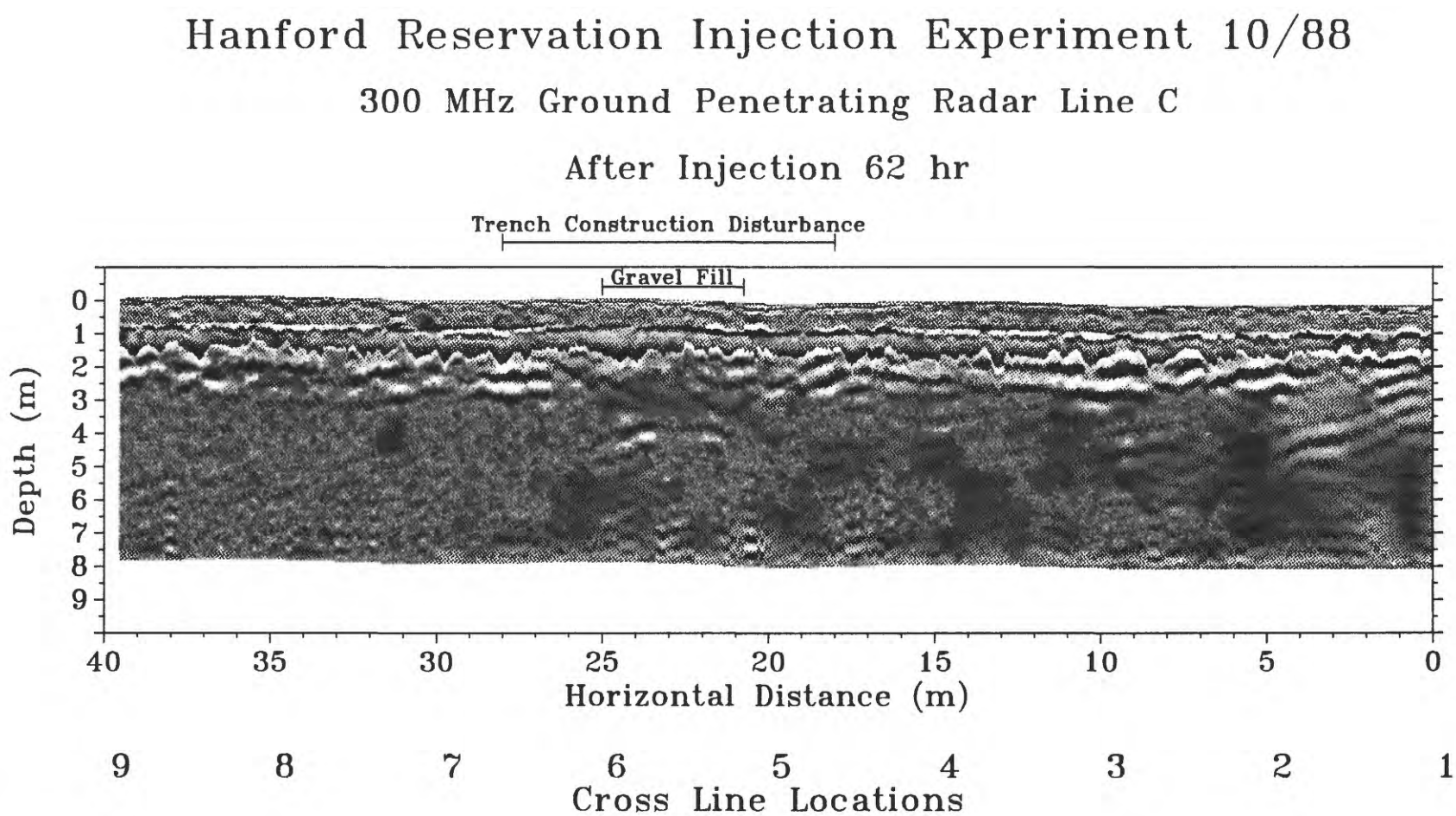

Figure 38 -

300 MHz ground penetrating radar section along line C (see location key in Figure 19) across the end of the trench near the injection riser 62 hours after injected ended.

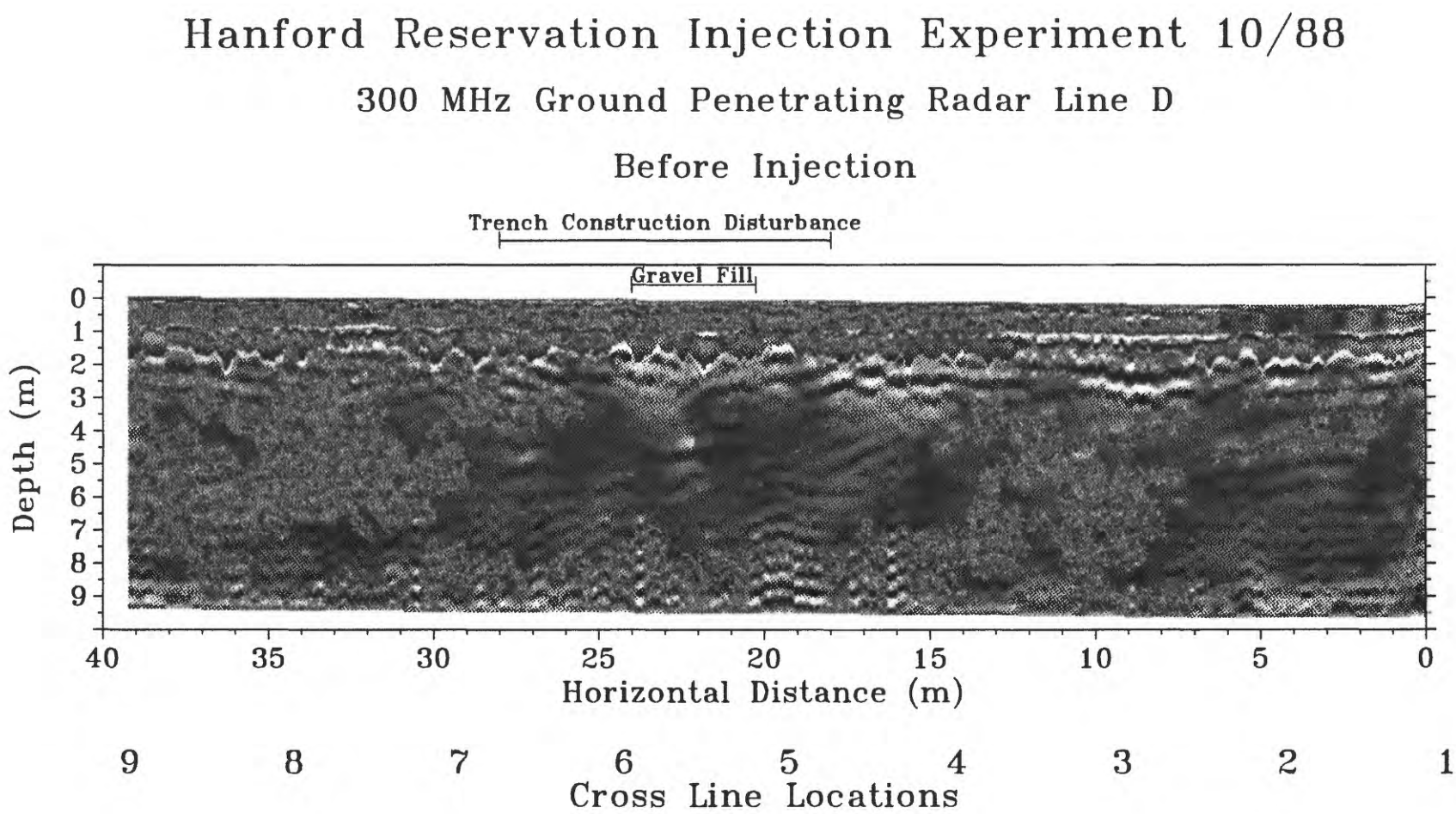

Figure 39 -

300 MHz ground penetrating radar section along line D (see location key in Figure 19) across the middle of the trench before injection.

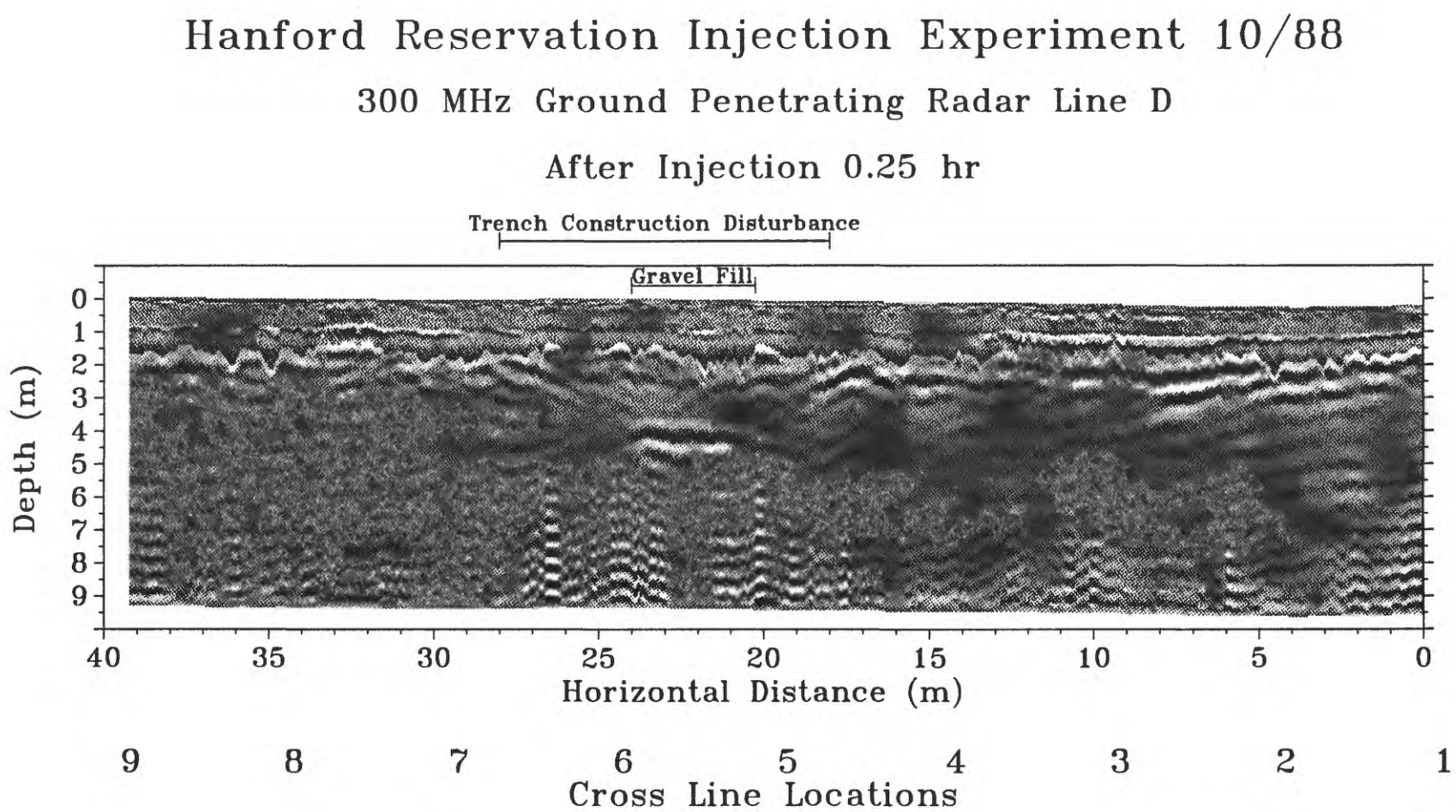

Figure 40 -

300 MHz ground penetrating radar section along line D (see location key in Figure 19) across the middle of the trench, 0.25 hour after injected ended.

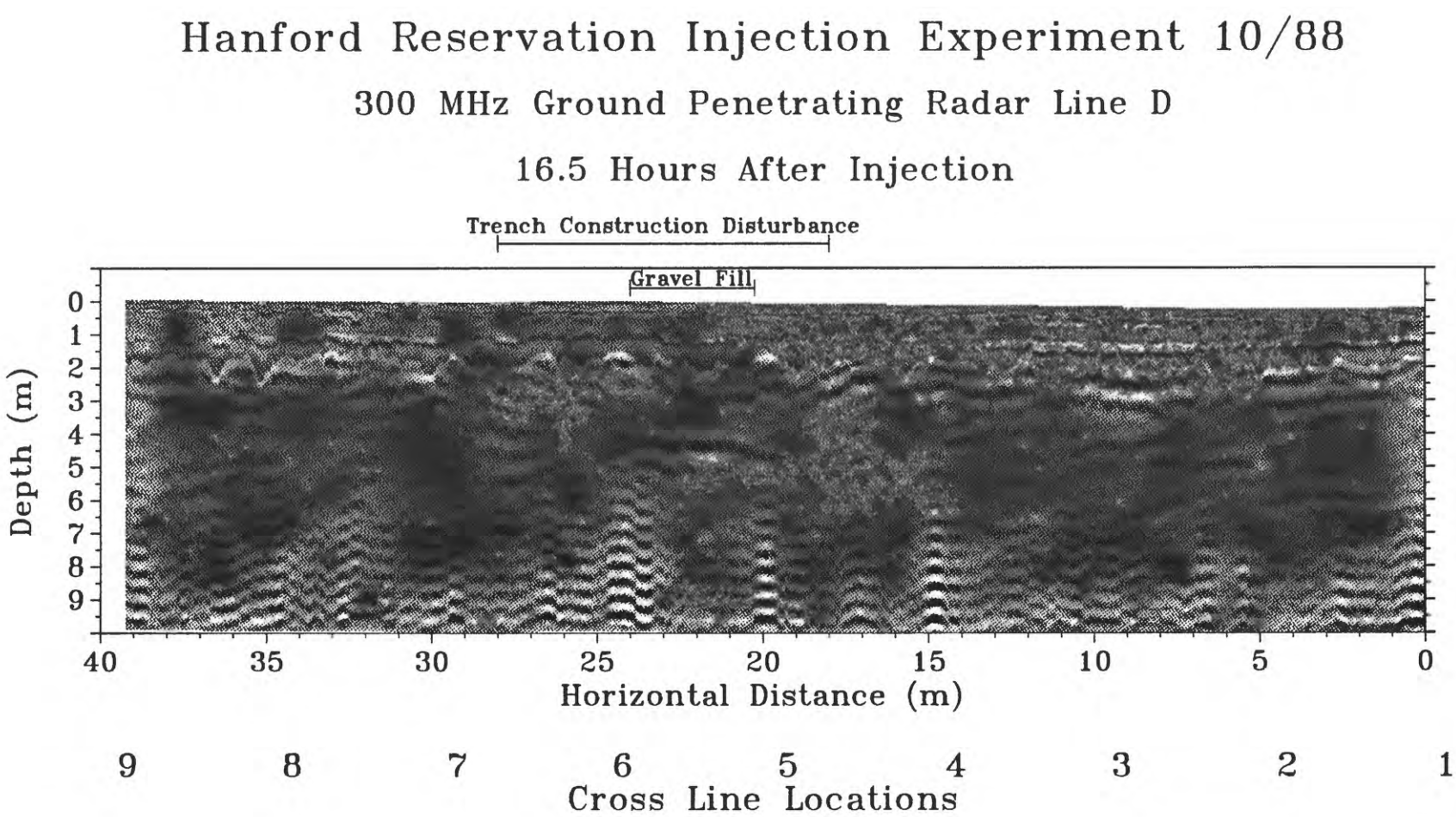

Figure 41 -

300 MHz ground penetrating radar section along line D (see location key in Figure 19) across the middle of the trench 16.5 hours after injected ended.

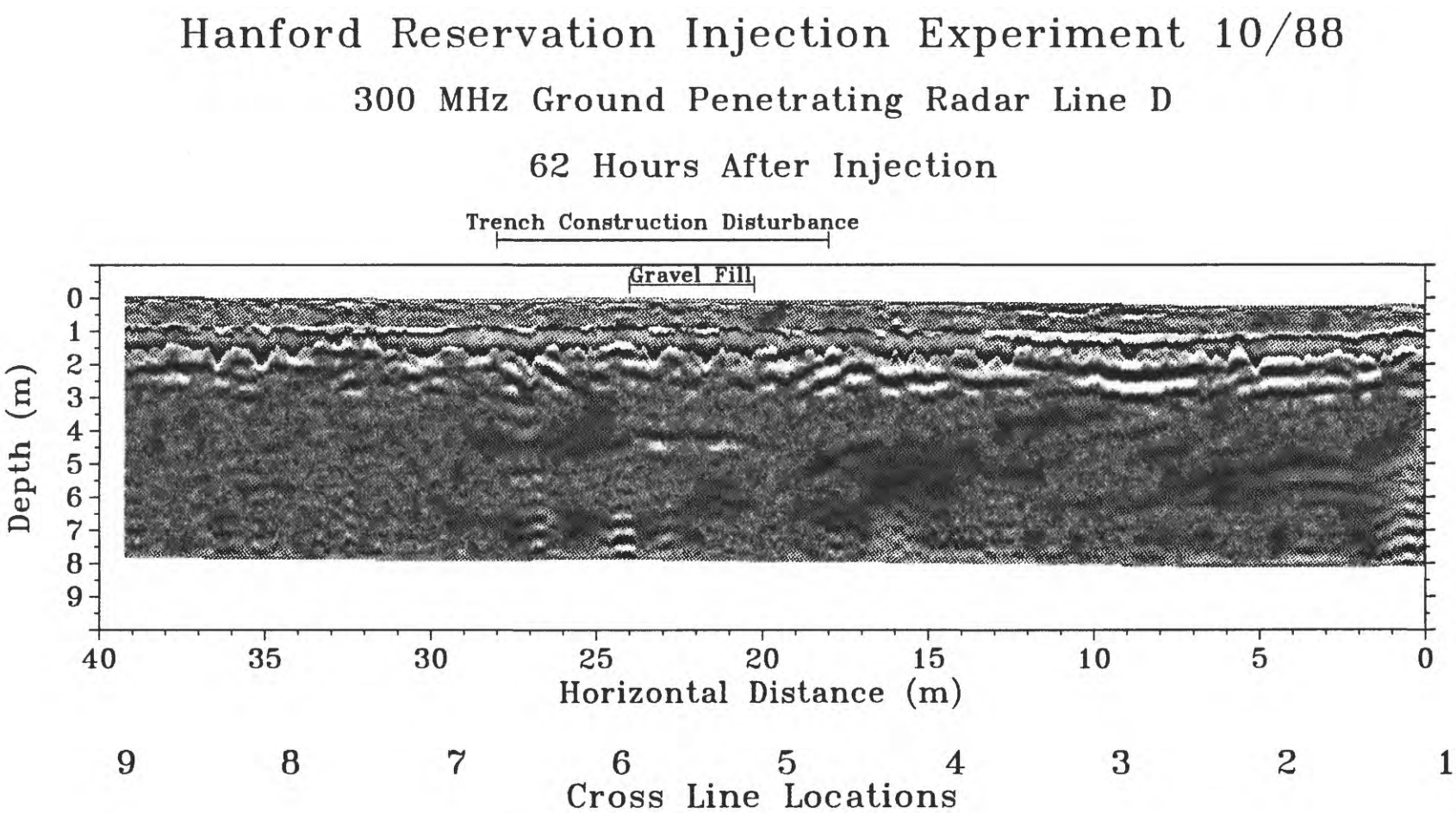

Figure 42 -

300 MHz ground penetrating radar section along line D (see location key in Figure 19) across the middle of the trench 62 hours after injected ended.

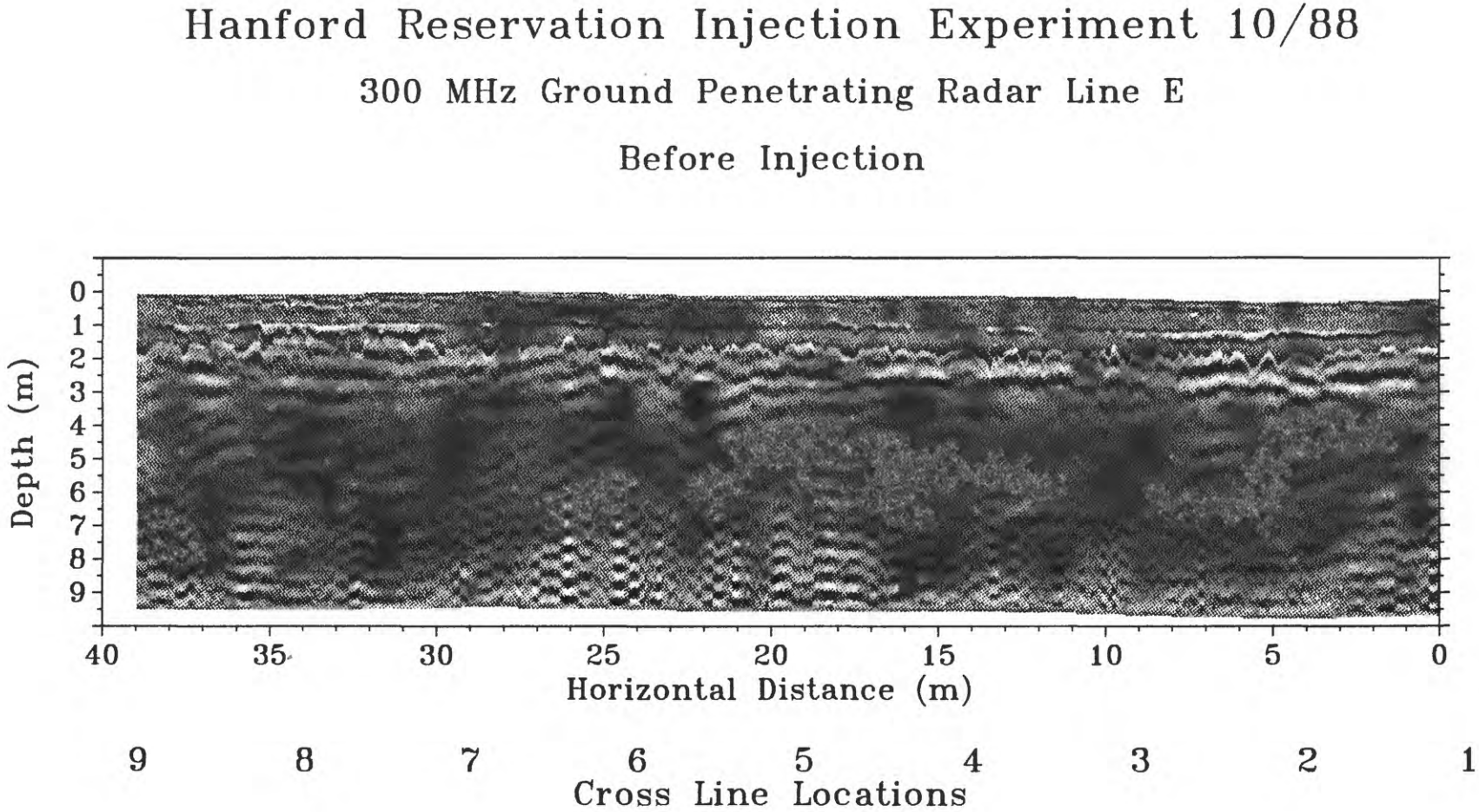

Figure 43 -

300 MHz ground penetrating radar section along line E (see location key in Figure 19) beyond the end of the gravel in the trench and before injection.

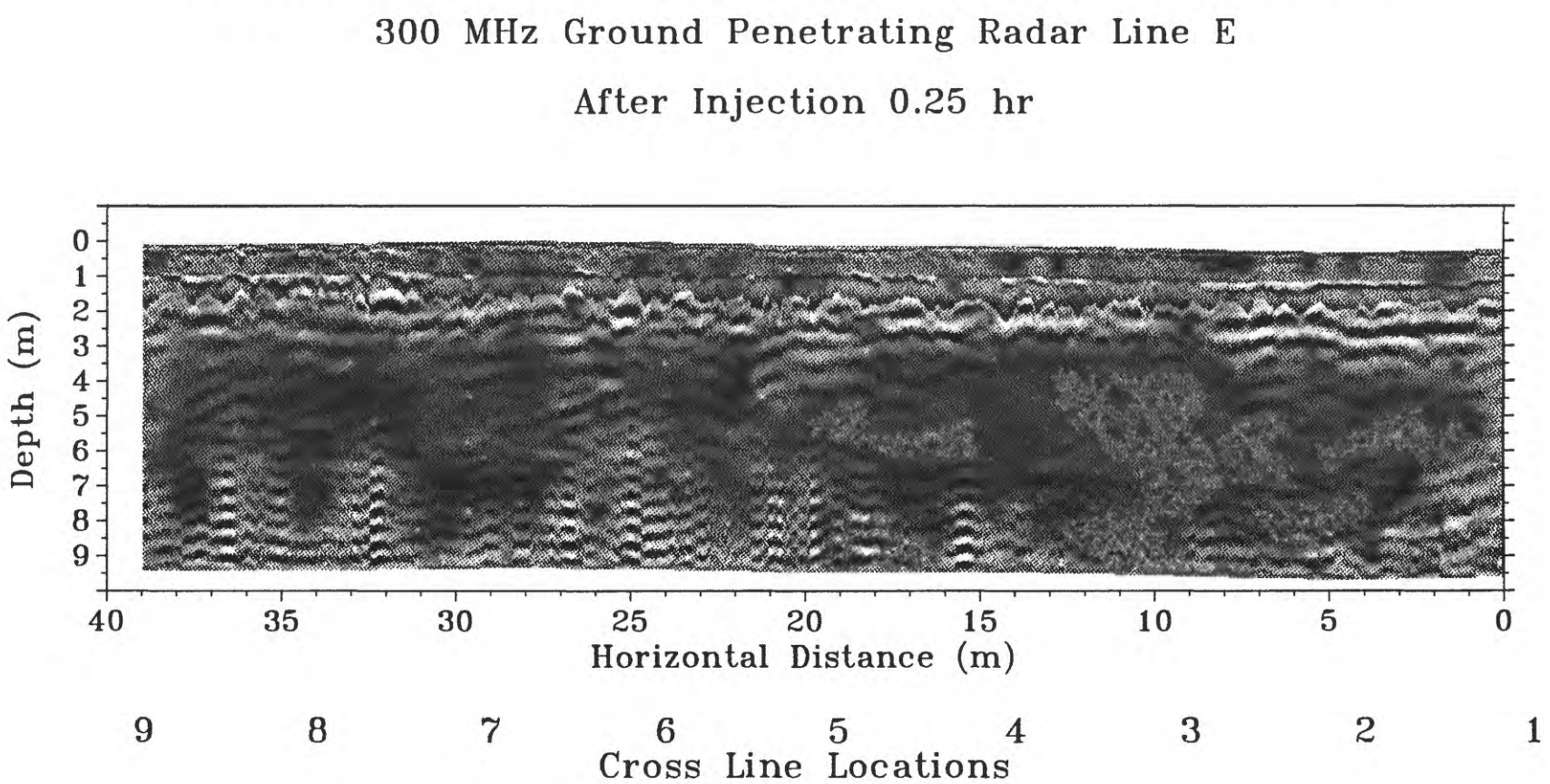

Figure 44 -

300 MHz ground penetrating radar section along line E (see location key in Figure 19) beyond the end of the gravel in the trench, 0.25 hour after injected ended.

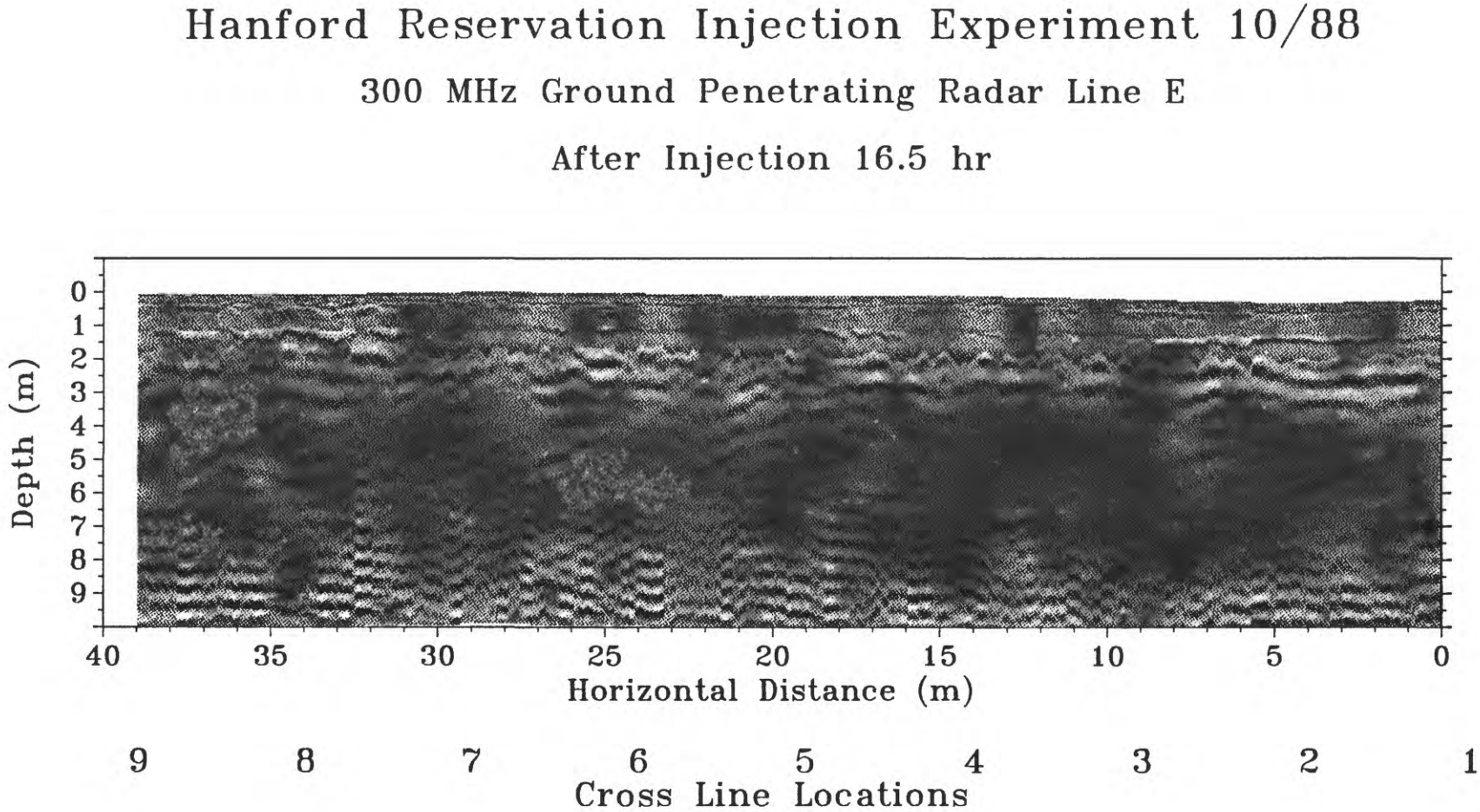

Figure 45 -

300 MHz ground penetrating radar section along line E (see location key in Figure 19) beyond the end of the gravel in the trench and 16.5 hours after injected ended.

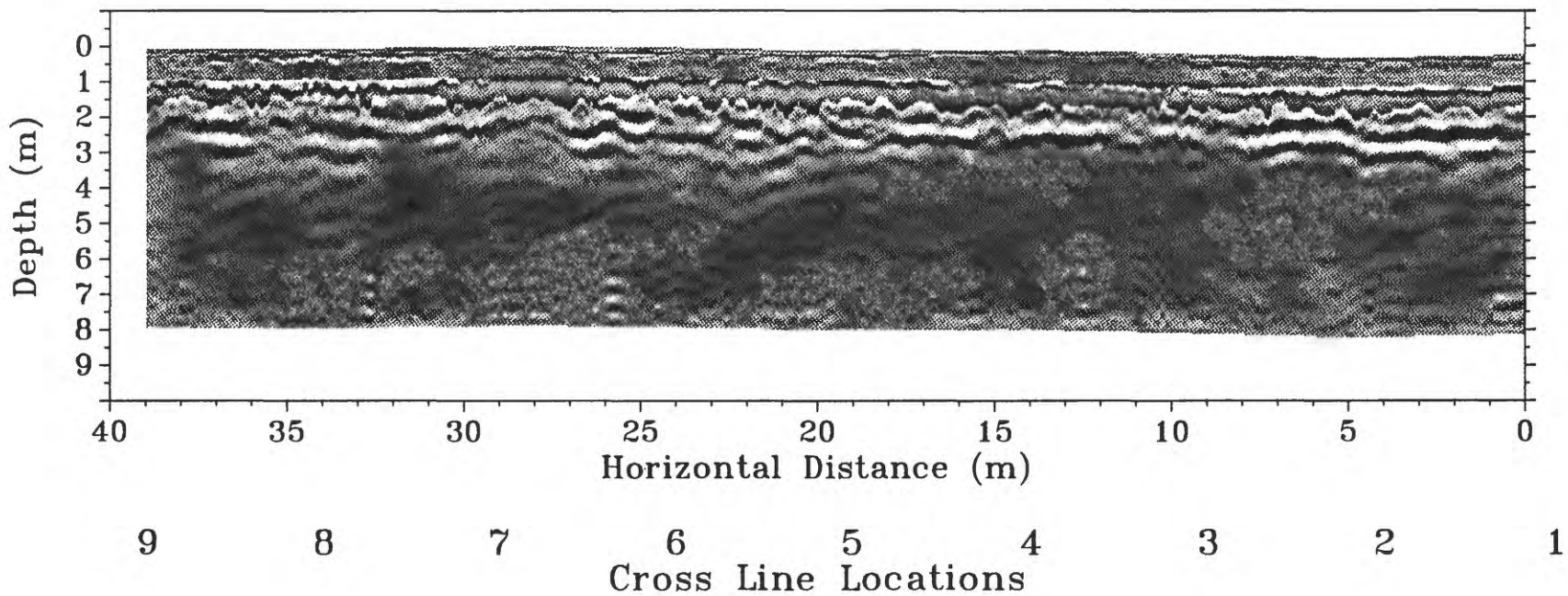

Figure 46 -

300 MHz ground penetrating radar section along line E (see location key in Figure 19) beyond the end of the gravel in the trench and 62 hours after injected ended.

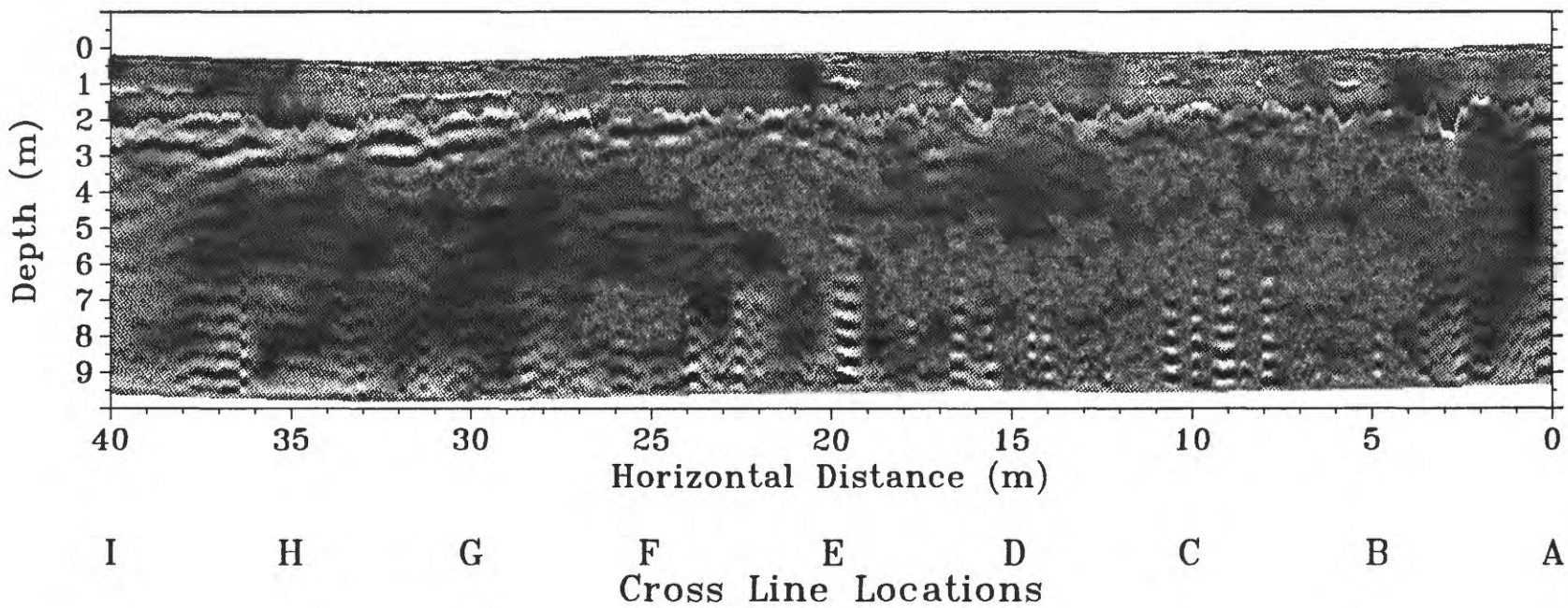

Figure 47 -

300 MHz ground penetrating radar section along line 5 (see location key in Figure 19) along the length of the gravel trench, just outside the gravel, before injection.

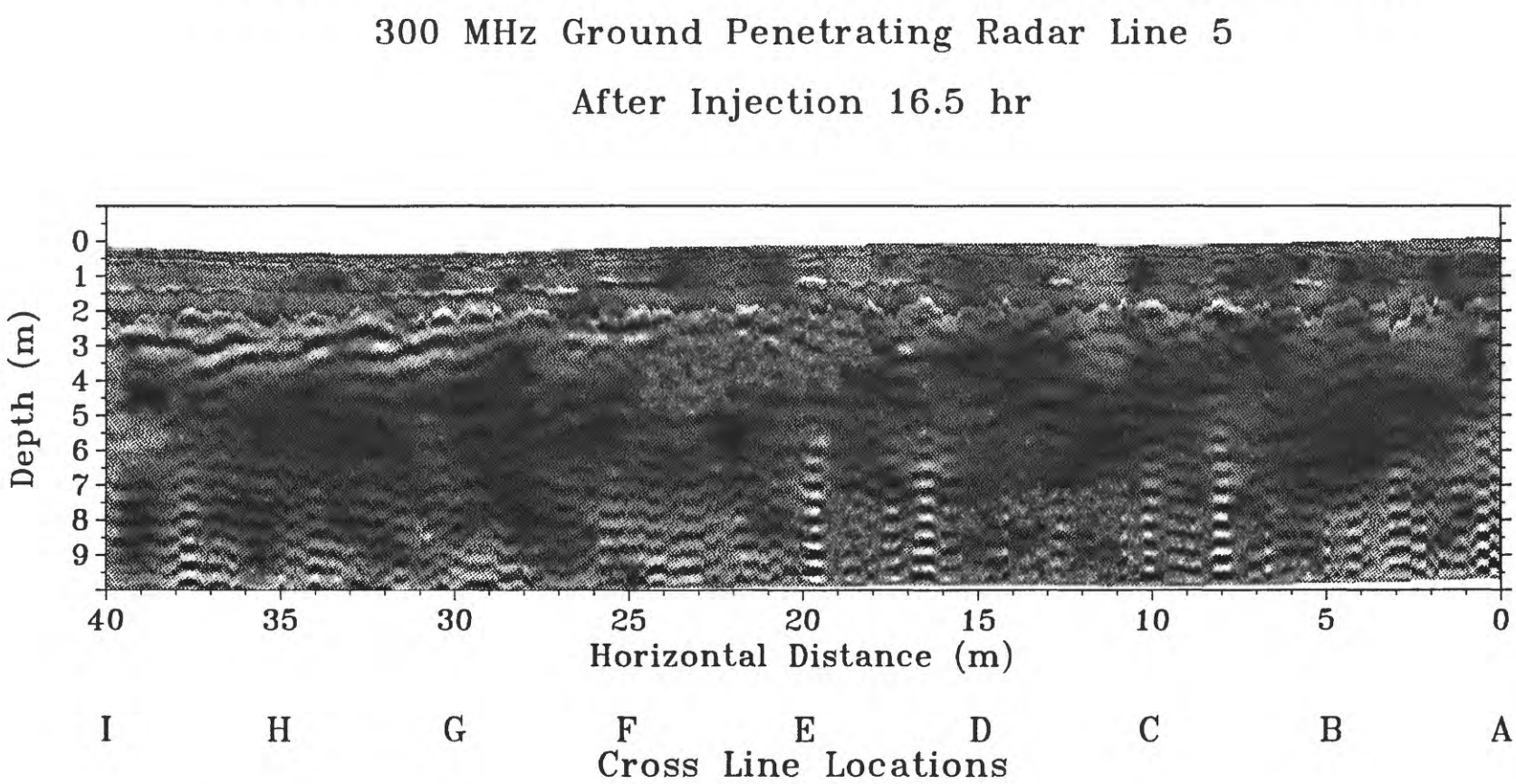

Figure 48 -

300 MHz ground penetrating radar section along line 5 (see location key in Figure 19) along the length of the gravel trench, just outside the gravel, 16.5 hours after injected ended.

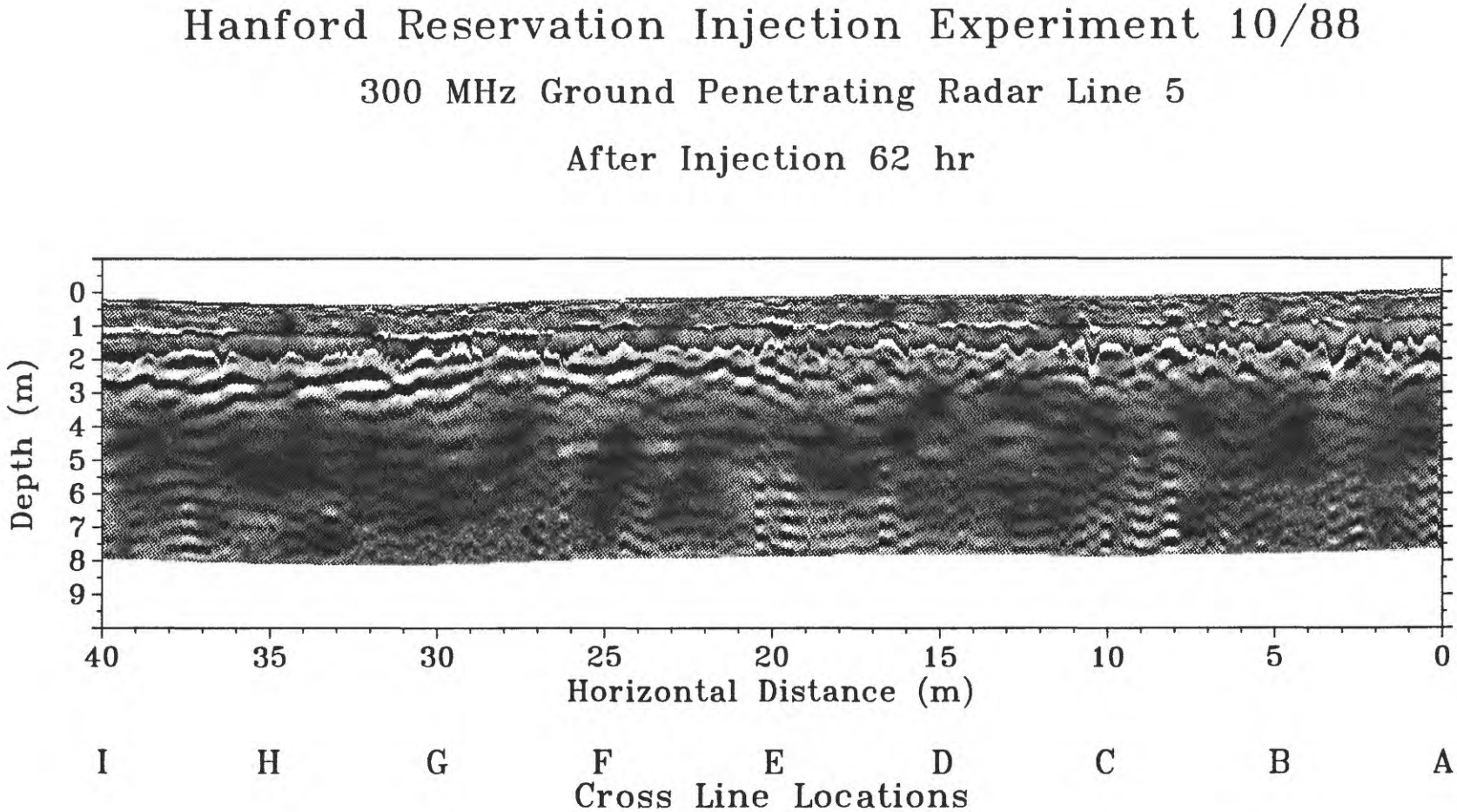

Figure 49 -

300 MHz ground penetrating radar section along line 5 (see location key in Figure 19) along the length of the gravel trench, just outside the gravel, 62 hours after injected ended.

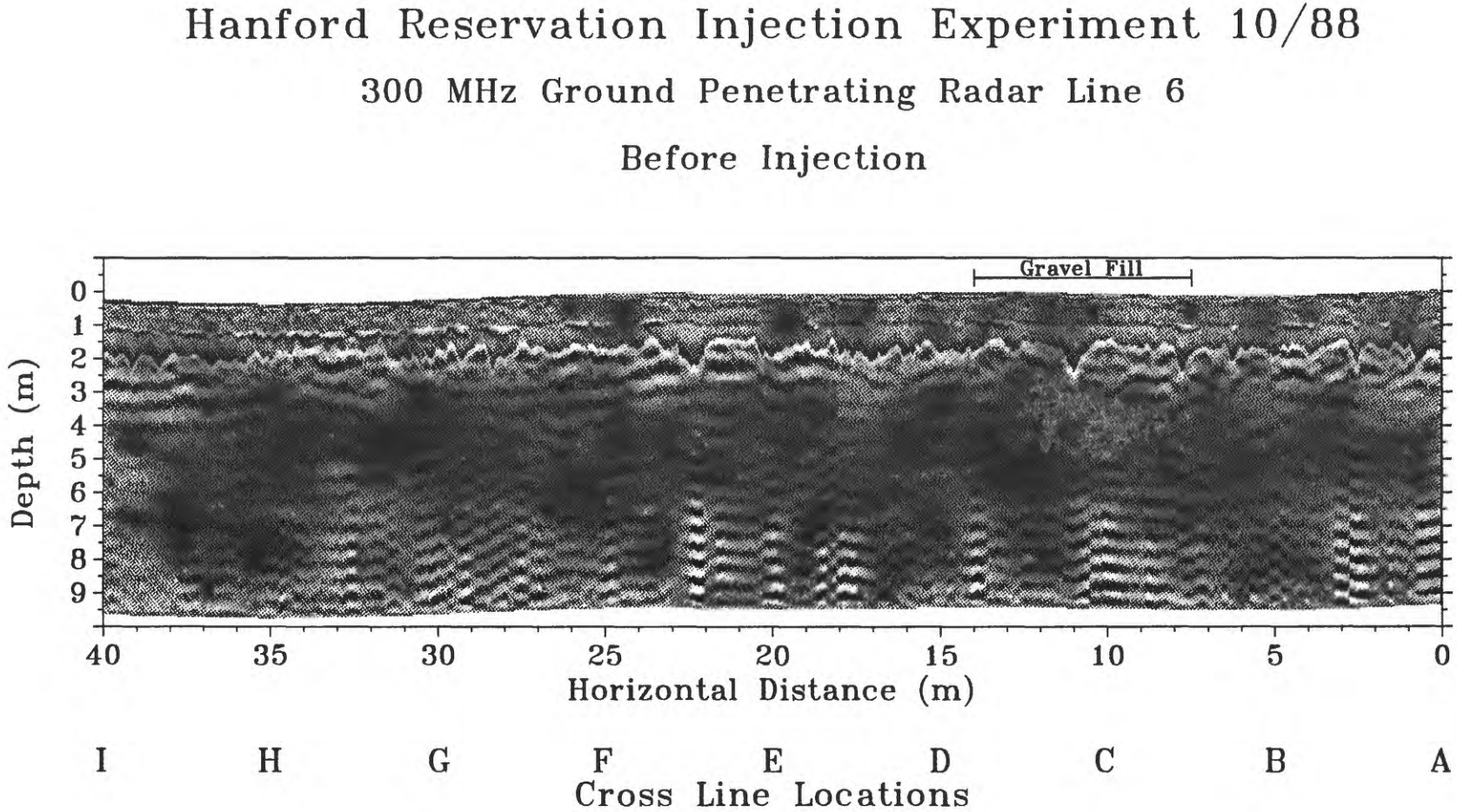

Figure 50 -

300 MHz ground penetrating radar section along line 6 (see location key in Figure 19) along the length of the gravel trench, before injection.

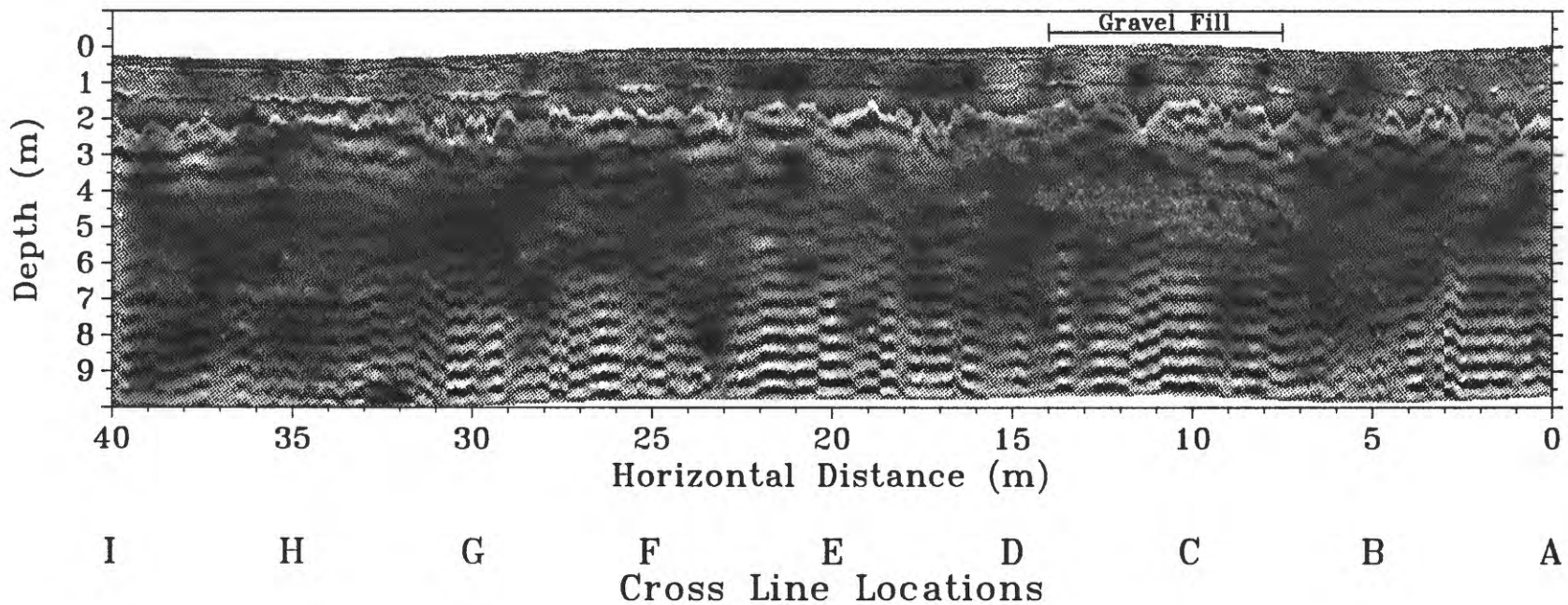

Figure 51 -

300 MHz ground penetrating radar section along line 6 (see location key in Figure 19) along the length of the gravel trench, 16.5 hours after injected ended.

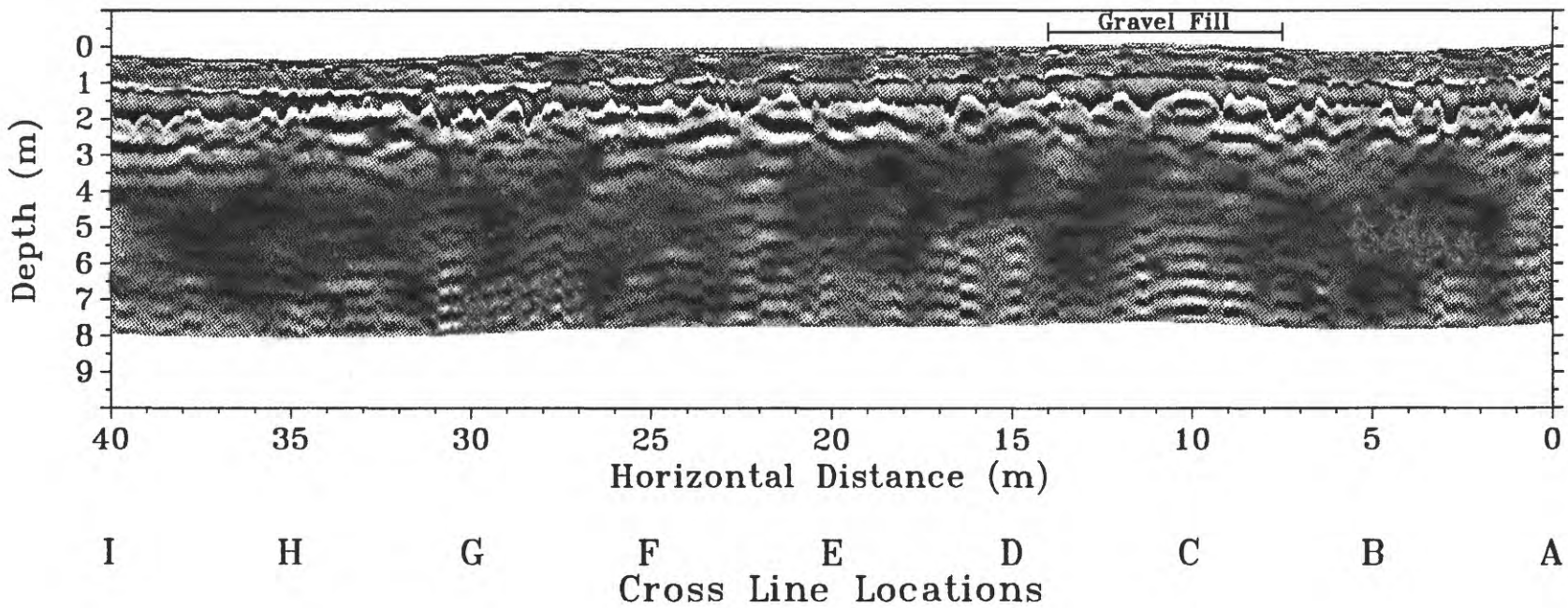

Figure 52 -

300 MHz ground penetrating radar section along line 6 (see location key in Figure 19) along the length of the gravel trench, 62 hours after injected ended.

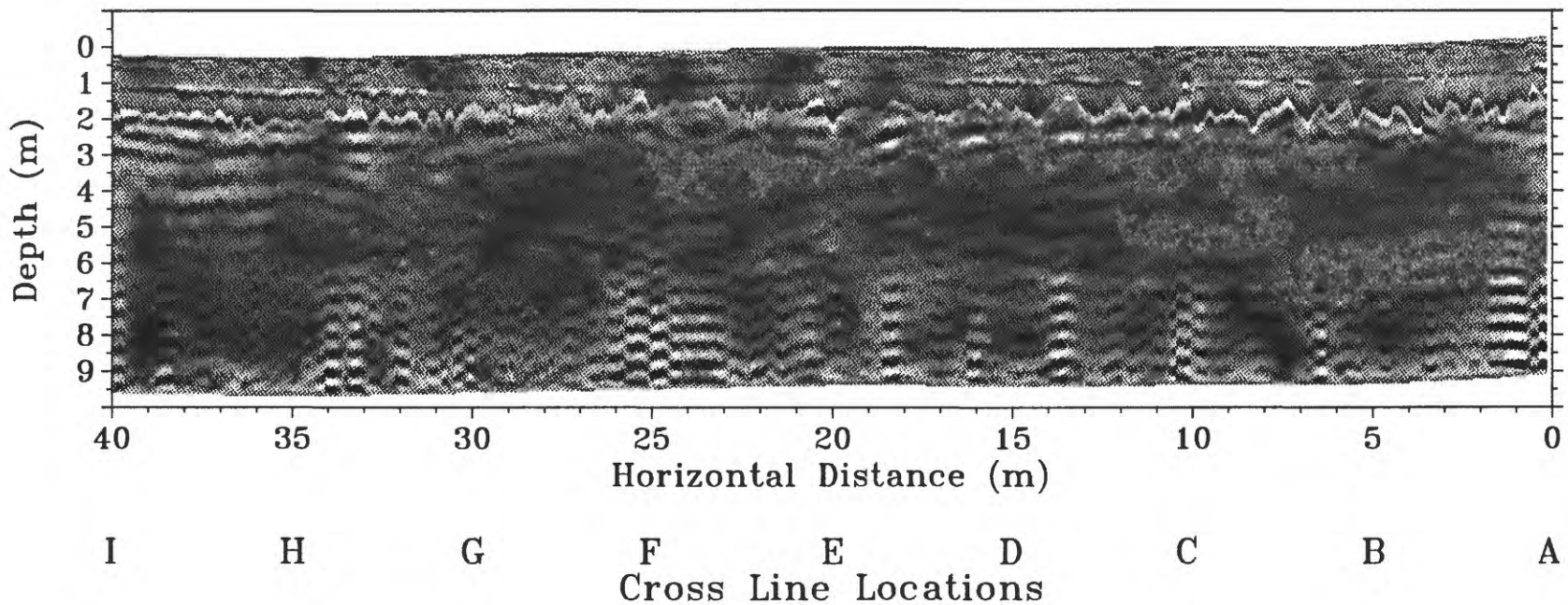

Figure 53 -

300 MHz ground penetrating radar section along line 7 (see location key in Figure 19) along the length of the gravel trench, just outside the gravel, before injection.

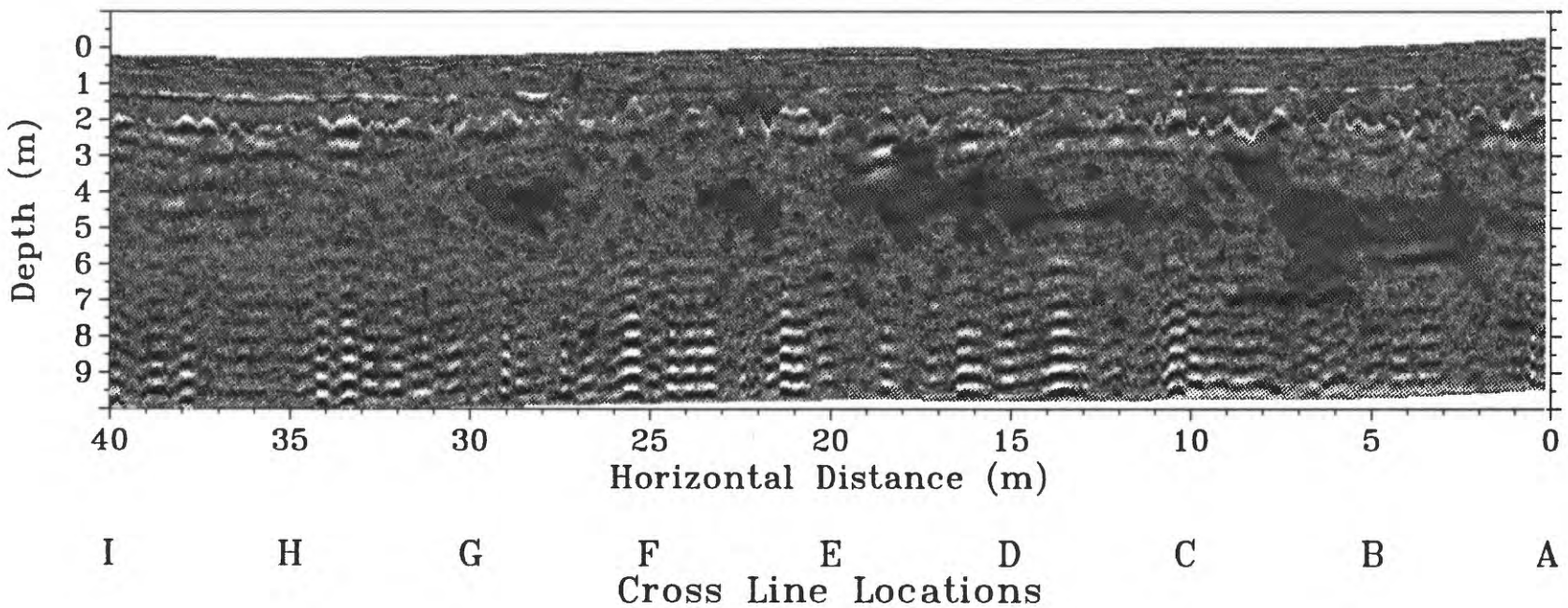

Figure 54 -

300 MHz ground penetrating radar section along line 7 (see location key in Figure 19) along the length of the gravel trench, just outside the gravel, 16.5 hours after injected ended.

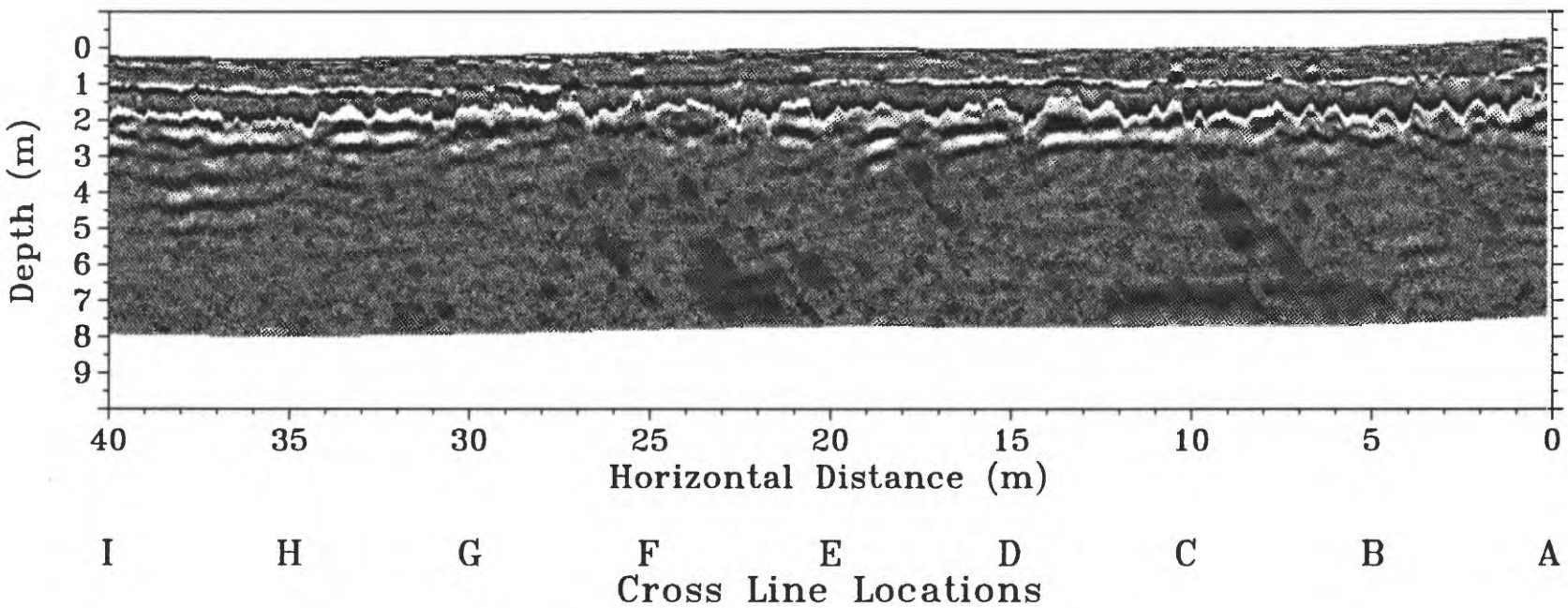

Figure 55 -

300 MHz ground penetrating radar section along line 7 (see location key in Figure 19) along the length of the gravel trench, just outside the gravel, 62 hours after injected ended.

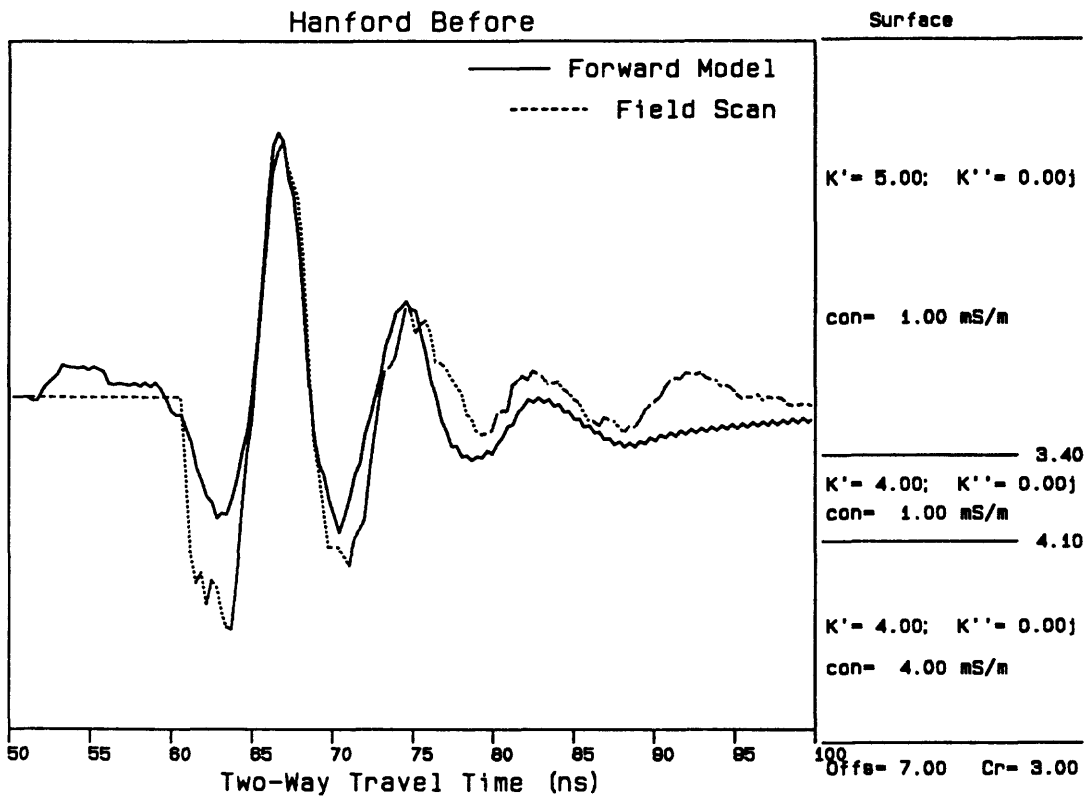

Figure 56 -

Full waveform forward model of ground penetrating radar data from center of line D at 22.5 m horizontal distance (Figure 39) before stabilization material injection. The reflector at 3.4 m depth near 60 ns two-way travel time is the dry gravel trench. The solid line is the forward model computed from the model parameters shown at the right side of the plot. K' and K" are relative dielectric permittivity. con is the DC electrical conductivity in mS/m. The rightmost number is depth in meters to each reflecting interface. Offs is a time offset to compensate for the GSSI SIR-7 arbitrary time zero. Cr is the coupling ratio to compensate for the lowering of the effective center frequency of the antenna by placing it on the ground (it's a ground loaded antenna) and for pulse broadening (dispersion) through the frequency dependent material properties of the ground.

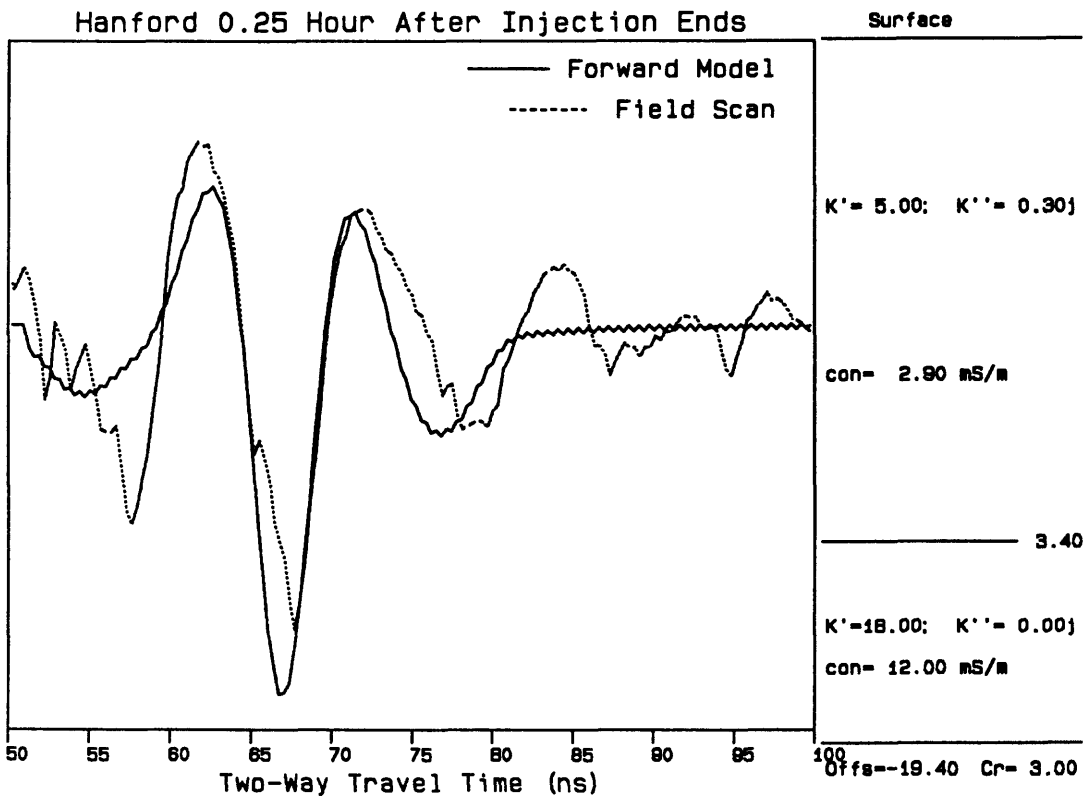

Figure 57 -

Full waveform forward model of ground penetrating radar data from center of line D at 22.5 m horizontal distance (Figure 40) during stabilization material injection, 0.25 hour after injection ended. The reflector at 3.4 m depth near 60 ns two-way travel time is the wet gravel trench. The solid line is the forward model computed from the model parameters shown at the right side of the plot. K' and K" are relative dielectric permittivity. con is the DC electrical conductivity in mS/m. The rightmost number is depth in meters to each reflecting interface. Offs is a time offset to compensate for the GSSI SIR-7 arbitrary time zero. Cr is the coupling ratio to compensate for the lowering of the effective center frequency of the antenna by placing it on the ground (it's a ground loaded antenna) and for pulse broadening (dispersion) through the frequency dependent material properties of the ground.

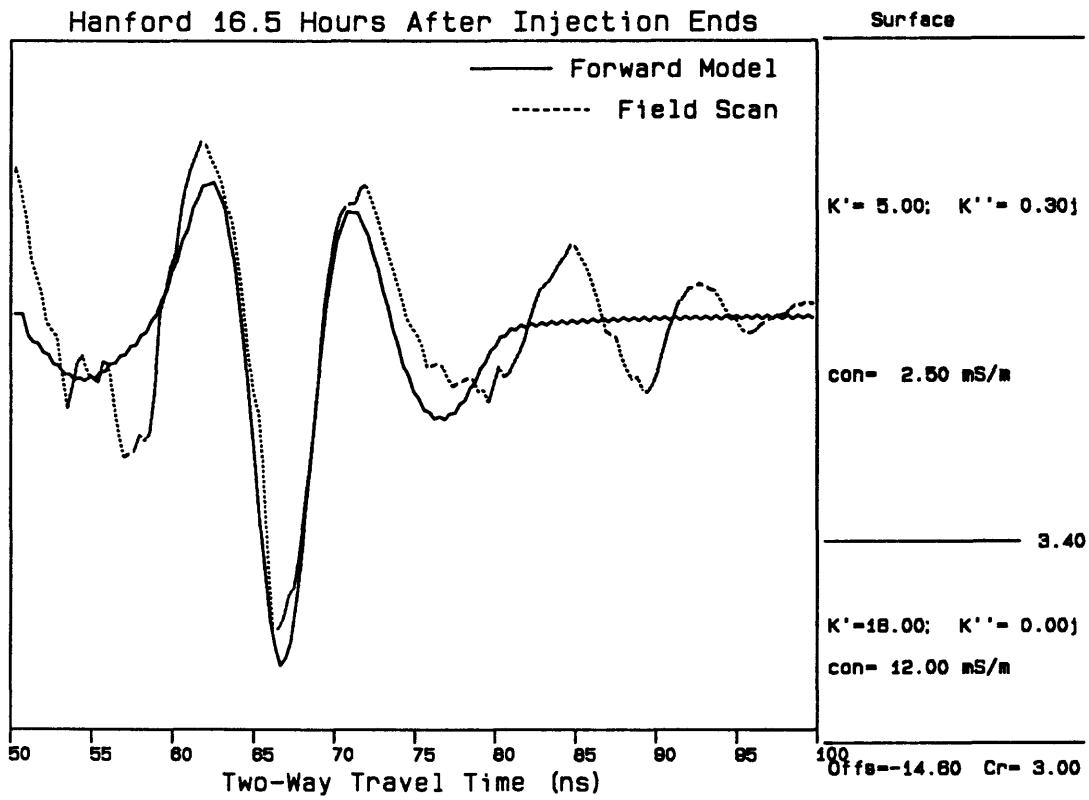

Figure 58 -

Full waveform forward model of ground penetrating radar data from center of line D at 22.5 m horizontal distance (Figure 41) 16.5 hours after stabilization material injected ended. The reflector at 3.4 m depth near 60 ns two-way travel time is the wet gravel trench. The solid line is the forward model computed from the model parameters shown at the right side of the plot. K' and K" are relative dielectric permittivity. con is the DC electrical conductivity in mS/m. The rightmost number is depth in meters to each reflecting interface. Offs is a time offset to compensate for the GSSI SIR-7 arbitrary time zero. Cr is the coupling ratio to compensate for the lowering of the effective center frequency of the antenna by placing it on the ground (it's a ground loaded antenna) and for pulse broadening (dispersion) through the frequency dependent material properties of the ground.

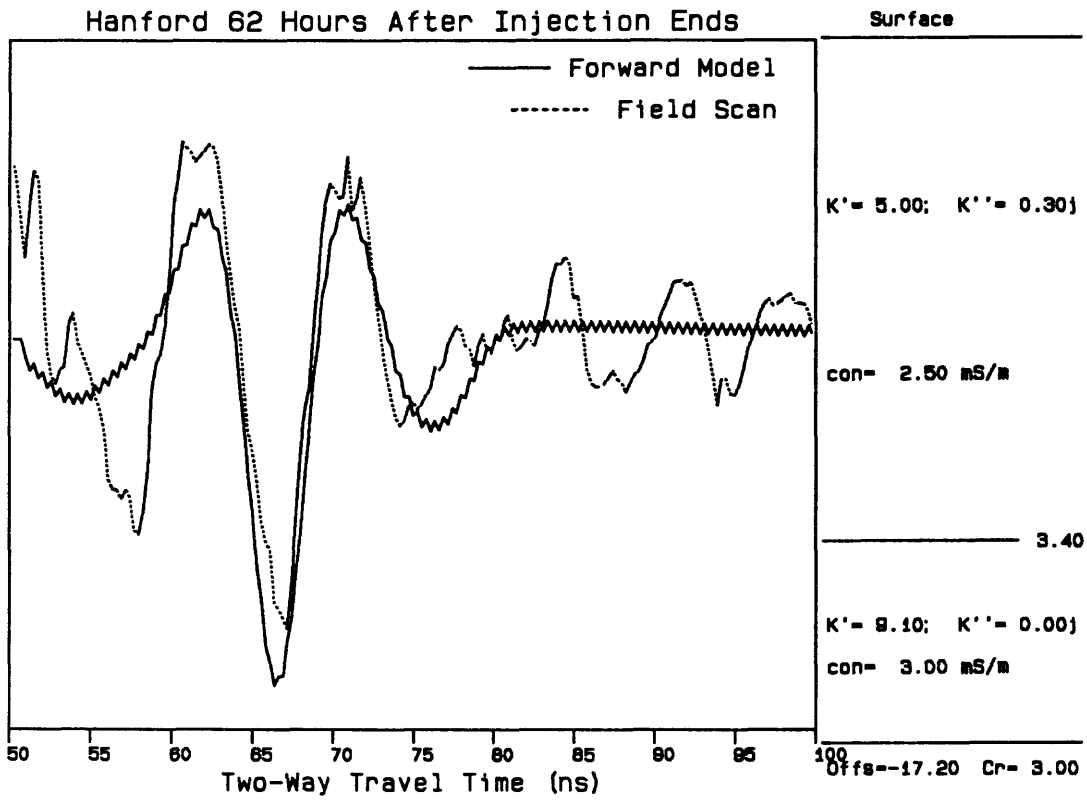

Figure 59 -

Full waveform forward model of ground penetrating radar data from center of line D at 22.5 m horizontal distance (Figure 42) 62 hours after stabilization material injected ended. The reflector at 3.4 m depth near 60 ns two-way travel time is the wet gravel trench. The solid line is the forward model computed from the model parameters shown at the right side of the plot. K' and K" are relative dielectric permittivity. con is the DC electrical conductivity in mS/m. The rightmost number is depth in meters to each reflecting interface. Offs is a time offset to compensate for the GSSI SIR-7 arbitrary time zero. Cr is the coupling ratio to compensate for the lowering of the effective center frequency of the antenna by placing it on the ground (it's a ground loaded antenna) and for pulse broadening (dispersion) through the frequency dependent material properties of the ground.